dupe

UCRL-51385

THE LLL ELECTRON AND PROTON SPECTROMETER ON NASA'S ORBITING GEOPHYSICAL OBSERVATORY 5

(Final Report for Experiment 6)

H. I. West, Jr.
R. M. Buck
J. R. Walton

May 29, 1973

Prepared for U.S. Atomic Energy Commission under contract No. W-7405-Eng-48

LAWRENCE LIVERMORE LABORATORY
University of California/Livermore

LAWRENCE LIVERMORE LABORATORY
University of California/Livermore, California/94550

UCRL-51385

THE LLL ELECTRON AND PROTON SPECTROMETER ON NASA'S ORBITING GEOPHYSICAL OBSERVATORY 5

(Final Report for Experiment 6)

H. I. West, Jr.
R. M. Buck
J. R. Walton

MS. date: May 29, 1973

Contents

Abstract 1
Introduction 1
Instrument and Inflight Operation 2
Electron Spectrometer 2
Proton Spectrometer 5
Dynamic Range 8
Magnetic Shielding 9
Pitch-Angle Scan Mechanism 9
Differential Discriminator and Proton Logic 11
Experiment Status and Failure 11
Raw Data Plots 12
Bibliography of Results 17
Reports 17
Talks 18
Publications 22
Resumé of Results 24
Inner Belt 24
Slot and Nearby Outer Belt 27
Pitch-Angle Distributions in the Outer Magnetosphere 29
Plasma Sheet Boundary Motion During a Substorm 50
The April 1969 Solar Particle Event 54
The November 18, 1968 Solar Particle Event 56
Highly-Anisotropic Proton Distributions Observed Interplanetary . . . 58
Concluding Remarks 60
Acknowledgments 61
References 62

THE LLL ELECTRON AND PROTON SPECTROMETER ON NASA'S ORBITING GEOPHYSICAL OBSERVATORY 5 (Final Report for Experiment 6)

Abstract

The LLL energetic electron and proton spectrometer on NASA's Orbiting Geophysical Observatory 5 (OGO-5) operated successfully from launch—March 4, 1968—until retirement in August 1971. Data recovery during this time was about 95 percent of the orbit except for the last few months. The electron spectrometer used a magnetic field for electron momentum selection which served also as an electron broom for a proton range-energy telescope. The energy range was ~60 to 2950 keV for electrons (seven channels) and 0.10 to ~94 MeV for protons (seven channels). The experiment was scanned relative to the stabilized OGO-5 for obtaining directional information. Excellent data were taken throughout the magnetosphere and in the interplanetary region (apogee 24 R_E). Studies were carried out in the areas of equatorial pitch-angle distributions, substorm dynamics and field topology, particle spectra (time history), particle spatial distributions, and solar particle events. Excellent data were available from other OGO-5 experiments for data correlation. This report covers instrumentation features that contributed significantly to the experiment's success and also presents a resumé of the experimental results.

Introduction

NASA's Orbiting Geophysical Observatory 5 (OGO-5), launched from the Eastern Test Range at 0800 LT March 4, 1968, operated successfully for nearly 3-1/2 yr. Our experiment (E-06) ran continuously during this period, with most of the experiment working properly.

E-06 grew out of a 1962 experiment (West, 1965) conducted on the U.S. Airforce satellite STARAD (1962 βK) to assess the effects of the Starfish high-altitude nuclear detonation on the earth's radiation belts (West et al., 1965). This experiment, consisting of a five-channel magnetic beta-ray spectrometer, worked well, giving three months of data in the inner belt and high-latitude regions of the outer belt. Because the satellite was spinning, we were able to measure pitch-angle distributions; this was important in interpreting the data.

In general, interpretation of the inner belt data was hampered by a paucity of pre-Starfish data. The STARAD results, along with those emerging from studies of the outer magnetosphere and the magnetotail by other investigators, pointed up the need for studying magnetospheric electrons with instruments able to make unique measurements in well-defined energy bins. Background effects would have to be low or accurately measured. Pitch-angle measurements would be required, particularly at the magnetic equator where such measurements can determine what is happening along the field line on the time scale of the bounce period; pitch-angle distributions also are sensitive to effects at other longitudes on the time scale of the azimuthal drift.

To complete the picture provided by the electrons, it was evident that low-energy proton measurements would be needed. In the OGO-5 experiment, this was accomplished by placing the proton detectors inside one of the electron-spectrometer magnets so that the magnet served the secondary purpose of an electron broom.

Other measurements on OGO-5 complemented our results. Initially, low-energy measurements were available via two electrostatic analyzer experiments, Unfortunately, these experiments met an early demise. At times, the plasma-wave measurements of Scarf et al. (dE/dt) were valuable. However, for our purposes, the most important information was the magnetic vector data for our pitch-angle studies, provided by the UCLA flux-gate magnetometer experiment. These were the major complementary data we needed for putting together the physics.

In this final report, we first describe the experiment's design and operation. Although no new technology of a patentable nature was found, there are some features of the instrumentation that may influence future experiments. We then present abstracts of pertinent reports, talks, and publications. This is followed by a resumé of results. In the resumé we include a discussion of future work that should be performed using the OGO-5 data.

Instrument and Inflight Operation

The instrument report by West et al. (1969) completely documents the LLL experiment. In this final report, we merely describe the instrument, emphasizing its unique features and inflight operation.

The experiment consisted of an electronics package, located in the main body of the satellite, and sensors on a boom called the OPEP-2 (Orbital Plane Experimental Package 2). Figure 1 shows the electronic functional makeup of the experiment. Figure 2 shows the important features of the spacecraft, whose proper orientation required that the solar paddles look directly at the sun and the OPEP shaft point to the earth's center. Table 1 gives the characteristics of the energy channels.

ELECTRON SPECTROMETER

The electron spectrometer used two small permanent magnets for momentum

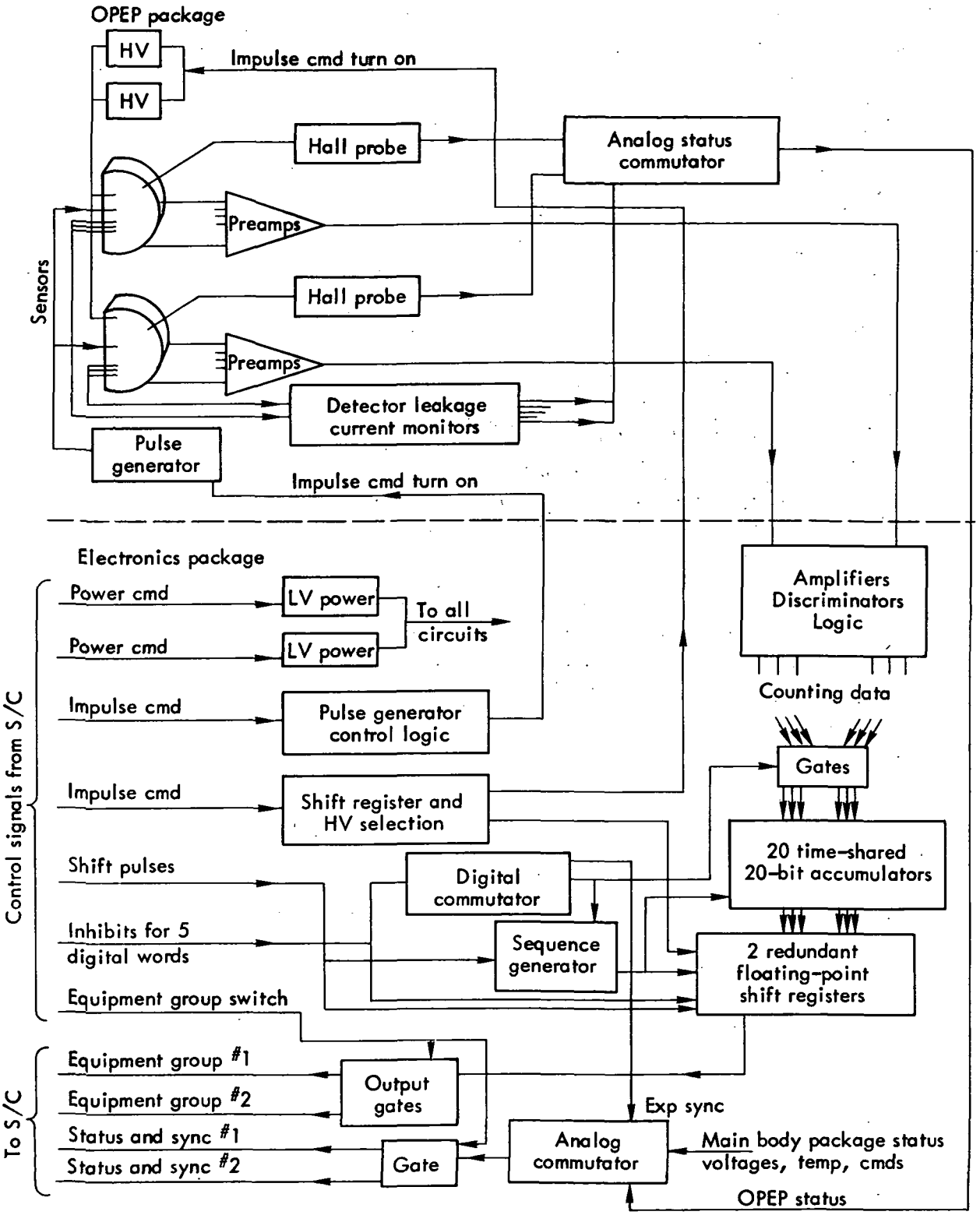

Fig. 1. Block diagram of the electronics.

analysis (180-deg first-order focusing) and solid-state detectors for particle detection (see Figs. 3 and 4).

Accurate evaluation of backgrounds was considered essential to the experiment's success. The backgrounds for

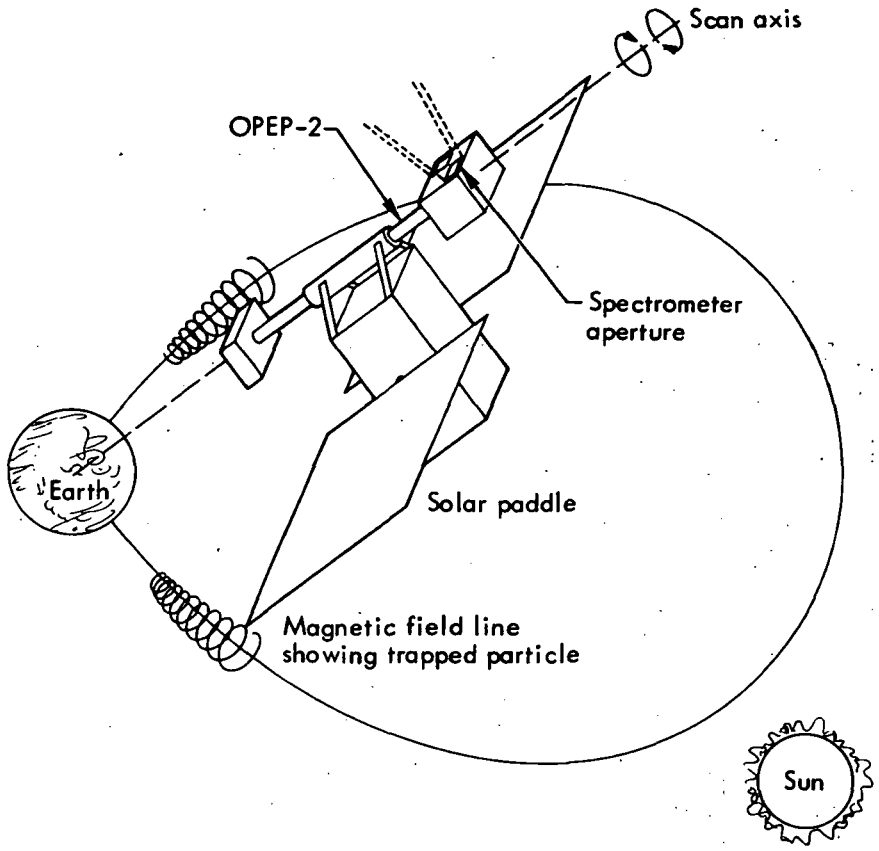

Fig. 2. Orientation of the experiment in the sun-earth-satellite system. Note that the OPEP shaft always points towards the center of the earth and the solar paddles always point towards the sun.

channels E_1 and E_2 were supplied by a single detector between the E_1 and E_2 detectors. For the other channels, individual detectors were used in a multiplexing arrangement. Figure 5 shows how the multiplexed pulses were handled such that the respective electron pulses and background pulses were routed to their respective scalars. The multiplexing arrangement, which worked so well for E_3 through E_7, was not used for E_1 and E_2 because of the increase in electronic noise that would have resulted.

An additional factor contributing to background reduction was the use of detectors thick enough to stop the electrons completely (at least for E_1 through E_6). Thus, a differential window could be positioned over the peak in the pulse-height distribution for the purpose of eliminating backgrounds more effectively (from bremsstrahlung and protons). Other experimenters, by contrast, have used thin solid-state detectors with a wide window set to count the wide range of pulse heights produced. While this is attractive with respect to simplicity, it results in a greater background, as proved by an analysis of the background spectrum.

The background evaluation procedure worked extremely well for all regions of space reached by OGO-5, including measurements in the inner belt and in

the interplanetary region during solar-particle events. In both cases, the major background problem was penetrating protons. In using the background data, we determined the sensitive-volume ratios of the respective detectors (~10 percent) before flight. These ratios were improved to ~±2 percent through study of penetrating galactic radiations during periods of minimum solar activity when OGO-5 was free from the influence of magnetospheric radiations. Normalization studies were made during 1968 and 1969, remaining quite constant during that period.

PROTON SPECTROMETER

Proton data were acquired from an array of proton detectors (range-energy telescope and single detector) in one of the electron spectrometer magnets. As shown in Fig. 4, the array was in line with the entrance aperture. Means were provided for estimating the backgrounds (by interchanged logic between detectors), but the results were not of the high accuracy available for the electrons. The electron-broom effect, provided by the spectrometer magnet shown in Fig. 4, was quite effective. Electron or

Table 1. Spectrometer characteristics.

Channel	Energy range	Geometry	Acceptance angle (deg)[a]
Electrons			
E_1	79 ± 23 keV	0.180 cm^2 keV sr	7.6
E_2	158 ± 36	0.277	5.9
E_3	266 ± 36	0.390	4.7
E_4	479 ± 52	0.605	3.5
E_5	822 ± 185	4.43	5.3
E_6	1530 ± 260	8.57	4.1
E_7	2820 ± 270	3.88	2.5
Protons			
P_1	0.10 - 0.15 MeV	2.06×10^{-3} cm^2 sr	12
P_2	0.23 - 0.57	1.3×10^{-2}	12
P_3	0.57 - 1.35	1.3×10^{-2}	12
P_4	1.35 - 5.40	1.3×10^{-2}	12
P_5	5.6 - 13.3	1.25×10^{-2}	12
P_6	14.0 - 46	1.72×10^{-2}	12
P_7	43 - 94	1.98×10^{-2}	12
O_1	< ~ 100	~$0.6 \times 4\pi$ cm^2	omni
Alpha			
α_1	5.9 - 21.6 MeV	1.3×10^{-2} cm^2 sr	

[a]Effective full width at 50% acceptance in the scan plane.

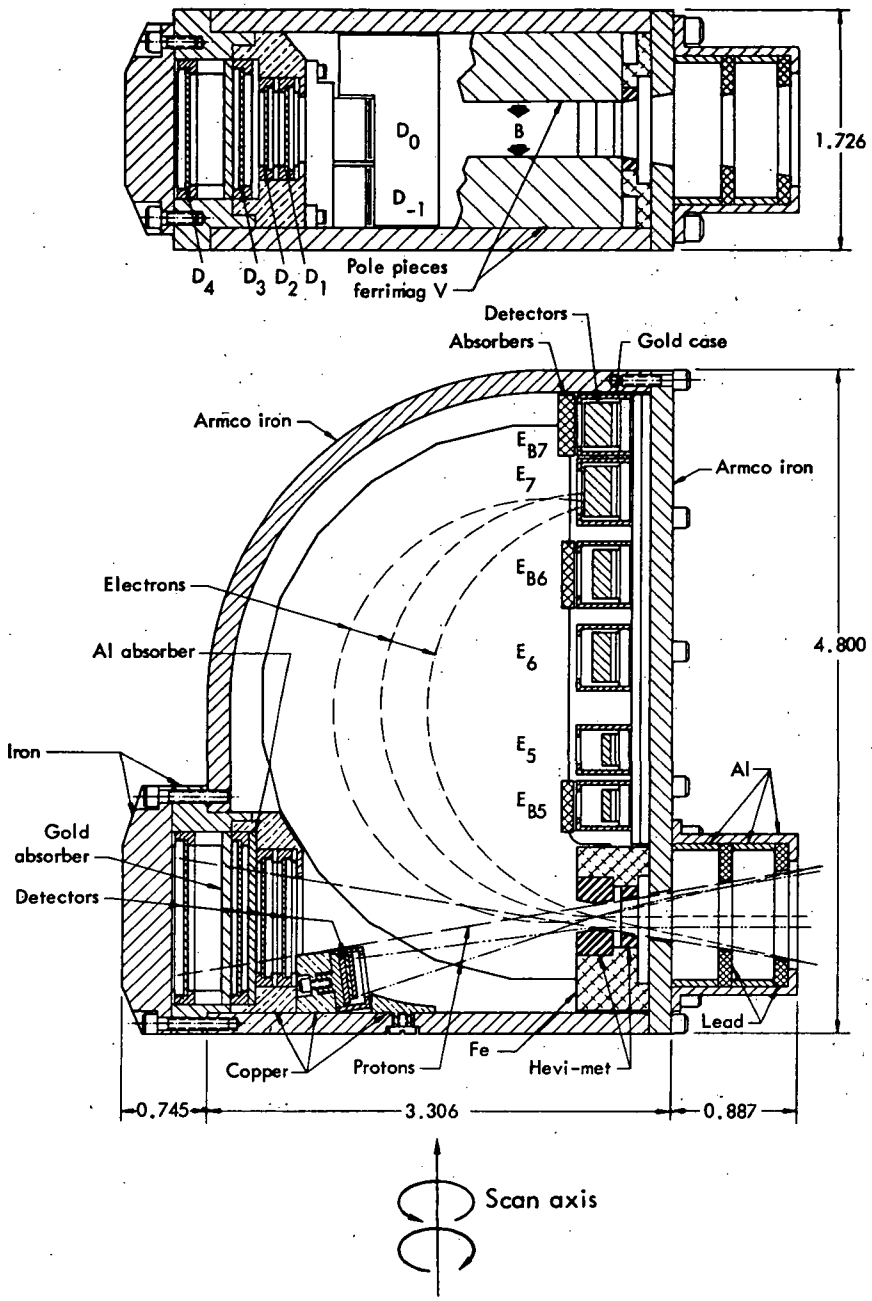

Fig. 3. The low-energy electron spectrometer.

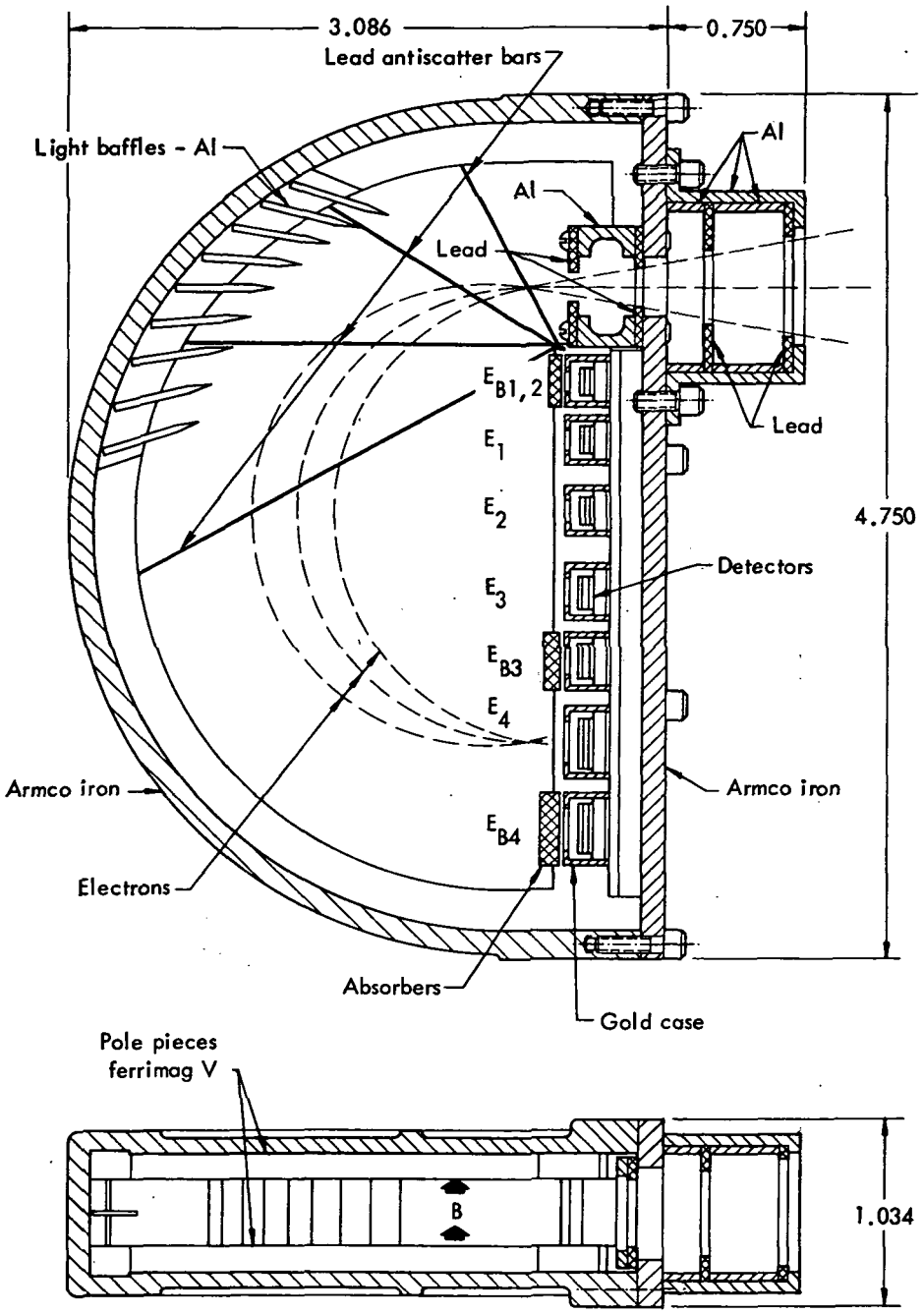

Fig. 4. The larger electron spectrometer and the proton detection system. The field of the electron spectrometer acts as an electron broom for the proton detection system. The field in the magnet is high enough to bend low-energy protons about 5 deg so the true geometry for the small side detector is greater than the apparent optical geometry.

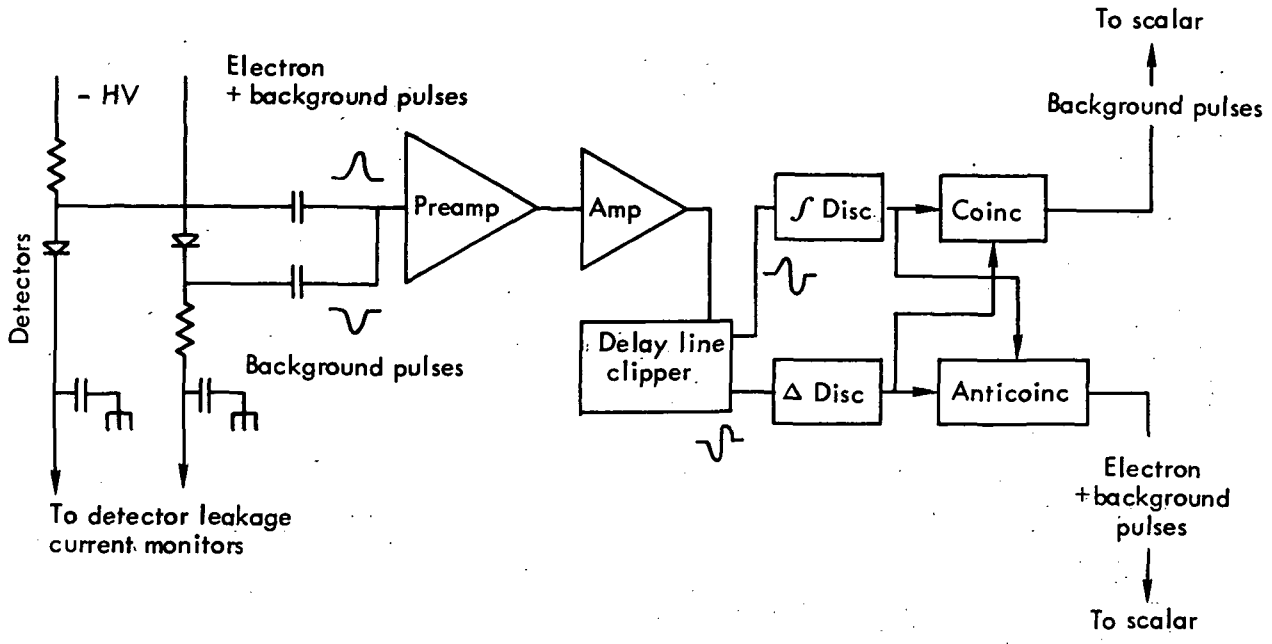

Fig. 5. Multiplexing arrangement for the detectors in the magnetic electron spectrometers. This procedure ensures that the background normalization, once determined, will be constant.

bremsstrahlung background was never a problem. However, penetrating protons were troublesome when we tried to acquire data in the inner belt and during relativistic solar-particle events. The proton data channels we used are listed in Table 1. Some other channels were provided (West et al., 1969), but these were not properly calibrated or used and will not be discussed here.

DYNAMIC RANGE

The geometric factors for the electron spectrometer were near optimum for most of the mission. For example, the maximum counting rates for E_1, E_2, and E_3 in the inner belt got to 10^5 counts/second, only on occasion. For these rates, count rate corrections could be properly made. By contrast, a factor-of-10 increase in the geometry for E_7 or an equivalent reduction in background would have been preferred for the inner belt. Larger geometry would have been desirable, at times, in the magnetotail. It was not realistic, however, with this type of instrumentation, to try to measure electrons in excess of about 1 MeV in the plasma sheet. The instrument was quite effective during solar particle events for E_1-E_5. Obviously, greater geometry would have been desirable. For example, it was only during the April 1969 solar electron event (the largest in the history of space measurements) that E_6 and E_7 provided useful data.

Because of the wide variation in proton fluxes and energies encountered, it is difficult to design a proton spectrometer that works well throughout the magnetosphere. A serious count-rate problem was encountered in measuring protons mirroring near the equatorial regions in the heart of the outer belt. The high

count rates in P_4 and P_5 were enough to cause partial paralysis of P_2 and P_3. The paralysis produced minima near 90 deg in the pitch-angle distributions for these channels. The paralysis was quite consistent. It was only with some reluctance, following studies with Flight Unit 2, that we had to abandon the result.

The experiment provided good measurements in most of the outer magnetosphere. Results in the magnetotail were confined to P_1, and P_2, and P_3. During solar particle events, P_1-P_5 were effective, with occasional significant results in P_6 and P_7. Alpha channel α_1 provided good data during solar particle events. However, due to a pulse-pileup problem, α_1 results were of no value for $L \lesssim 4$, at least in the region of appreciable trapped proton populations.

MAGNETIC SHIELDING

The magnetic field of the larger electron spectrometer magnet between pole pieces was about 2700 G; the field of the smaller spectrometer magnet was about 860 G. The magnets were so mounted that their external dipoles partially cancelled. Because the cancellation did not reduce the stray field adequately, we installed additional shielding: a single sheet of 4-mil Conetic* about 1/2 in. from the spectrometers. The Conetic had to be annealed carefully before assembly and not "work hardened" afterwards. The package "depermed" to a residual field of about 12 γ at 1 ft, which was quite acceptable for the mission.

PITCH-ANGLE SCAN MECHANISM

Because OGO-5 was oriented with respect to the earth and the sun, the aperture of the experiment had to be scanned relative to the spacecraft. The OPEP's were scannable at 1.5 deg/sec as a normal spacecraft function, but this capability generally could not be used because OPEP-1 and -2 were tied together rigidly; all OPEP experiments would have scanned as a consequence. Hence a special mechanism had to be provided on OPEP-2 for scanning our experiment.** It operated almost continuously during the 3-yr mission with no evident sign of malfunction. On alternate orbits inside 4 R_E, the mechanism was turned off so a companion experiment on the same scan platform could look forward in the plane of the orbit (the OPEP "gyro mode"). This reduced our inner-belt data coverage by half.

We encountered a serious problem with respect to the spacecraft scan mechanism. The requirement that our experiment viewing-direction be tied into the coordinate system of the vector magnetometer to ±1 deg did not seem to be fully understood by the spacecraft people. The spacecraft system determined the shaft

*Conetic is a trade name, product of the Magnetic Shield Division, Perfection Mica Company. Reference to a company or product name does not imply approval or recommendation of the product by the University of California or the U.S. Atomic Energy Commission to the exclusion of others that may be suitable.

**This mechanism was supplied through the efforts of R. Browning, and later H. Burdick, of the NASA-Goddard Space Flight Center.

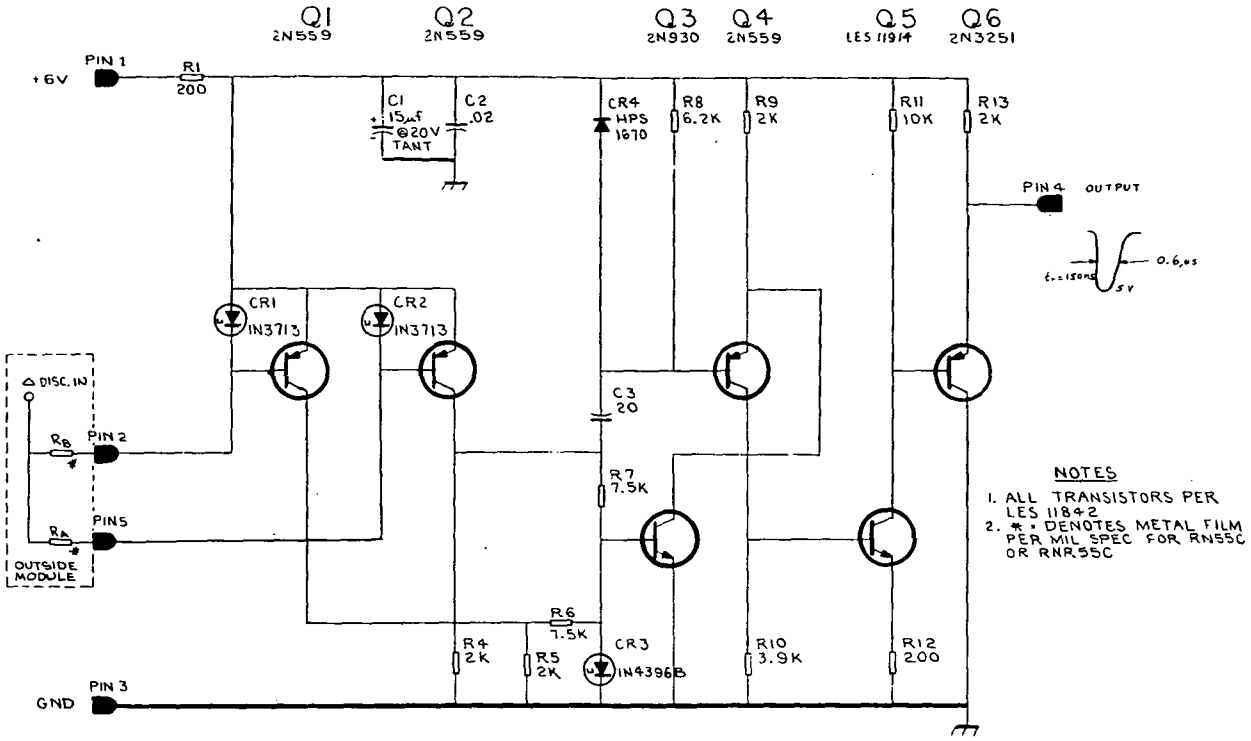

Fig. 6. Differential discriminator. This LLL circuit design is capable of zero standby power and wide operating temperature; it is fast and cannot be tricked by overload pulses, even those lasting tens of microseconds.

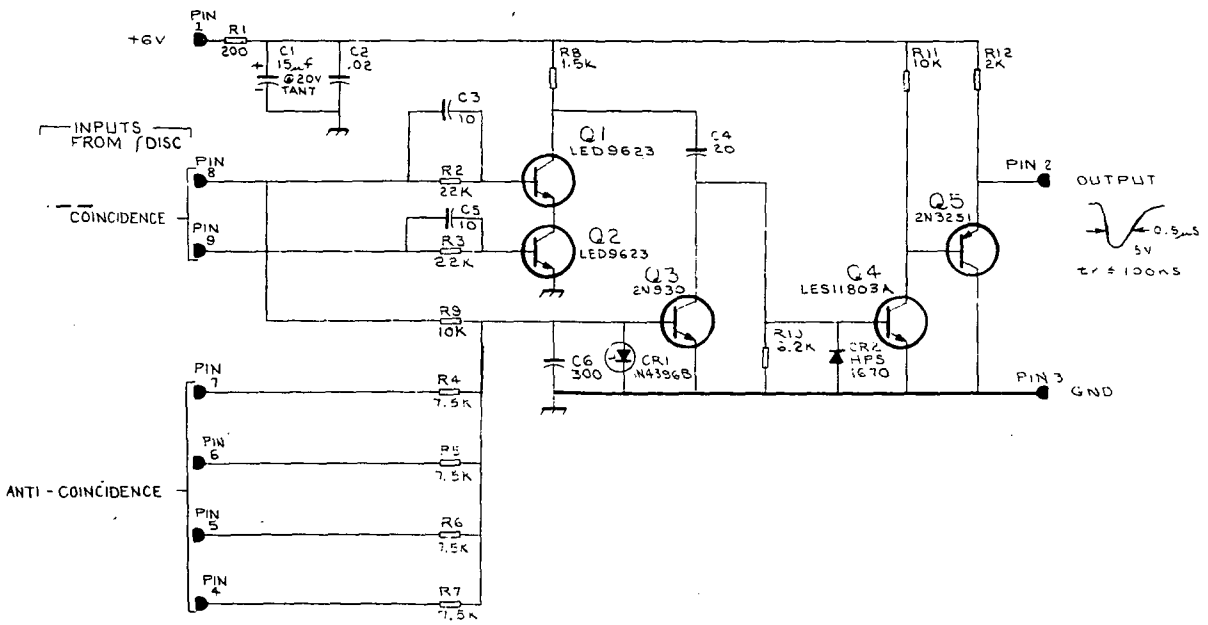

Fig. 7. Typical proton logic circuit. The anticoincidence portion of the circuit (CR1, Q3, R_9, R_4, R_5, R_6, R_7) is identical in principle to that used in the discriminator (Fig. 6).

angle through the use of selsin angle resolvers. This system, capable of fractional degree accuracy, was calibrated at best to 5 deg. Thus, we had to effect an inflight calibration using trapped particle fluxes in predictable regions. Part of this calibration effort is still going on.

DIFFERENTIAL DISCRIMINATOR AND PROTON LOGIC

A circuit designed at LLL prior to the start of the OGO-5 work proved invaluable in implementing our experiment design. Figures 6 and 7 show its use. The circuit uses zero standby power, is fast, and cannot be tricked by overload pulses. Although it has been reported (McQuaid, 1966; West et al., 1969), it does not seem to be widely used.

A differential discriminator (Fig. 6), which is easily expandable to multichannel use, was employed in the electron system. Negative pulses are supplied to integral discriminators 1 (CR1, Q1) and 2 (CR2, Q2). Tripping discriminator 1 results in anticoincidence of the differentiated pulse from discriminator 2 (the output comes in the trailing edge of the pulse from discriminator 2); this occurs through the tripping of tunnel diode CR3, which in turn saturates transistor Q3. Note that once CR3 is tripped, via current through R6 and R7, it stays in conduction until discriminator 2 is turned off (the current through R7 is sufficient to maintain the tripped condition). Thus, long saturating pulses at the input cannot produce an output. Also note that Q3 is in hard conduction when CR3 is on; this means a delay of ~0.7 μsec before Q3 comes out of conduction, so that the anticoincidence function is maintained for this period. The tunnel diode and transistor are temperature-compensating, ensuring that the delay is constant over a wide temperature range.

Figure 7 shows a similar system used in the proton logic. Q1, Q2, and Q6 form a standard series-coincident circuit. CR1 and Q3 form the anticoincidence logic, which operates as previously discussed. In this case, current through R9 plus current from either R4, R5, R6, or R7 results in anticoincidence.

EXPERIMENT STATUS AND FAILURES

A large amount of "housekeeping" data were brought out of the experiment in order to keep track of its status. Once every orbit, near apogee, an inflight pulse generator was exercised to check out the system. This test always gave positive results, an important factor in establishing the credibility of the data.

Some partial failures were observed. In August 1968, we discovered that noise associated with the Goddard Space Flight Center (GSFC) scan mechanism was getting into the bottom channels of the proton telescope. The problem was most pronounced in P_2 and usually could be localized to a small range of scan angles.

For the first few weeks of OGO-5's operation, we encountered occasional problems in the electronically associated channels E_7, EB_7, O_1, and O_2. Noise, seldom lasting more than 10 min at a time, was being generated, probably as a result of bulk or surface leakage in either the E_7 or EB_7 detector. After the first few weeks, this noise disappeared and was never a problem afterwards.

In the Spring of 1971, a detector problem appeared in the associated channels E_6 and EB_6 (the two detectors were multiplexed into the same preamplifier). The channels became noisy. However, E_6 responded to outer belt fluxes and, based on the resulting spectrum, appeared to give correct results. We found that just prior to this time, OGO-Operations had turned off the experiment; in restoring it, personnel had failed to turn on the experiment's high voltage. After the high voltage had been on for a few weeks, the noise disappeared. We cite this as the kind of solid-state detector failure that can occur after prolonged operation in a space environment (3 yr).

RAW DATA PLOTS

We used two plotting schemes for routine examinations of our data: a 20-min plot and a 2-hr plot. Many of these, for 1963 and 1969, are available at the National Space Science Data Center.

Figure 8 is a 20-min plot of E_5 data obtained at the heart of the inner belt. The I's are the electron data (4.6-sec averages) and the O's are backgrounds (4.6-sec averages, counted only one-quarter of the time). The zig-zag pattern gives the magnetic aspect angle, which is read from the scale at the upper right of the plot. The normalization of the background to the electron data is 1.01 ± 0.02. The electron-to-background ratios in the inner belt for the lower energy channels (E_1-E_4) are considerably better than for the E_5 data. Figure 9 shows P_2 data obtained the same time as the E_5 data; the background normalization is 1.0.

Figure 10 shows E_5 data in a 2-hr plot overlapping the time period of Fig. 8. The electron data are 4.6-sec averages, and the background data are 73.7-sec averages. Because of the long averages for the background, some of the background structure has been averaged out. The scatter of points in the electron data is due, of course, to the scan modulation of the data.

Figure 11 shows P_2 data in a 2-hr plot covering the same period as the E_5 data. Note that saturation effects are occurring for the period 1724 to 1820 UT.

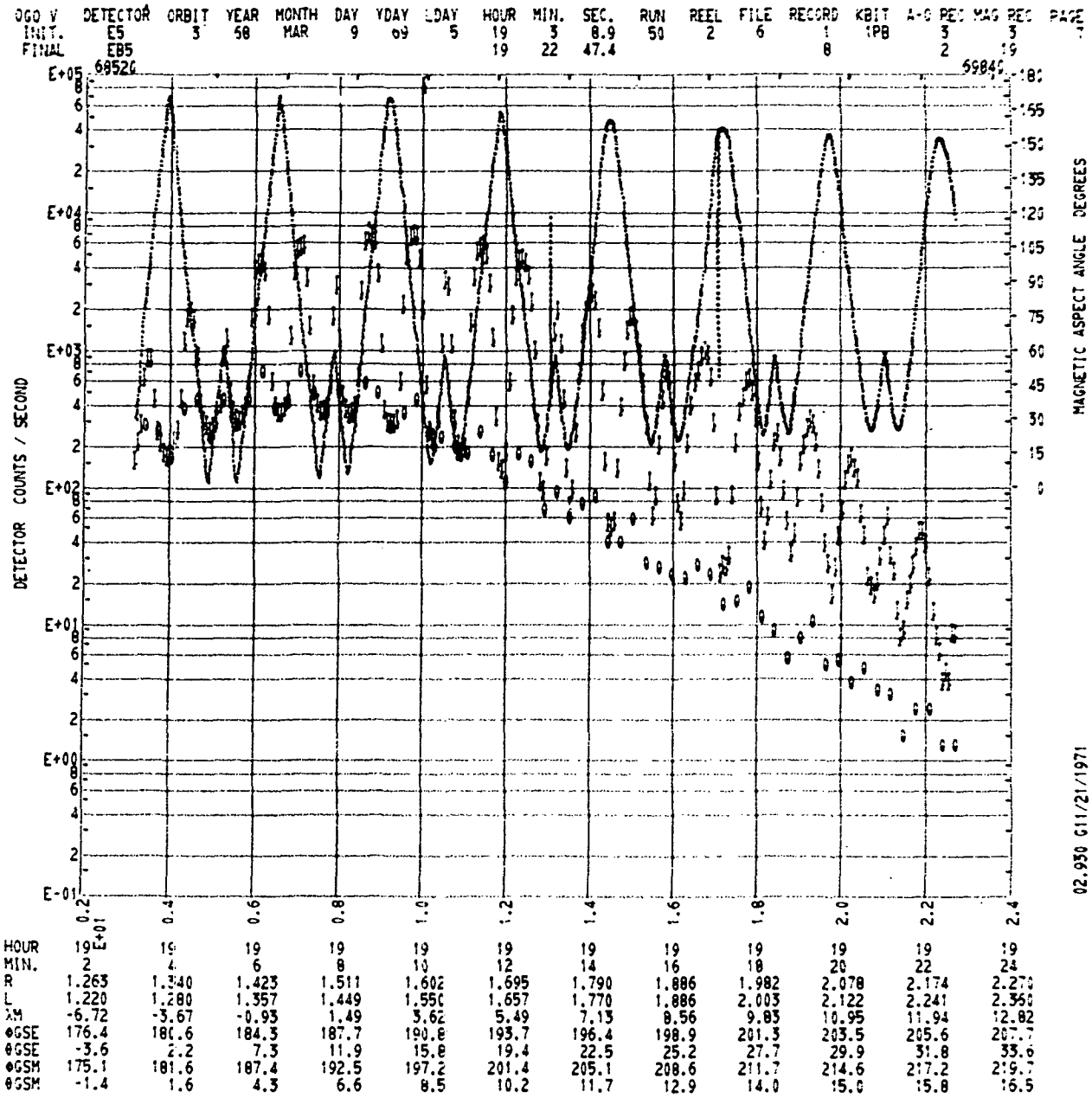

Fig. 8. E_5 inner-belt data in a 20-min plot. The flags are electron data and the O's background. The background normalization is close to 1.00. These data are typical of the E_1 - E_5 data in the inner belt where background due to high energy penetrating protons is a potential problem. The coordinates along the abscissa are: universal time, R in R_E, L in R_E, λ_m (magnetic latitude), ψ_{GSE} (solar ecliptic azimuth), θ_{GSE} (elevation above the ecliptic plane), ψ_{GSM} (solar magnetospheric azimuth), and θ_{GSM} (solar magnetospheric elevation).

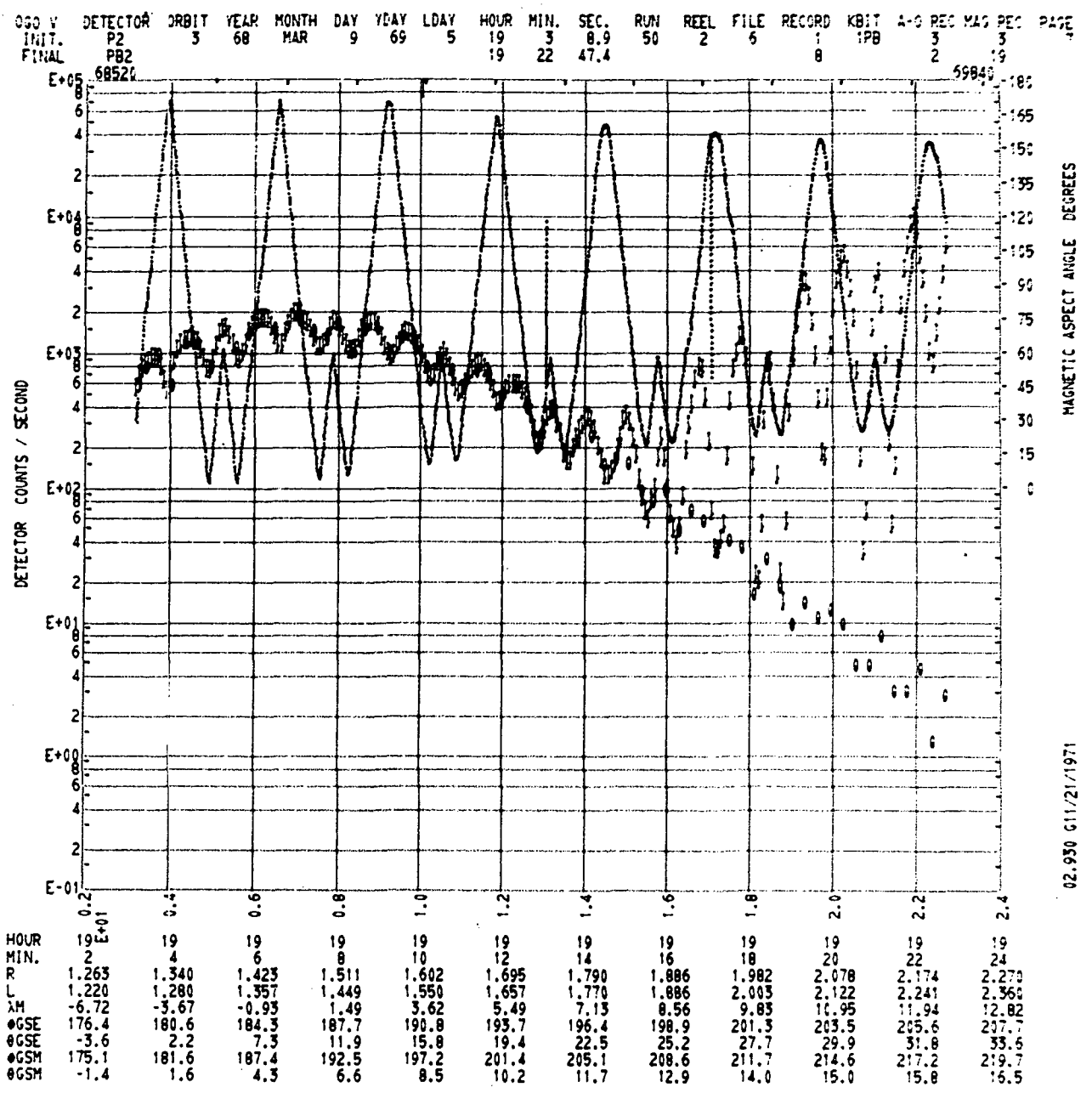

Fig. 9. P_2 inner-belt data in a 20-min plot. The background normalization is close to 1.00.

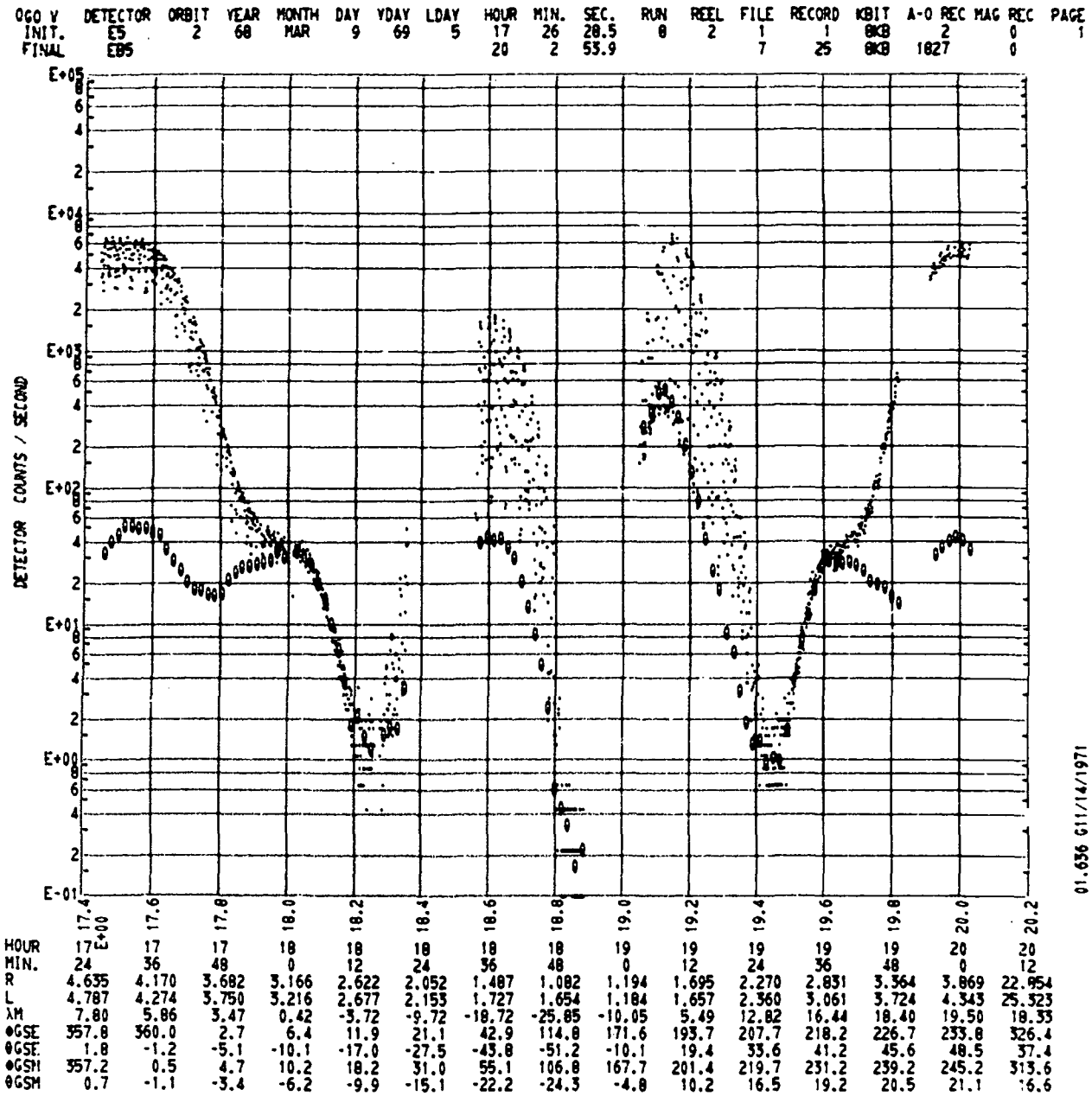

	E+00														
HOUR	17	17	17	18	18	18	18	18	19	19	19	19	19	20	20
MIN.	24	36	48	0	12	24	36	48	0	12	24	36	48	0	12
R	4.635	4.170	3.682	3.166	2.622	2.052	1.487	1.082	1.194	1.695	2.270	2.831	3.364	3.869	22.854
L	4.787	4.274	3.750	3.216	2.677	2.153	1.727	1.654	1.184	1.657	2.360	3.061	3.724	4.343	25.323
λM	7.80	5.86	3.47	0.42	-3.72	-9.72	-18.72	-25.85	-10.05	5.49	12.82	16.44	18.40	19.50	18.33
ϕGSE	357.8	360.0	2.7	6.4	11.9	21.1	42.9	114.8	171.6	193.7	207.7	218.2	226.7	233.8	326.4
θGSE	1.8	-1.2	-5.1	-10.1	-17.0	-27.5	-43.8	-51.2	-10.1	19.4	33.6	41.2	45.6	48.5	37.4
ϕGSM	357.2	0.5	4.7	10.2	18.2	31.0	55.1	106.8	167.7	201.4	219.7	231.2	239.2	245.2	313.6
θGSM	0.7	-1.1	-3.4	-6.2	-9.9	-15.1	-22.2	-24.3	-4.8	10.2	16.5	19.2	20.5	21.1	16.6

Fig. 10. E_5 data in a 2-hr plot.

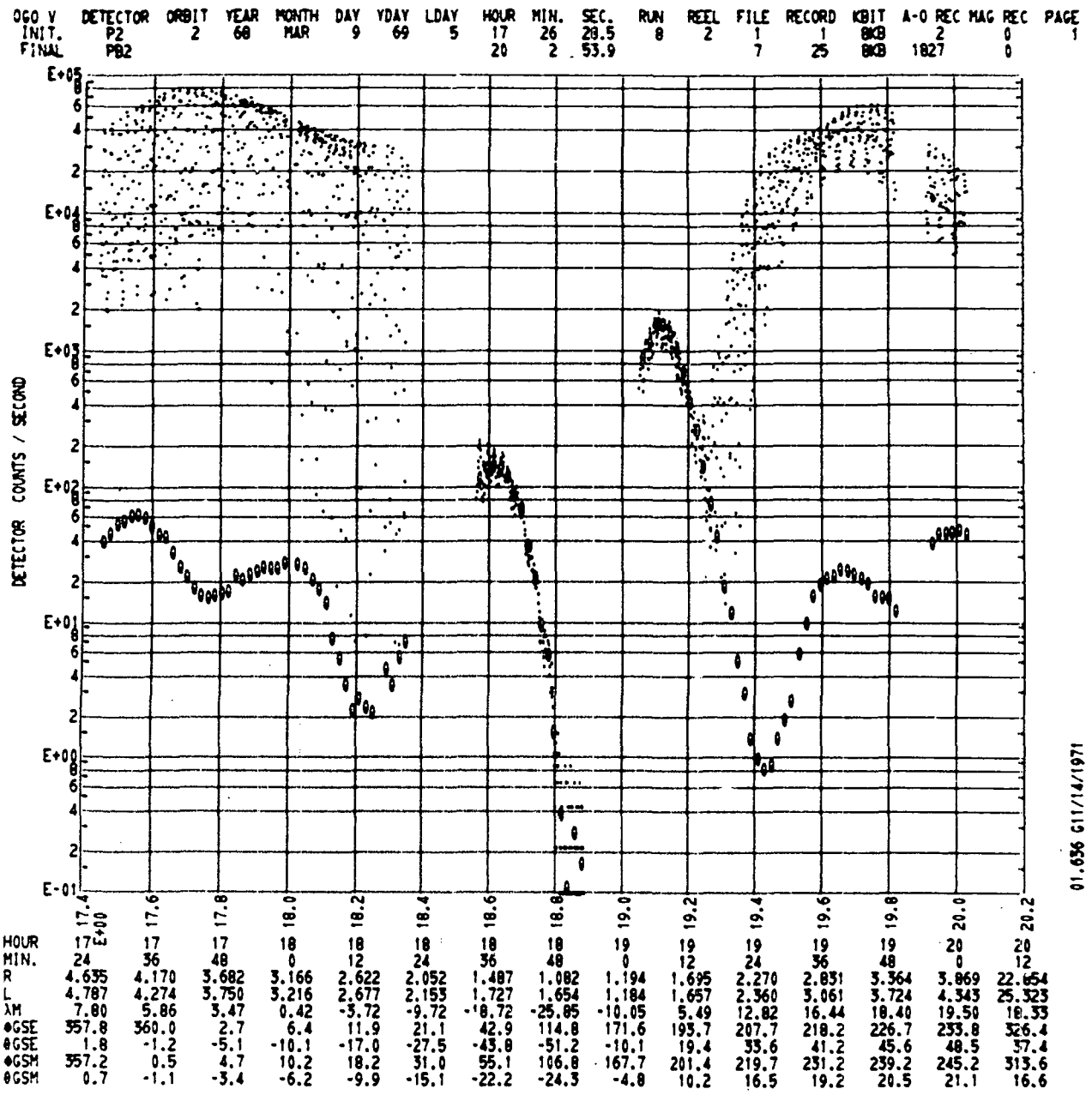

Fig. 11. P_2 in a 2-hr plot.

Bibliography of Results

REPORTS*

The LRL Electron and Proton Spectrometer on NASA's Orbiting Geophysical Observatory V(E) (Instrumentation and Calibration)

H. I. West, Jr., J. H. Wujek, J. H. McQuaid, N. C. Jenson, R. G. D'Arcy, Jr., R. W. Hill, and R. M. Bogdanowicz

Lawrence Livermore Laboratory, University of California
Livermore, California

Lawrence Livermore Laboratory Report UCRL-50572, June 1969

The design, construction, and calibration of the LLL electron and proton experiment on the OGO-V satellite are described. A brief account of postlaunch results is included. The electron spectrometer consists of two small permanent magnets used for energy analysis with electron detection provided by solid-state detectors. Background detectors are also provided. The energy range covered is approximately 60 to 2950 keV in 7 differential energy channels. Geometrical factors vary from 0.18 to 8.6 cm^2-keV-sr.

The proton spectrometer consists of a single solid-state detector and a range energy telescope of four solid-state detectors situated in line with the entrance aperture of the larger of the electron spectrometer magnets. The energy range is 0.1 to 94 MeV in 7 differential energy channels. The geometrical factor for the lowest energy channel (0.1 to 0.15 MeV) is 2.06×10^{-3} cm^2-sr and for the rest of the proton channels 1.3 to 1.9×10^{-2} cm^2-sr. Data handling in the experiment is primarily digital using a binary floating-point compressional scheme. The experiment apertures are scanned relative to the stabilized spacecraft for obtaining pitch-angle distributions.

The LLL Electron and Proton Spectrometer on NASA's Orbiting Geophysical Observatory V (The data user's guide to the microfilm records)

H. I. West, Jr.

Lawrence Livermore Laboratory, University of California
Livermore, California

Lawrence Livermore Laboratory Report UCRL-51037, June 1972

This report provides background for using data from the LLL energetic-particle experiment conducted on OGO-5. These data have been plotted on both 20-min and 2-hr

*We give the abstracts of reports here because this information is not as readily obtainable as the talks and publications that follow. Also, the latter information is summarized in the resumé of results.

scales. Data from the UCLA magnetometer experiment have been plotted to the 20-min scale for correlative purposes. In addition, tables of pertinent attitude-orbit data have been plotted. Many of these data are available on microfilm from the National Space Science Data Center.

The LLL Electron and Proton Spectrometer on NASA's Orbiting Geophysical Observatory V(E): The Three-Way Merged Tape (An Archival Data Base)

M. M. Zeligman and J. R. Walton

Lawrence Livermore Laboratory, University of California
Livermore, California

Lawrence Livermore Laboratory Report UCRL-51314, November 1972

This is a description of a data base that can be used for archival records. The data are combined from three sources and thus the name of the resultant tape: The Three-Way Merged Tape.

The data contained on these tapes came from the following sources:

The LLL Electron and Proton Spectrometer (Experiment E-06) on NASA's Orbiting Geophysical Observatory V(E).

Attitude-orbit tapes containing the satellite ephermeris provided by Goddard Space Flight Center.

Magnetometer tapes provided by Drs. Paul J. Coleman and C. T. Russell with data from the Triaxial Fluxgate Magnetometer Experiment (Experiment E-14) on OGO-5.

TALKS

Observations of Energetic Electrons and Protons on OGO-V

Harry I. West, Jr., Raymond G. D'Arcy, Richard W. Hill, John R. Walton, and G. Allen McGregor

Lawrence Livermore Laboratory, University of California
Livermore, California

International Symposium on the Physics of the Magnetosphere
Washington, D.C., September 3-13, 1968

Electron and Proton Pitch Angle Distributions in the Outer Magnetosphere

Harry I. West, Jr., Richard W. Hill, John R. Walton, and Richard M. Buck

Lawrence Livermore Laboratory, University of California
Livermore, California

Raymond G. D'Arcy, Jr.

Bartol Research Foundation, Franklin Institute
Swarthmore, Pennsylvania

EOS Trans., Amer. Geophys. Union 50, 659, 1969

Observations of Magnetopause Crossings by OGO-5

K. W. Ogilvie and J. D. Scudder

NASA-Goddard Space Flight Center
Greenbelt, Maryland

H. I. West

Lawrence Livermore Laboratory, University of California
Livermore, California

EOS Trans., Amer. Geophys. Union 50, 661, 1969

Anisotropic Angular Distribution of Protons and Electrons from the Cosmic Ray Solar Flare of November 18, 1968

Raymond G. D'Arcy

Bartol Research Foundation, Franklin Institute
Swarthmore, Pennsylvania

Harry I. West, Jr.

Lawrence Livermore Laboratory, University of California
Livermore, California

EOS Trans. Amer. Geophys. Union 51, 410, 1970

Simultaneous Measurements of Solar Flare Electron Spectra in Interplanetary Space and Within the Earth's Magnetosphere

Harry I. West, Jr.

Lawrence Livermore Laboratory, University of California
Livermore, California

A. L. Vampola

Space Physics Laboratory, The Aerospace Corporation
El Segundo, California

EOS Trans., Amer. Geophys. Union 51, 411, 1970

Electron Spectra in the Slot and the Outer Radiation Belt

H. I. West, Jr., R. M. Buck, and J. R. Walton

Lawrence Livermore Laboratory, University of California
Livermore, California

EOS Trans., Amer. Geophys. Union 51, 806, 1970

Evidence for Thinning of the Plasma Sheet During the August 15, 1968 Substorm

R. M. Buck and H. I. West, Jr.

Lawrence Livermore Laboratory, University of California
Livermore, California

R. G. D'Arcy, Jr.

Bartol Research Foundation, Franklin Institute
Swarthmore, Pennsylvania

EOS Trans., Amer. Geophys. Union 51, 810, 1970

OGO-5 Observations of Substorm-Associated Energetic Electrons on 15 August 1968

Margaret G. Kivelson and Thomas A. Farley

Institute of Geophysics and Planetary Physics, University of California
Los Angeles, California

Harry I. West, Jr.

Lawrence Livermore Laboratory, University of California
Livermore, California

EOS Trans., Amer. Geophys. Union 51, 810, 1970

The Butterfly Pitch Angle Distribution of Electrons in the Postnoon to Midnight Region of the Outer Magnetosphere as Observed on OGO-5

H. I. West, Jr., R. M. Buck, and J. R. Walton

Lawrence Livermore Laboratory, University of California
Livermore, California

EOS Trans., Amer. Geophys. Union 53, 486, 1972

Energetic Protons as Probes
of Magnetospheric Particle Gradients

R. M. Buck and H. I. West, Jr.

Lawrence Livermore Laboratory, University of California
Livermore, California

R. G. D'Arcy

Bartol Research Foundation, Franklin Institute
Swarthmore, Pennsylvania

EOS Trans., Amer. Geophys. Union 53, 486, 1972

Energetic Particles Near the Noon Magnetopause
as Observed on OGO-5

R. M. Buck and H. I. West, Jr.

Lawrence Livermore Laboratory, University of California
Livermore, California

American Geophysical Union meeting
Washington, D. C., Spring 1973

Inner Belt Electrons in 1968 Observed on OGO-5

H. I. West, Jr. and R. M. Buck

Lawrence Livermore Laboratory, University of California
Livermore, California

American Geophysical Union meeting
Washington, D. C., Spring 1973

A Unified View of Electron Pitch-Angle Distributions
in the Equatorial Regions
of the Outer Magnetosphere—OGO-5 Observations

H. I. West, Jr.

Lawrence Livermore Laboratory, University of California
Livermore, California

Invited paper, American Geophysical Union meeting
Washington, D. C., Spring 1973

PUBLICATIONS

Simultaneous Observations of Solar-Flare Electron Spectra in Interplanetary Space and Within Earth's Magnetosphere

H. I. West, Jr.

Lawrence Livermore Laboratory, University of California
Livermore, California

A. L. Vampola

Space Physics Laboratory, The Aerospace Corporation
Los Angeles, California

Phys. Rev. Lett. 26, 458, 1971

Energetic Electrons and Protons Observed on OGO-5, March 6-10, 1970

H. I. West, Jr., J. R. Walton, and R. M. Buck

Lawrence Livermore Laboratory, University of California
Livermore, California

R. G. D'Arcy, Jr.

Bartol Research Foundation, Franklin Institute
Swarthmore, Pennsylvania

Solar Geophys. Data ESSA Report UAG-12, 124, 1971

Shadowing of Electron Azimuthal-Drift Motions Near the Noon Magnetopause

H. I. West, Jr., R. M. Buck, and J. R. Walton

Lawrence Livermore Laboratory, University of California
Livermore, California

Nature Phys. Sci. 240, 6, 1972

Energetic Electron and Proton Solar Particle Observations on OGO-5, January 24-30, 1971

H. I. West, Jr., R. M. Buck, and J. R. Walton

Lawrence Livermore Laboratory, University of California
Livermore, California

R. G. D'Arcy, Jr.

Bartol Research Foundation, Franklin Institute
Swarthmore, Pennsylvania

Solar Geophys. Data ESSA UAG Report UAG-24, Part 1, 113, 1972

Electron Pitch-Angle Distributions
Throughout the Magnetosphere as Observed on OGO-5

H. I. West, Jr., R. M. Buck, and J. R. Walton

Lawrence Livermore Laboratory, University of California
Livermore, California

J. Geophys. Res. 78, 1064, 1973

Satellite Studies of Magnetospheric Substorms on August 15, 1968
7. OGO-5 Energetic Proton Observations—Spatial Boundaries

R. M. Buck and H. I. West, Jr.

Lawrence Livermore Laboratory, University of California
Livermore, California

R. G. D'Arcy, Jr.

Bartol Research Foundation, Franklin Institute
Swarthmore, Pennsylvania

J. Geophys. Res. 78, 3103, 1973

Satellite Studies of Magnetospheric Substorms on August 15, 1968
6. OGO-5 Energetic Electron Observations—
Pitch-Angle Distributions in the Nighttime Magnetosphere

H. I. West, Jr., R. M. Buck, and J. R. Walton

Lawrence Livermore Laboratory, University of California
Livermore, California

J. Geophys. Res. 78, 3093, 1973

Resumé of Results

Initially, the perigee of OGO-5 was 291 km and apogee was ~24 R_E. The orbit inclination was 31 deg at launch (March 1968), increasing slowly to 54 deg in 1971. The orbital period was ~2-1/2 days. The experiment obtained useful data throughout the orbit. During most of 1968 and part of 1969, OGO-5 made many inbound passes during which it stayed close to the geomagnetic equator from about 15 R_E into 4 R_E. This, coupled with the fact that OGO-5 provided about 95 percent data coverage during the mission, meant that we were able to do an extraordinarily good job of acquiring data in the equatorial regions of the magnetosphere.

During most of the time that the pitch-angle scan mechanism was in operation, our experiment scanned so as to look out perpendicular to the earth's radius (the choice was dictated by the operational makeup of the spacecraft). Consequently, our angular coverage in much of the magnetosphere varied from 90 deg to the dip angle of the local magnetic field. Equatorial coverage thus meant complete pitch-angle coverage and, of course, equatorial pitch-angle measurements also meant a complete knowledge of what was going on along the field lines. Away from the equator, in a dipole-like field, the coverage was largely limited to pitch angles near 90 deg. Near the noon magnetopause, however, the field configuration is close to being circular and here, even at high latitudes (45 deg geomagnetic), good pitch-angle coverage was available. Conversely, in the magnetotail during substorm growth phases, the magnetic field approached the radial direction. During these times, the pitch-angle coverage could be as limited as 90 ± 20 deg. When needed, complementary electron data from the UCLA scintillation counter experiment were available.* As will be seen later, the limited pitch-angle coverage in the magnetotail had its compensations; it was ideal for using the proton east-west effect in the study of the plasma sheet boundary during substorms.

The experimental results are discussed below in terms of the inner belt, the slot and near-by outer belt, pitch-angle results in the outer magnetosphere, plasma sheet boundary during substorms, and solar particles. Some of this work is published or in publication, while the rest is in process of completion.

INNER BELT

Data were studied in the inner belt region for those orbits during which the experiment scanned. The values of $j_\perp$ at discrete L-shell crossings were obtained and were plotted in terms of $j_\perp$ vs λ_d (here, λ_d is the magnetic latitude as determined from the dipole equations $B/B_0 = (1/\cos^6\lambda_d)(4-3\cos^2\lambda_d)^{1/2}$.

Figure 12 shows an example of the ordering of the data. To a good order of approximation,** we and others (e.g., Pfitzer et al., 1966) find that the shape of

*This experiment, conducted by T. Farley and M. Kivelson, consisted of six scintillation counters looking in different directions.

**This is a reasonable approximation well away from the loss cone.

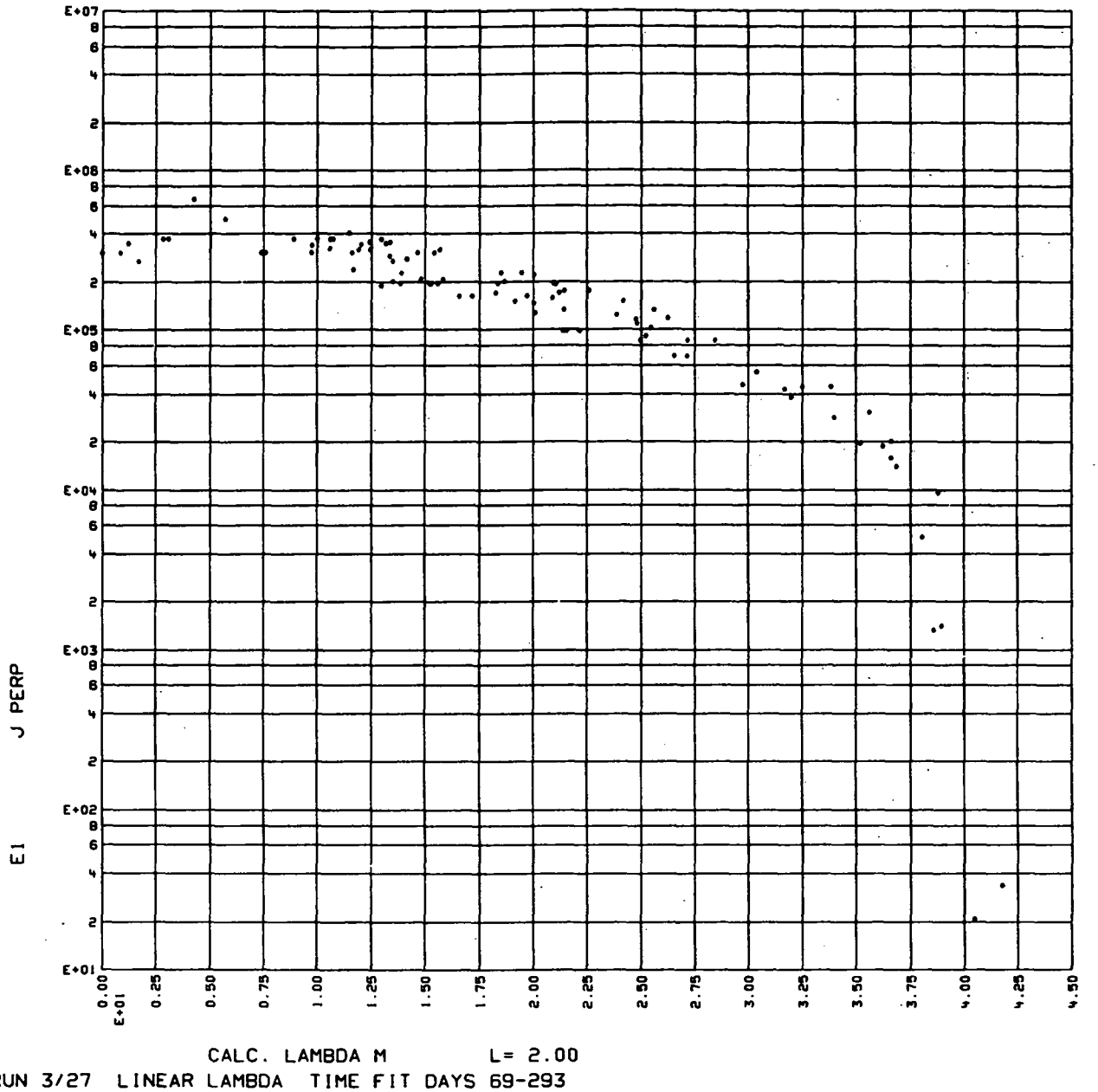

Fig. 12. E_1 $j_\perp$-fluxes for L = 2 in 1968 plotted as a function of λ_d. Note that the λ_d used here is derived from the dipole equation. These low-energy electrons showed little decay during 1968 whereas the higher energies showed appreciable changes (especially E_4 and E_5).

the distribution ($j_\perp$-vs-λ_d being equivalent to $j_\perp$-vs-equatorial-pitch-angle) is independent of energy. This finding has allowed us to order the data in terms of equatorial $j_\perp$ - values.

L-plots of equatorial fluxes for 1968 and early 1969 are shown in Fig. 13. The curves starting at L = 1.3 indicate the flux in early 1968. All energies except E_1 decayed slowly until the large inner-belt injection during the October 31-November 1, 1968, magnetic storms. The poststorm radiation belt rearrangement effects also are indicated in Fig. 13;

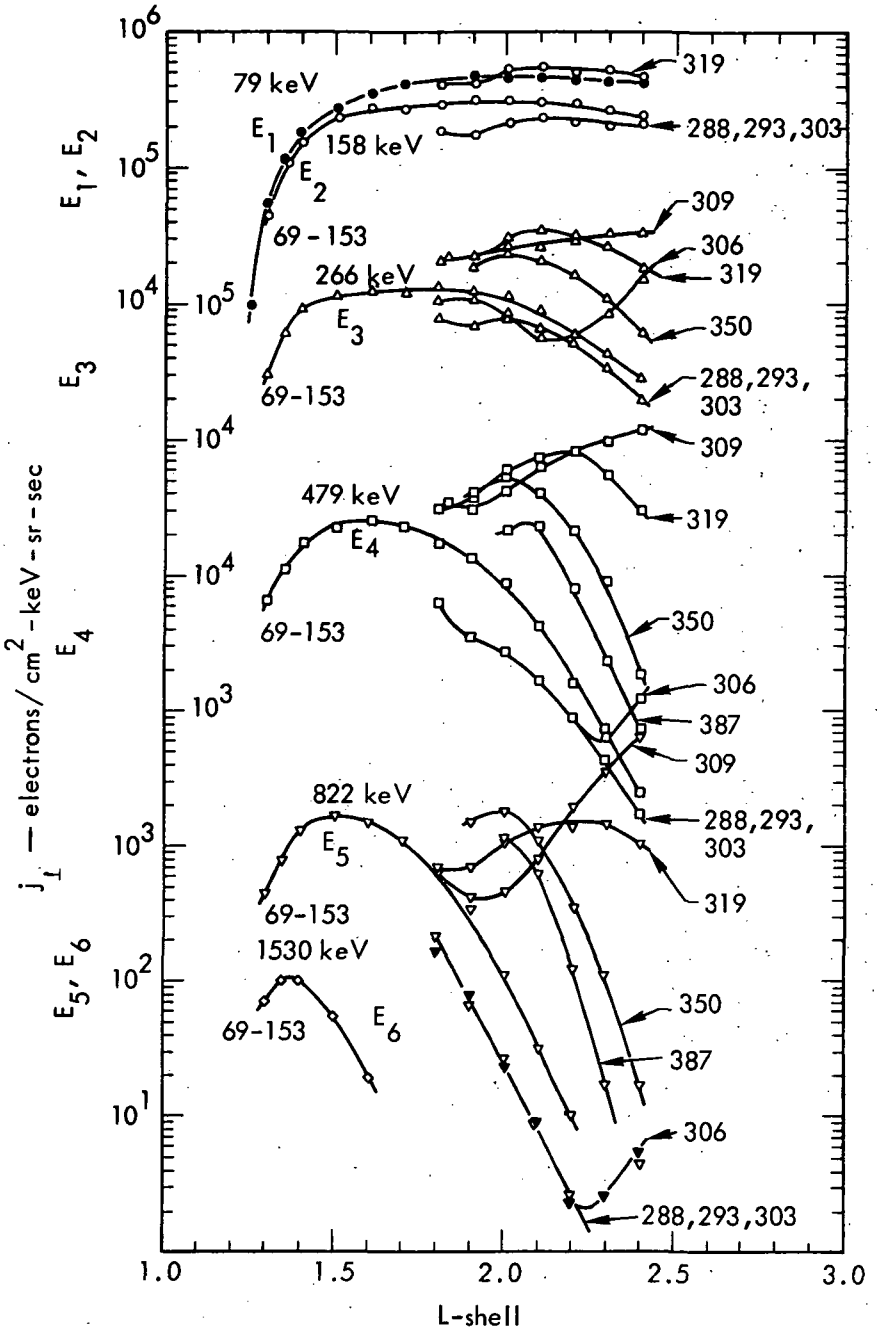

Fig. 13. Equatorial $j_\perp$-values for 1968 plotted as a function of L. Major inner-belt injection occurred on Days 305 and 306. The various curves show the rearrangement effects that occurred following injection.

unfortunately, the perigee crossing was at L = 1.8 on November 1, so that deep inner-belt coverage was not possible.

It is surprising how stable the E_1 fluxes are. They did not rise appreciably during the major injection even though the fluxes of the next higher energy channel (E_2) rose above those in E_1. Conversely, we are fascinated by the relatively rapid changes in E_4 and E_5. We believe the data in E_6 (Fig. 13) to be a Starfish residual. The E_7 fluxes were of comparable

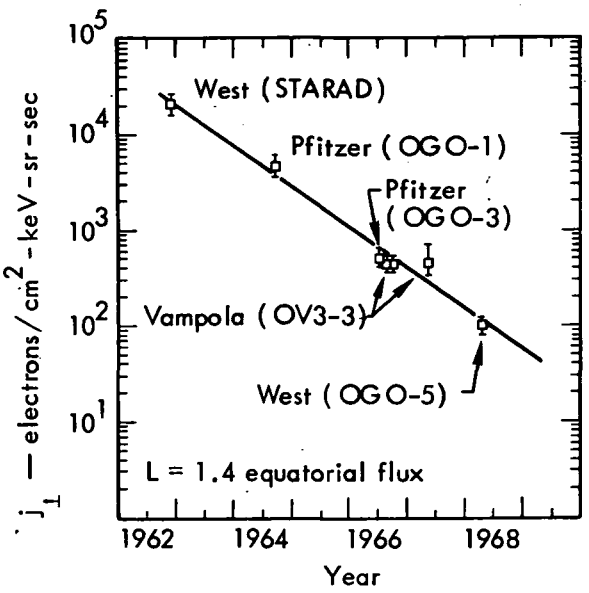

Fig. 14. Long-term decay of 2-MeV electrons at L = 1.4. All data points were determined by magnetic electron spectrometers. The data sources are indicated on the figure.

level but are not plotted in Fig. 13 due to the greater difficulty in extracting these data.

With our 1968 data, we combined earlier data obtained in 1962 by West (1965), in 1964 by Pfitzer (1968) and Pfitzer et al. (1968), and in 1966 and 1967 by Vampola (private communication). An energy of 2 MeV, which seems well above the electron energies involved in the usual inner belt dynamics, is chosen for the L = 1.4 data plotted in Fig. 14. The e-fold decay rate is ~370 days. Starfish electrons are no longer important in radiation belt dynamics.

Electron spectra typical of the mid-latitude regions are shown in Fig. 15 for the period before the major injection event. The data are normalized to point out the spectral hardening as we approach the earth. The spectrum changed greatly as a result of the October-November injection.

SLOT AND NEARBY OUTER BELT

In the inner belt, the pitch-angle distributions are largely independent of energy. In the outer belt, by contrast, we find a marked energy dependence. A good example of data we acquired is presented in Lyons et al. (1972), their Fig. 6; these authors used our data as a point-in-proof of their electron pitch-angle diffusion theory. The pitch-angle data, along

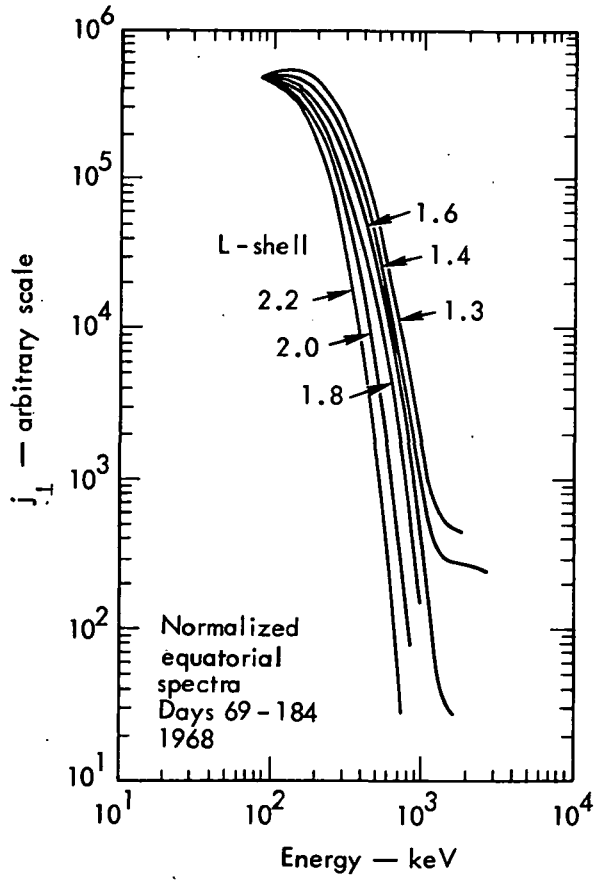

Fig. 15. Typical inner-belt electron spectra in the period March 4 to October 31, 1968. The spectra are normalized to facilitate comparison. Major changes occurred in the spectra following injection on October 31-November 1.

with the theoretical comparisons, are shown in Fig. 16. Other examples are shown in Fig. 17. Salient features of these results are the flat pitch-angle distributions prevailing at the higher energies and the appearance of what may be described as a bell-shaped distribution sitting on a broader flat distribution for the lower energy electrons. At present, it has not been established whether these features are time-independent; possibly some of them evolve during storm time injection and are modified later. The resolution of this point is the subject of further investigation. Unfortunately, the OGO-5 equatorial data coverage in this region is not as complete as we would like.

We have carried out a study of storm-time injection and decay. The data were obtained during a relatively mild storm (peak $D_{ST} = -94\gamma$) on June 11, 1968. Preliminary results were presented by West et al. (1970). Pitch-angle corrections based on studies described in the previous paragraph still need to be made; hence, we still consider the results preliminary.

Plots of $j_\perp$-vs-L provide part of the picture. Figures 18 and 19 show data from Day 158, 1968, obtained three days before the storm. Figure 20 presents storm-time data for Day 163. Figure 21 shows data on Day 176, 13 days after the storm. At this time, the outer belt is believed to have been in diffusive equilibrium.

Taking $j_\perp$ from such plots as Figs. 18 through 21, we have prepared the time plots shown in Figs. 22 and 23 for L = 3.5 and L = 4.5. No pitch-angle corrections have been made; this may account for some of the scatter in the data. Features to be specially noted are

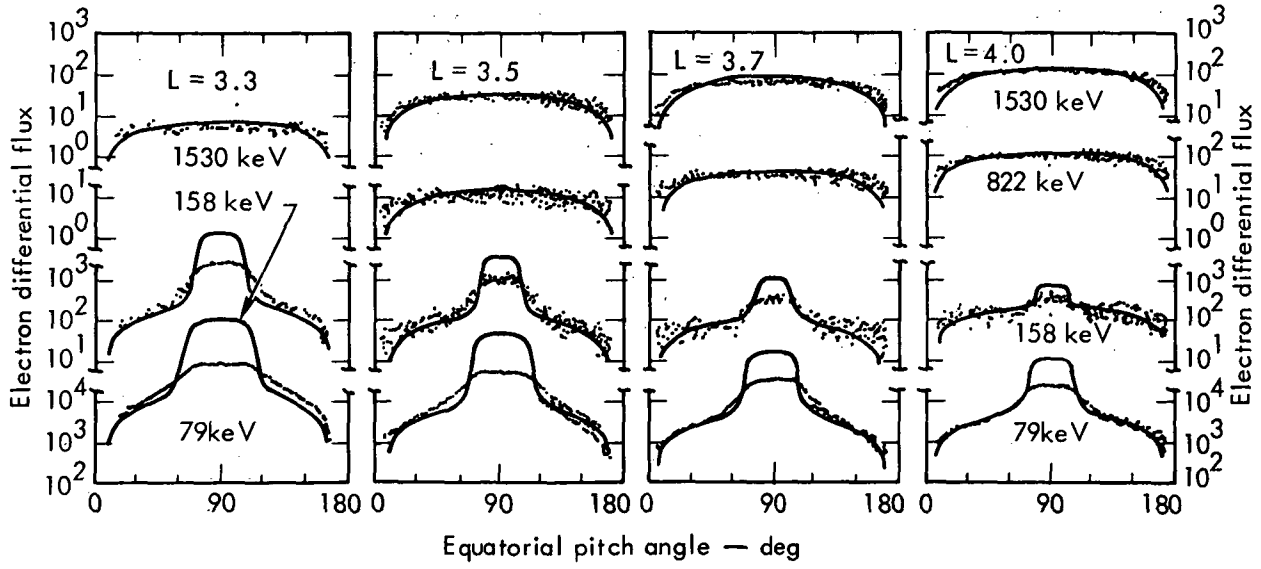

Fig. 16. Electron equatorial pitch-angle distributions obtained April 25, 1968, compared with theory (solid line). [After Lyons et al. (1972)]. Lyons et al. calculate a combination of cyclotron and Landau resonant diffusion driven by the average observed band of plasmaspheric whistler-mode radiation (hiss). There can be no doubt that they have pinpointed the major effects controlling the energetic electron fluxes in this region of space.

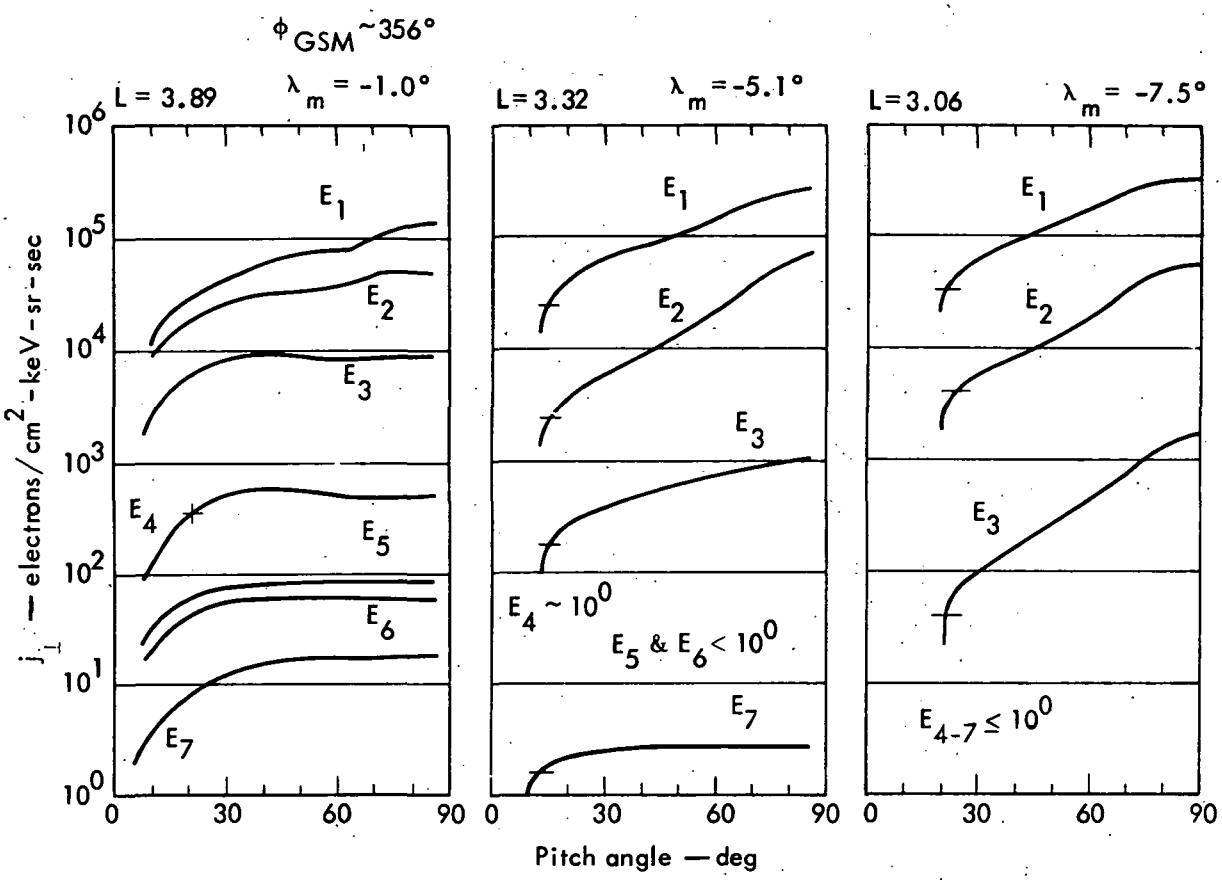

Fig. 17. Electron pitch-angle distributions obtained March 30, 1968. This is another example of slot-region pitch-angle data similar to that shown in Fig. 16. For perspective, note the corresponding radial profile data in Fig. 26.

the drop in the high energy fluxes during storm time and the rise of the low-energy fluxes; the relatively rapid decay of E_2, E_3, and E_4; and the growth of E_5, E_6, and E_7 followed by slow decay. Obviously, the decay rates are energy-dependent. For shells ~3 to 4.5, the lower energy channels E_1 - E_4 have e-fold decay rates of 1.4 to 3 days. The decay rates for E_5 are 3 to 4 days, for E_6 are 6 to 7 days, and for E_7 are 10 to 14 days.

The electron spectrum can change markedly as a function of time. Figures 24 and 25 show the post-recovery diffusion effects for L = 3.5 and L = 4.5. The curves are annotated to show the number of days after the storm. Figure 26 shows the changes in spectrum as a function of L-shell for Day 181. Note the evolution of a marked high-energy peak in the slot region. This is characteristic of the slot at weeks to months after injection.

PITCH-ANGLE DISTRIBUTIONS IN THE OUTER MAGNETOSPHERE

We have had a major preoccupation with these data; accounts of our efforts are to be found in West et al. (1969) and West et al. (1972 a,b,; 1973 a,b). We

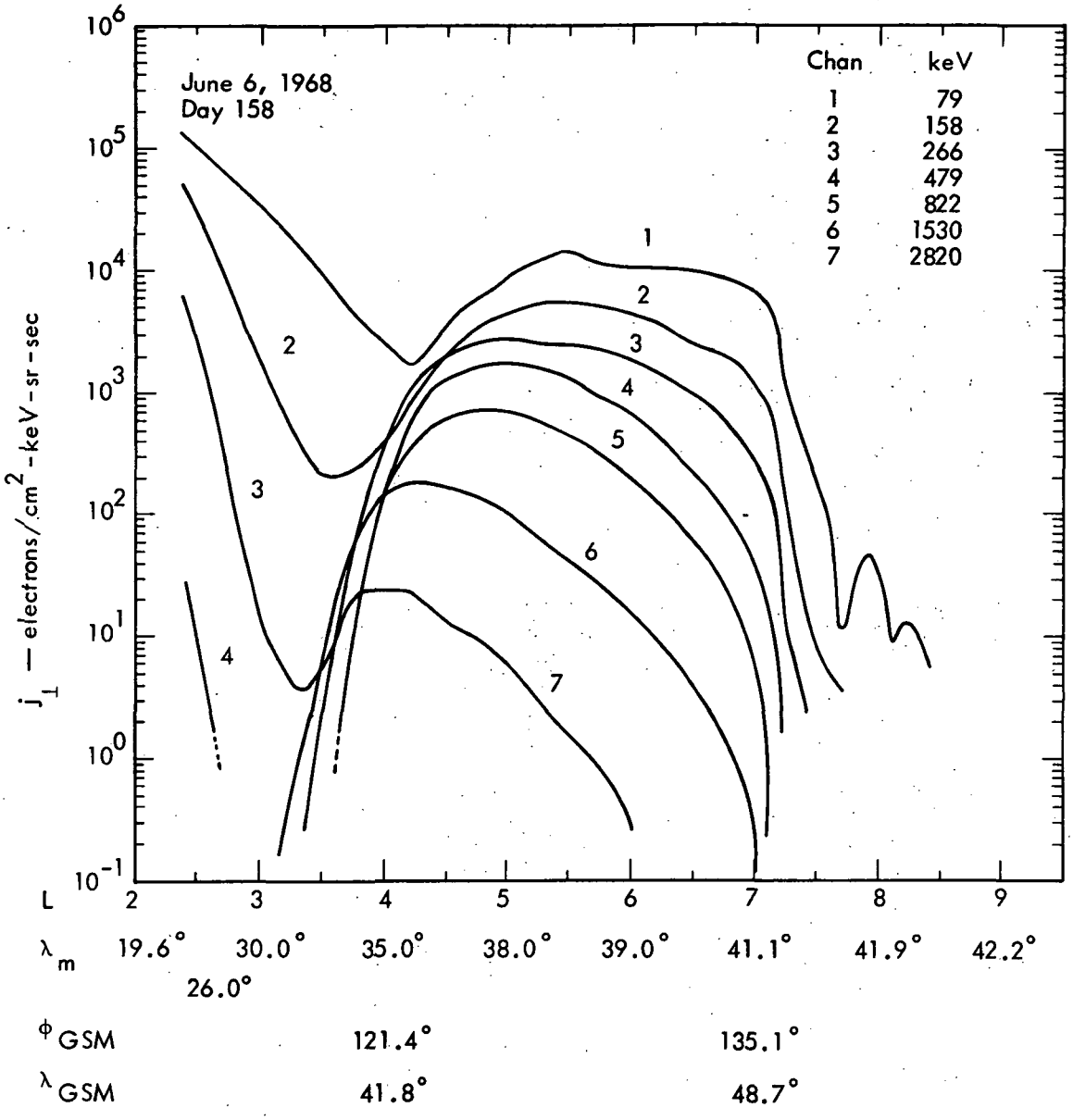

Fig. 18. Outbound radial flux profile on Day 158, 1968. This quiet-time data (also Fig. 19) sets the stage for the changes that occurred during the storm on Day 163, 1968.

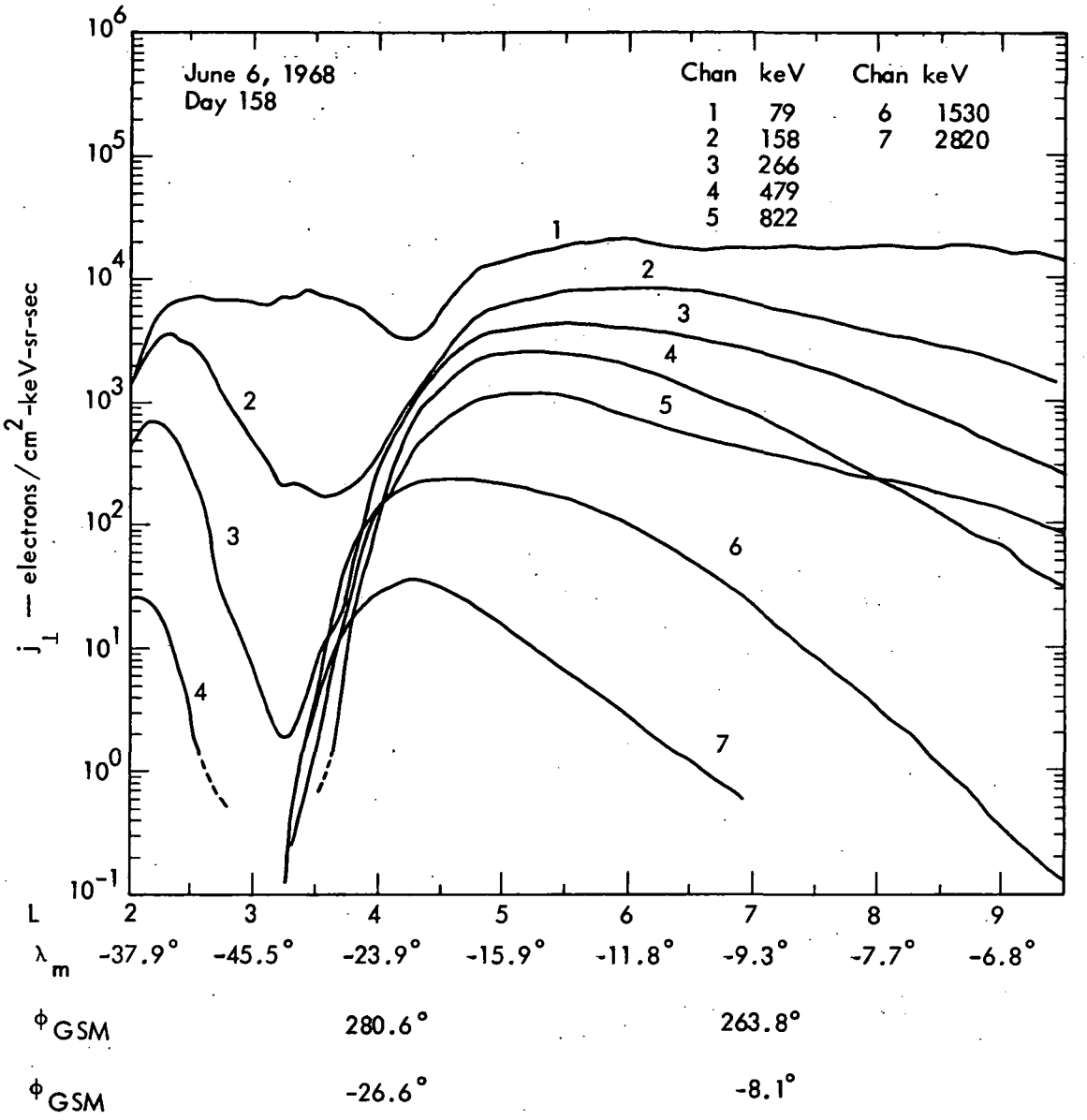

Fig. 19. Inbound radial flux profile on Day 158, 1968.

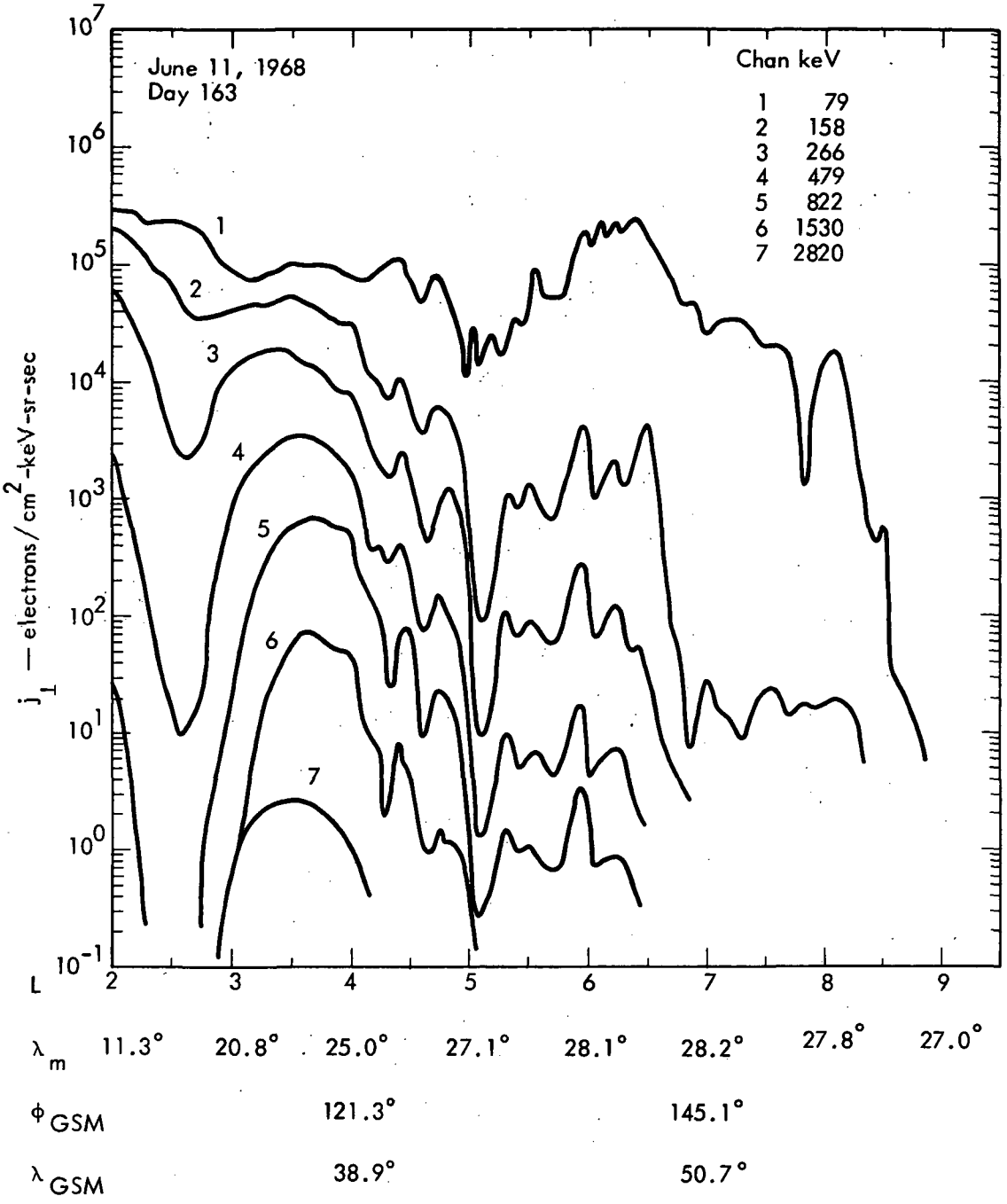

Fig. 20. Outbound radial flux profile on Day 163, 1968.

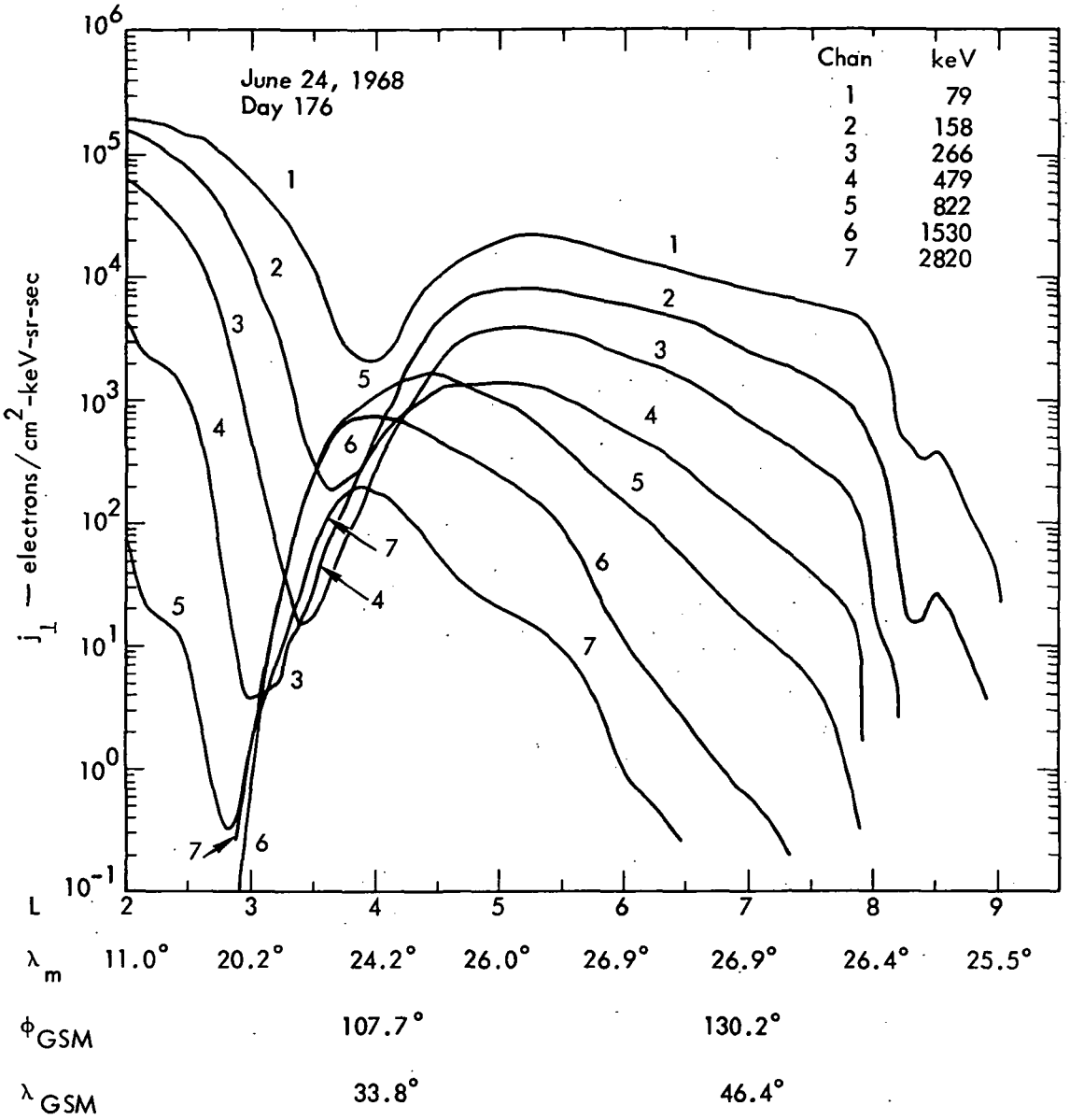

Fig. 21. Outbound radial flux profile on Day 176, 1968. The electrons should be in a state of diffusive equilibrium at this time.

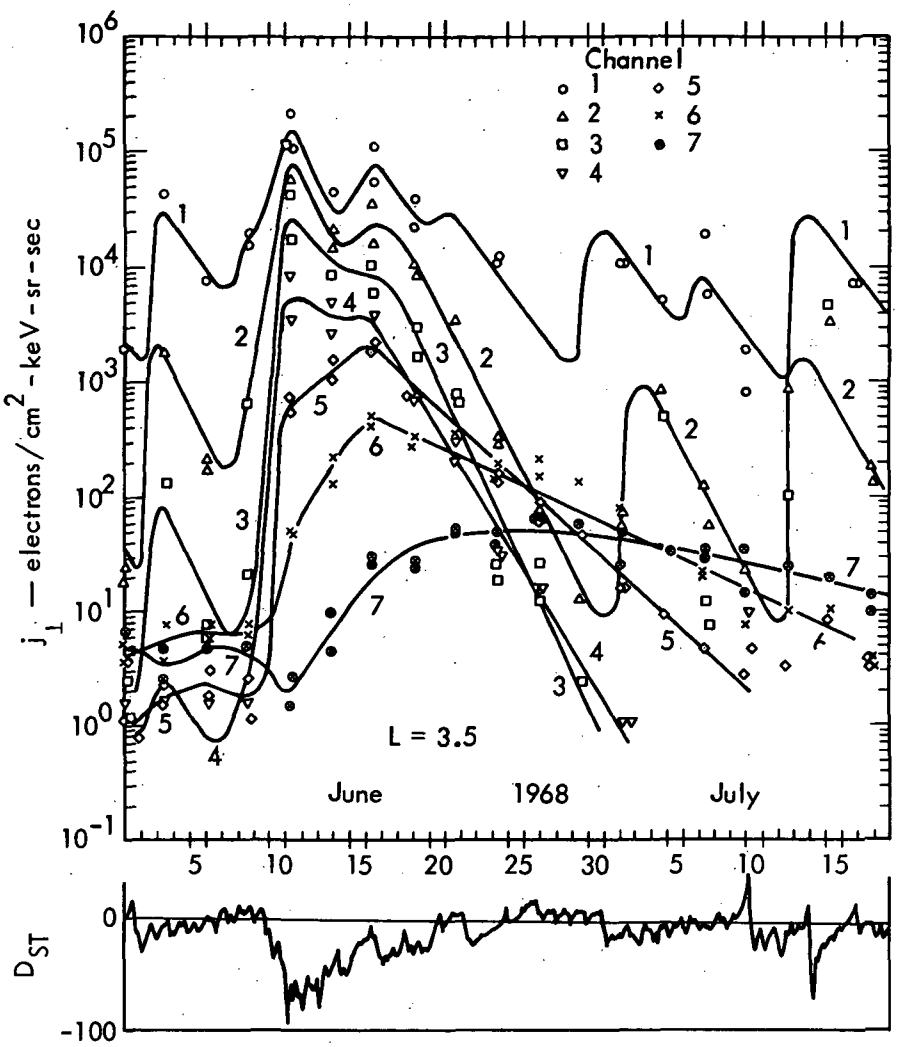

Fig. 22. Time history of $j_\perp$-fluxes on L-shell 3.5 before, during and after the June 11, 1968, magnetic storm (Day 163). These data are preliminary since pitch-angle corrections have not been made.

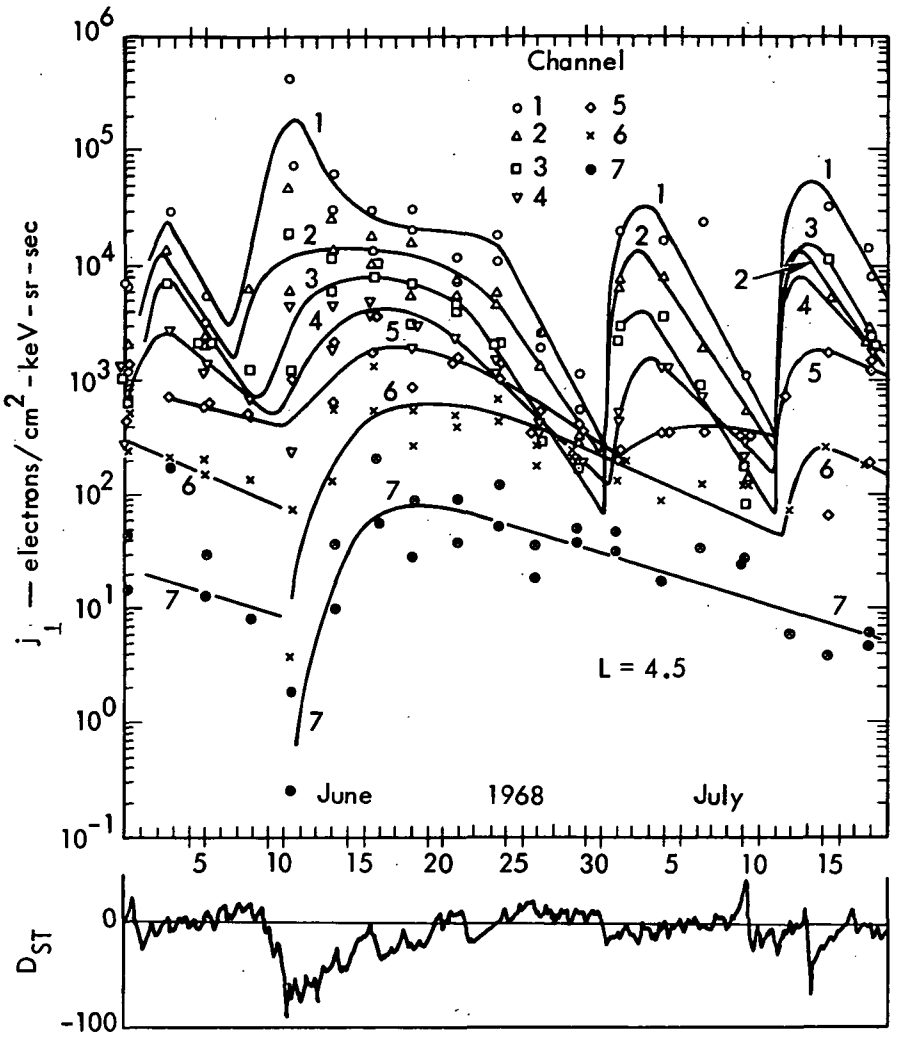

Fig. 23. Time history of the $j_\perp$-fluxes on L-shell 4.5 before, during, and after the June 11, 1968, magnetic storm (Day 163). These data are preliminary since pitch-angle corrections have not been made.

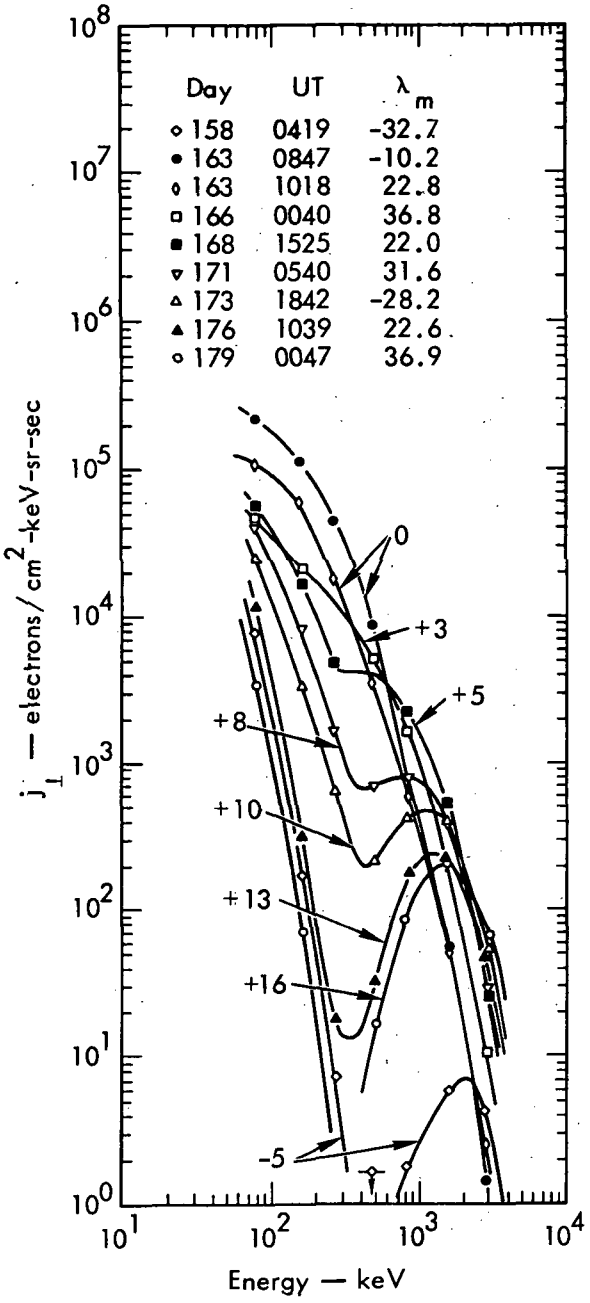

Fig. 24. Changes in spectra at L-shell 3.5 as a function of time after the June 11, 1968, storm. The various spectra are labeled, to show number of days following the storm.

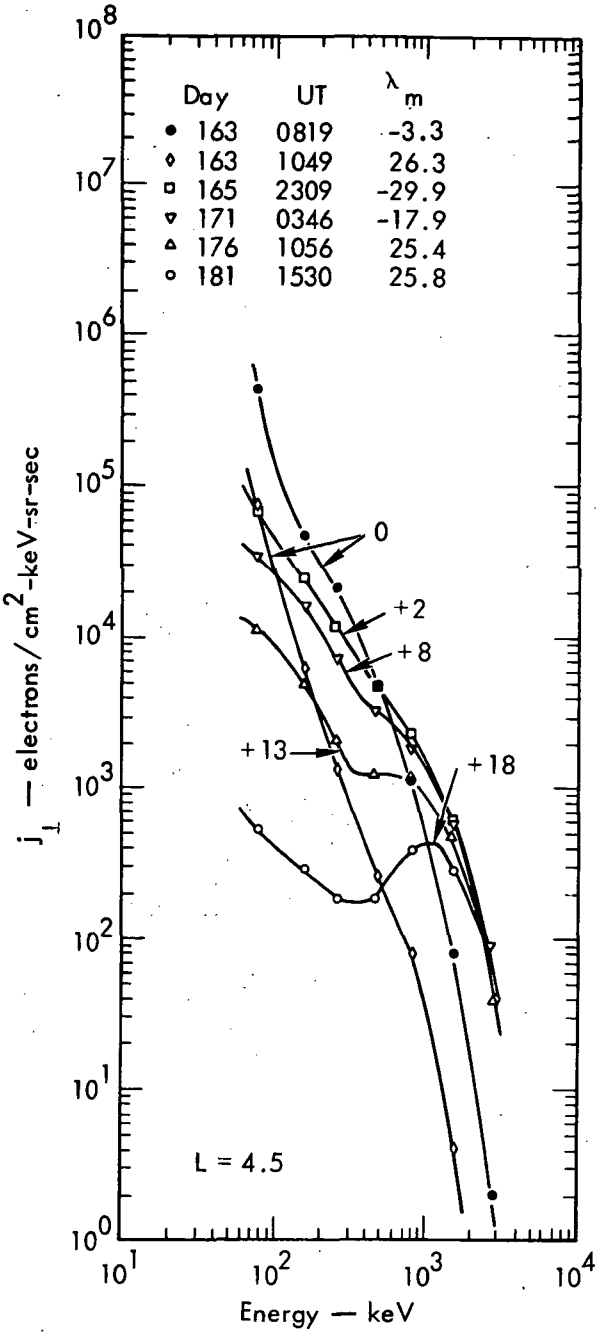

Fig. 25. Changes in spectra at L-shell 4.5 as a function of time after the June 11, 1968, storm. The various spectra are labeled to show number of days following the storm.

have studied the equatorial pitch-angle distributions of electrons at all local times throughout the magnetosphere. As a result, we have acquired an overall view we wish to present. We have also studied the proton pitch-angle distributions. These data are more subjective than the electron results, not as well understood, and, hence, discussed more briefly.

We start in the prenoon magnetosphere. The electron pitch-angle distributions in this region are always normal. (Here we are referring to distributions that are symmetrical and peaked at 90 deg and have a loss cone. They are often shaped like the normal probability distribution and are encountered all the way to the magnetopause.) The radial profile of $j_\perp$-vs-L for March 30, 1968 (Fig. 27) provides perspective for presenting some pitch-angle data. Figures 17, 28, and 29 show the pitch-angle results acquired. These results are quite typical of this region of the magnetosphere.

As electrons drift through the noon magnetosphere at extended distances, changes can occur as a result of drift-shell splitting. Assuming adiabaticity, we find that the equatorially mirroring particles follow contours of constant B. Constant-B contours obtained by Fairfield (1968) for an average magnetosphere are shown in Fig. 30. Conversely, as shown by Roederer (1967, 1969), particles with small equatorial pitch-angles drift so as to keep the length of their bounce path approximately constant, all-the-while maintaining a constant mirror field. If, for example, we examine data at 9 R_E and 0900 local time and contrast them with data at 9 R_E and 1500 local time, we might expect to find changes in electron fluxes having pitch-angles near 90 deg. An effect indeed occurs, as exemplified by the radial profile data in Fig. 31 and the pitch-angle data in Fig. 32. We call these pitch-angle distributions with minima near 90 deg "butterfly" distributions. We consistently find this effect of "magnetopause shadowing" in the equatorial region beyond roughly the constant-B

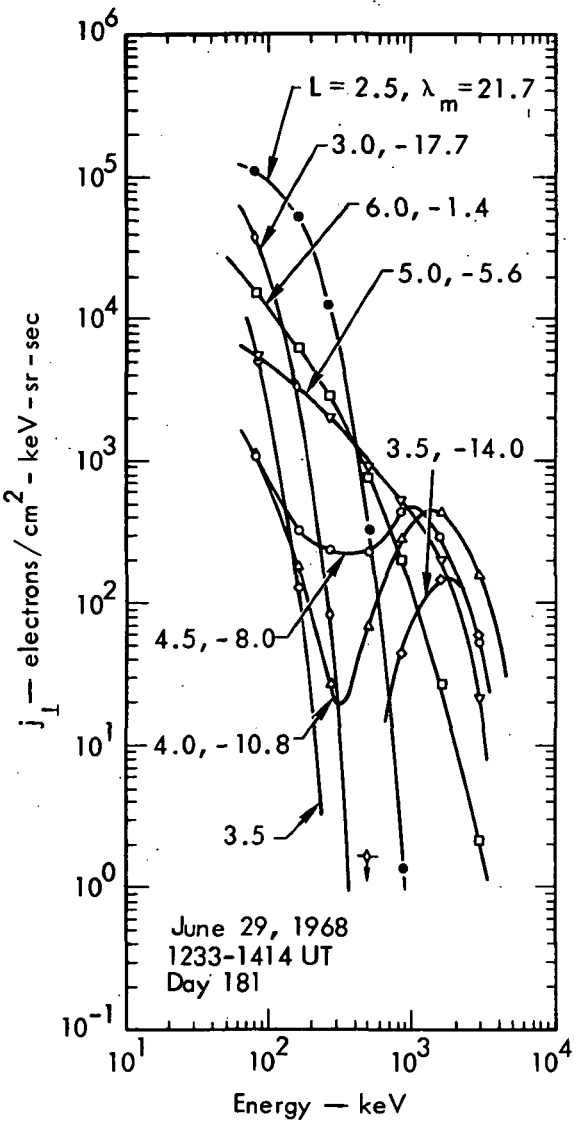

Fig. 26. Changes in spectra as a function of L-shell on June 29, 1968.

contour that maps from noon to about 7 R_E at local midnight (see Fairfield's data in Fig. 30).

Starting near dusk, as we go into the nighttime magnetosphere, another aspect of drift-shell splitting comes into play. The appearance of a tail-like magnetic field further contributes to the generation of the butterfly distribution. This effect, which we call "configuration-change drift-shell splitting," is well known. By contrast, the effect of magnetopause

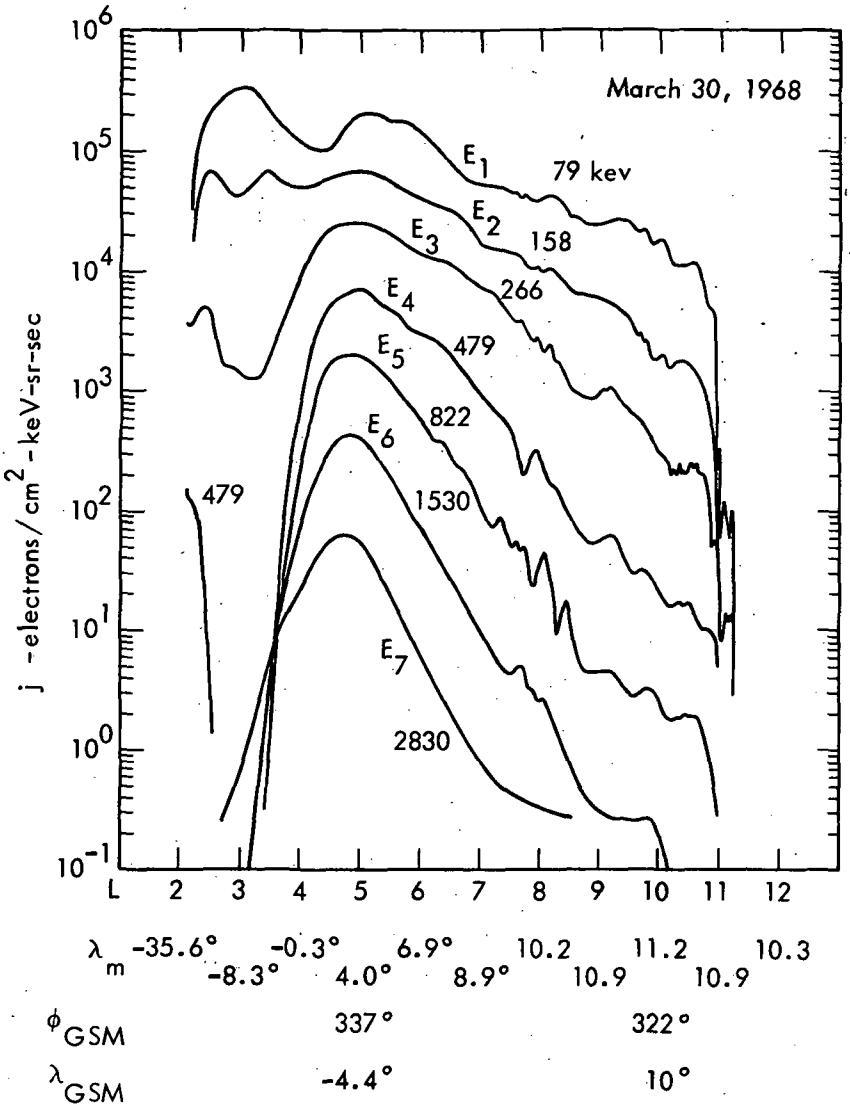

Fig. 27. Radial flux profile on March 30, 1968.

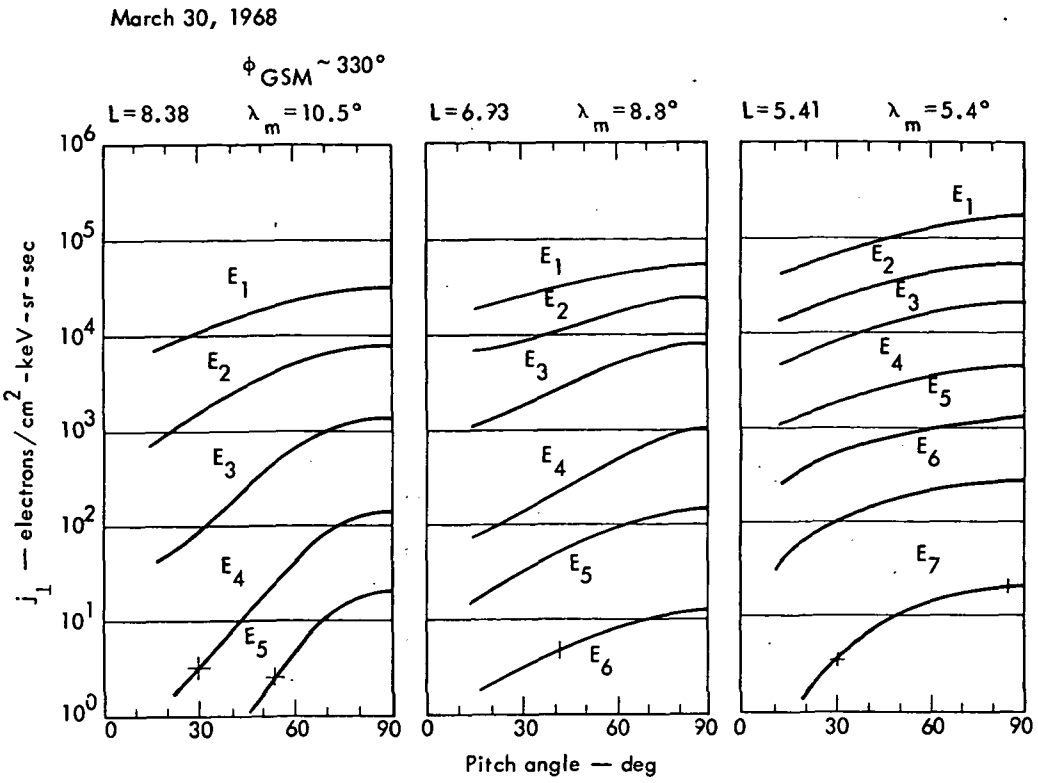

Fig. 28. Typical outer-belt pitch-angle distributions obtained on the morning side of the earth March 30, 1968.

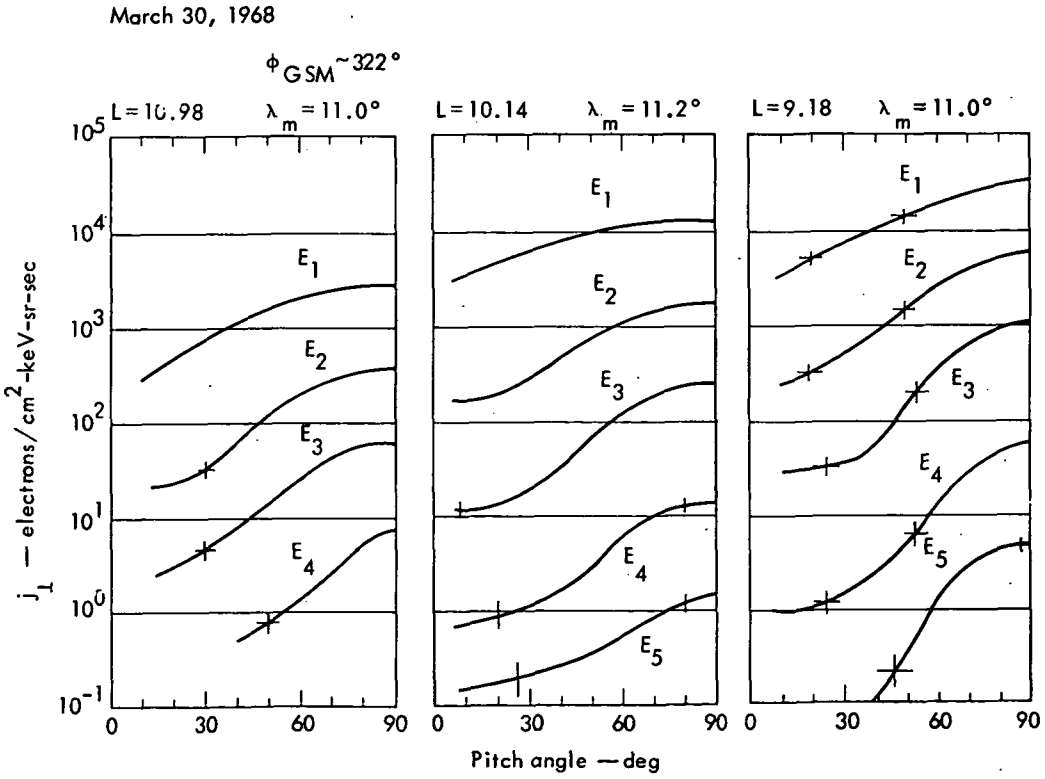

Fig. 29. Typical pitch-angle distributions near the morning magnetopause obtained March 30, 1968.

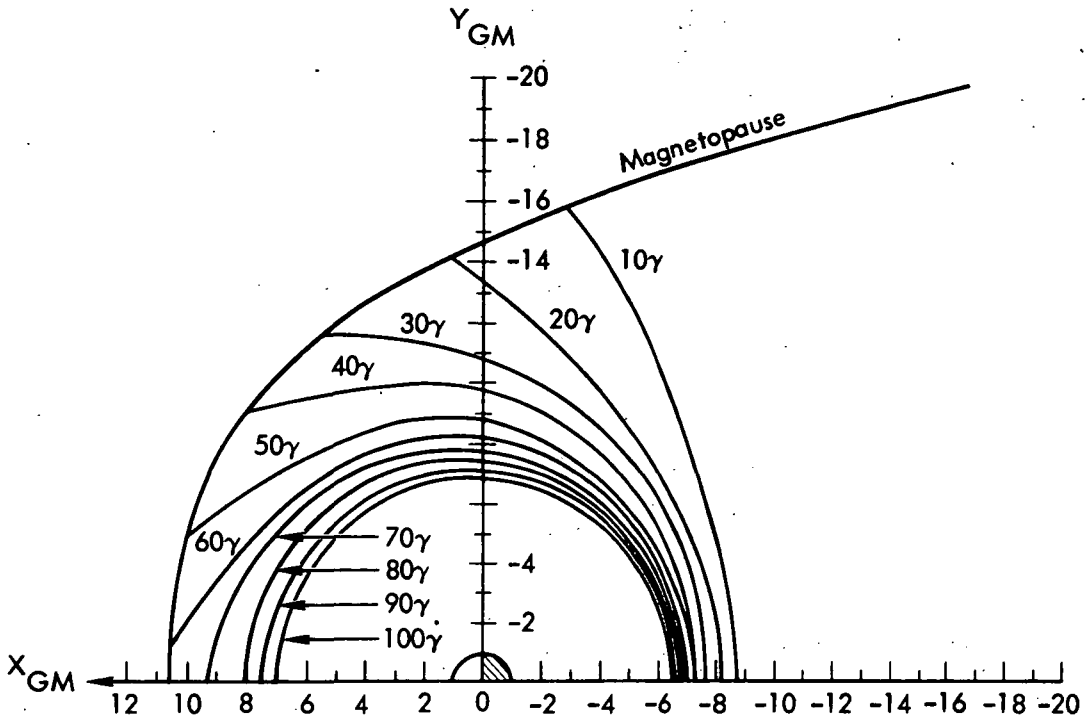

Fig. 30. Contours of constant equatorial-B for an average magnetosphere [after Fairfield (1968)]. Equatorially mirroring particles drift at constant-B as long as the first adiabatic invariant remains conserved.

shadowing is an original discovery of this experiment.

An example of the effects we obtained in a quiet magnetosphere is shown in the radial profiles of Fig. 33 and the corresponding pitch-angle distributions in Fig. 34. Inside ~9 R_E, we attribute most of the butterfly distribution to configuration-change drift-shell splitting; beyond roughly 9 R_E, the results are due to the combined action of both shell-splitting effects. As indicated earlier, we might expect to find the crossover point of these effects more in the range 7 to 8 R_E. Although some other data are more in agreement with this expectation, there seems to be a discrepancy indicating an area of future work. Serlimitsos (1966) and Haskell (1969) have also observed the butterfly distribution deep in the nighttime magnetosphere. They attribute the distribution to configuration-change drift-shell splitting only, overlooking the effect of magnetopause shadowing.

The almost complete dropout in the perpendicular fluxes beyond 9 R_E, as shown in Fig. 33, is quite typical of the premidnight outer magnetosphere during periods of magnetic quiet. During disturbed periods, some disruption of the butterfly distribution occurs. The filling in of the perpendicular fluxes occurs more readily for the lower energies; however, in general, it is electrons, showing the deep dropout in $j_\perp$, which drift into the substorm region. For our purposes, this is ~2300 ± 2 local time. The transition to

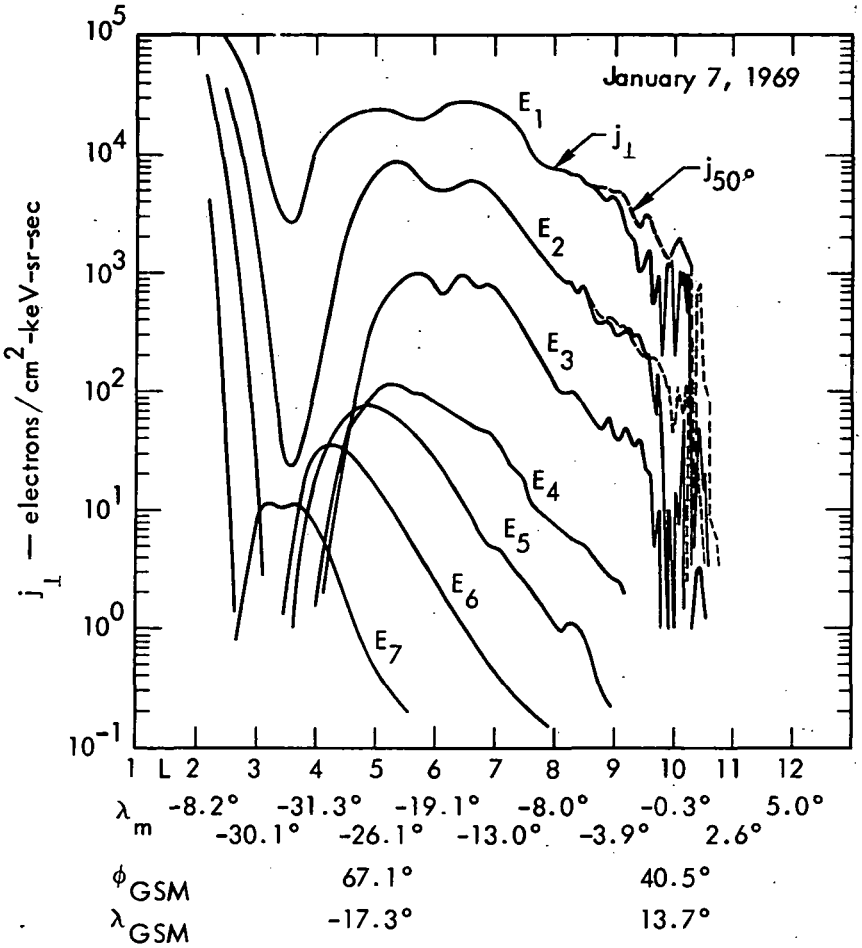

Fig. 31. Radial profile of electrons in the afternoon magnetosphere obtained January 7, 1968. Note beyond 8.5 R_E that $j_\perp$ is no longer the dominate flux in pitch angle. The relatively large fluctuations in $j_\perp$ may be due to the fact that these electrons in their eastward azimuthal drift were closer to the magnetopause than were the peak fluxes (at ~50-deg pitch angles).

a tail-like field in the regions near midnight can mean the demise of the butterfly distribution. We attribute this change to a transition from guiding-center motion of the electrons to one in which they get caught up in the field reversals of the neutral sheet (Speiser, 1965, 1967, 1971). It is expected that the electrons can alternate between these two modes until they either precipitate or drift out of the interaction region. Figures 35 and 36 show data acquired during the famous substorm of 0714 UT, August 15, 1968. (For the pitch-angle data see West et al., 1973; this was part of a nine-paper substorm study.) Prior to the start of the substorm growth phase, the field was close enough to a dipole configuration to maintain the butterfly distribution. As the substorm developed, the higher-energy electrons changed to isotropy, followed by the lower-energy electrons on a time scale of a few

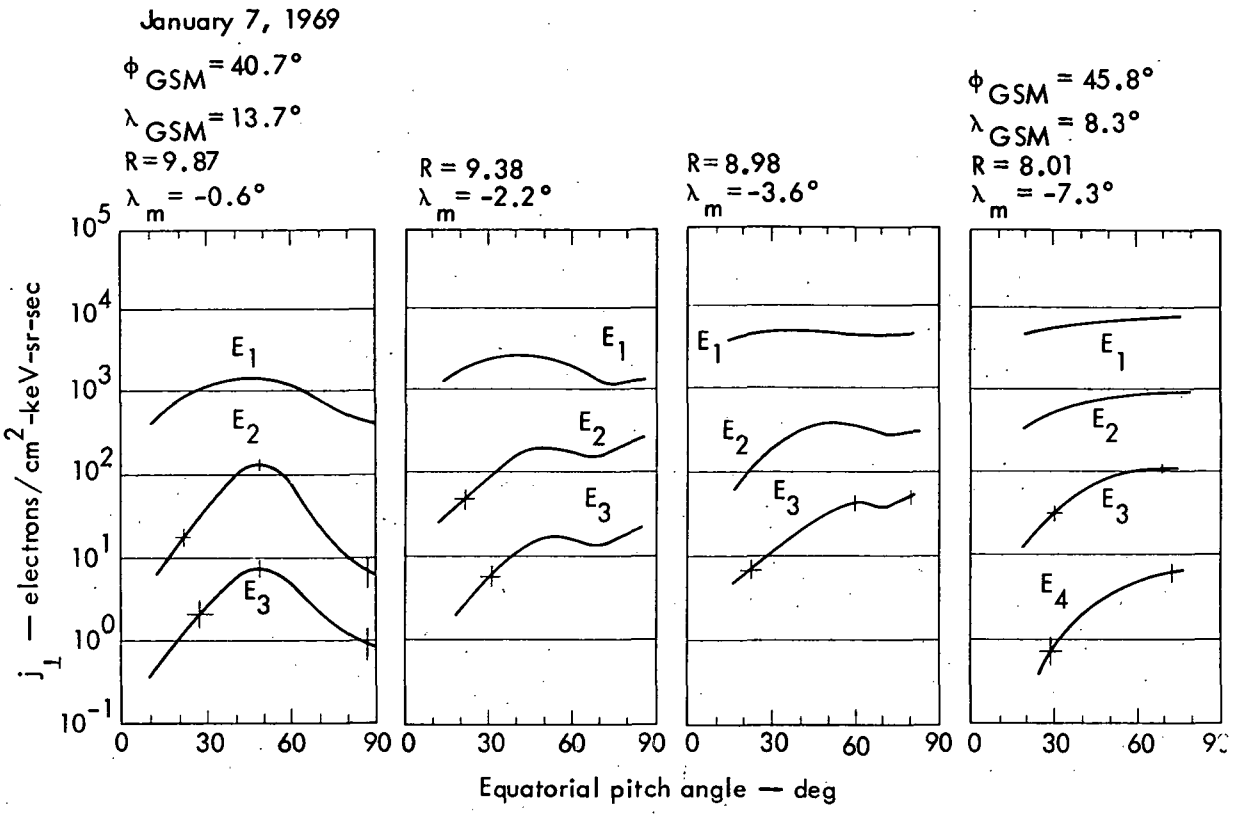

Fig. 32. Pitch-angle distribution of electrons postnoon in the distant magnetosphere January 7, 1968. These pitch-angle distributions were transformed to the magnetic equator under the assumption that the position of the dipole equator is still meaningful this close to the magnetopause.

minutes. Substorm expansion occurred at 0714 UT. With the resulting occurrence of a dipole-like magnetic field, fresh electrons showing the butterfly distribution drifted in from dusk. Magnetic and wave-particle effects disturbed the distributions so that the undisturbed butterfly distribution was not observed until about 0740 UT, which is near the end of the substorm recovery phase.

Another example of substorm effects is shown in Fig. 37. Here we show data obtained near midnight. The data have been plotted to 4.6-sec averages and are shown in time sequence without any selection of angle. The pitch angles of the particles being detected are indicated by the panel marked "scan." Of course, only qualitative pitch-angle information can be obtained from these plots. By virtue of the experiment-satellite orientation, the outer envelope of "scan" is equal to the field inclination and its complement; when the envelope is narrow, we have a tail-like field and when wide, a dipole-like field.

In the bottom four panels we show the UCLA magnetometer data in geocentric solar magnetospheric (GSM) coordinates. Four well-defined substorms occurred on this inbound pass; expansion onsets occurred at 1700, 2012, 2255, and 0108 UT as the field direction began to rotate to a more dipolar direction. The

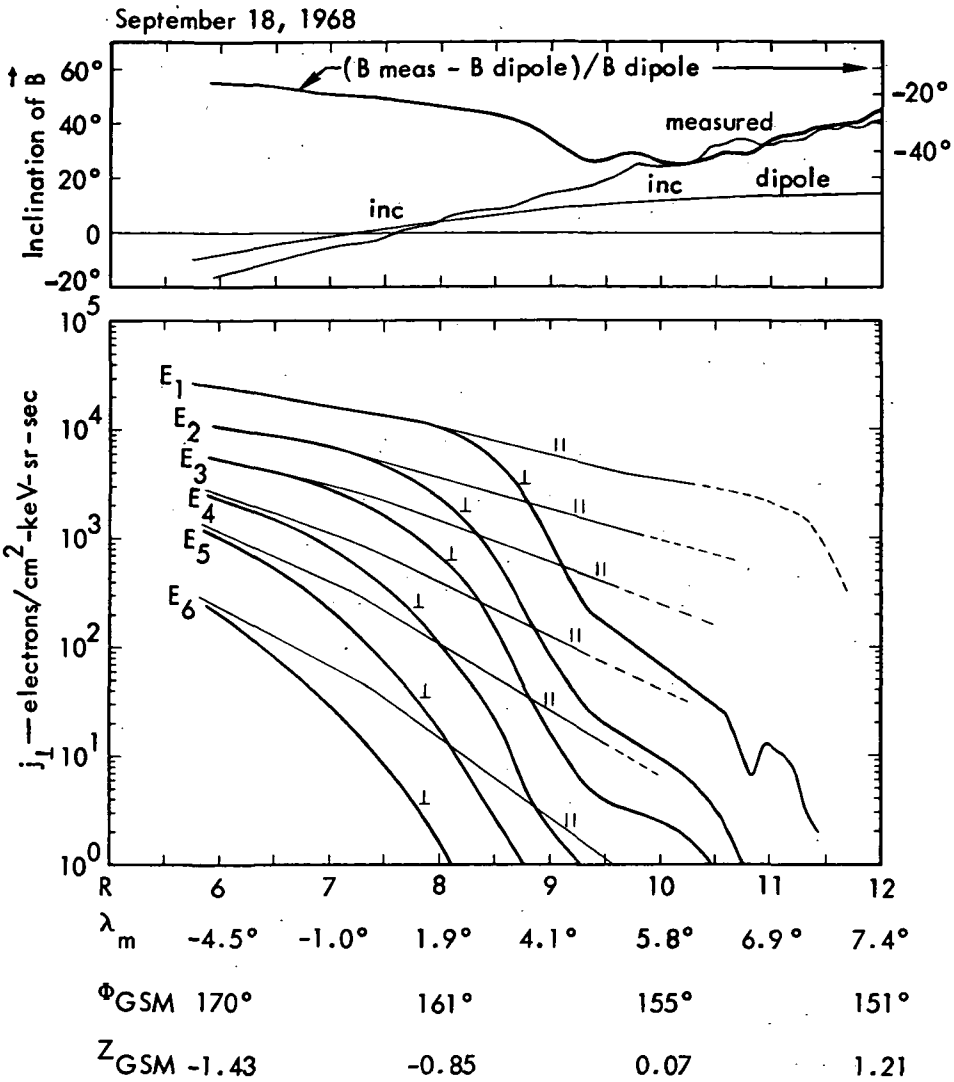

Fig. 33. The radial flux profile for September 18, 1968. The fluxes labeled $j_{||}$ are in reality the peak fluxes in the butterfly distribution at pitch angles of 20 to 40 deg. Beyond about 9.5 R_E, the magnetic field became somewhat tail-like, so the physical constraints placed on the field of view of our spectrometer meant we could not view at much less than 25 deg. The lower energy distributions peaked at higher angles than the higher energies, accounting for the more complete coverage in $j_{||}$ at low energies. The dashed curves indicate some extrapolation in the data. $K_p = 0^+$.

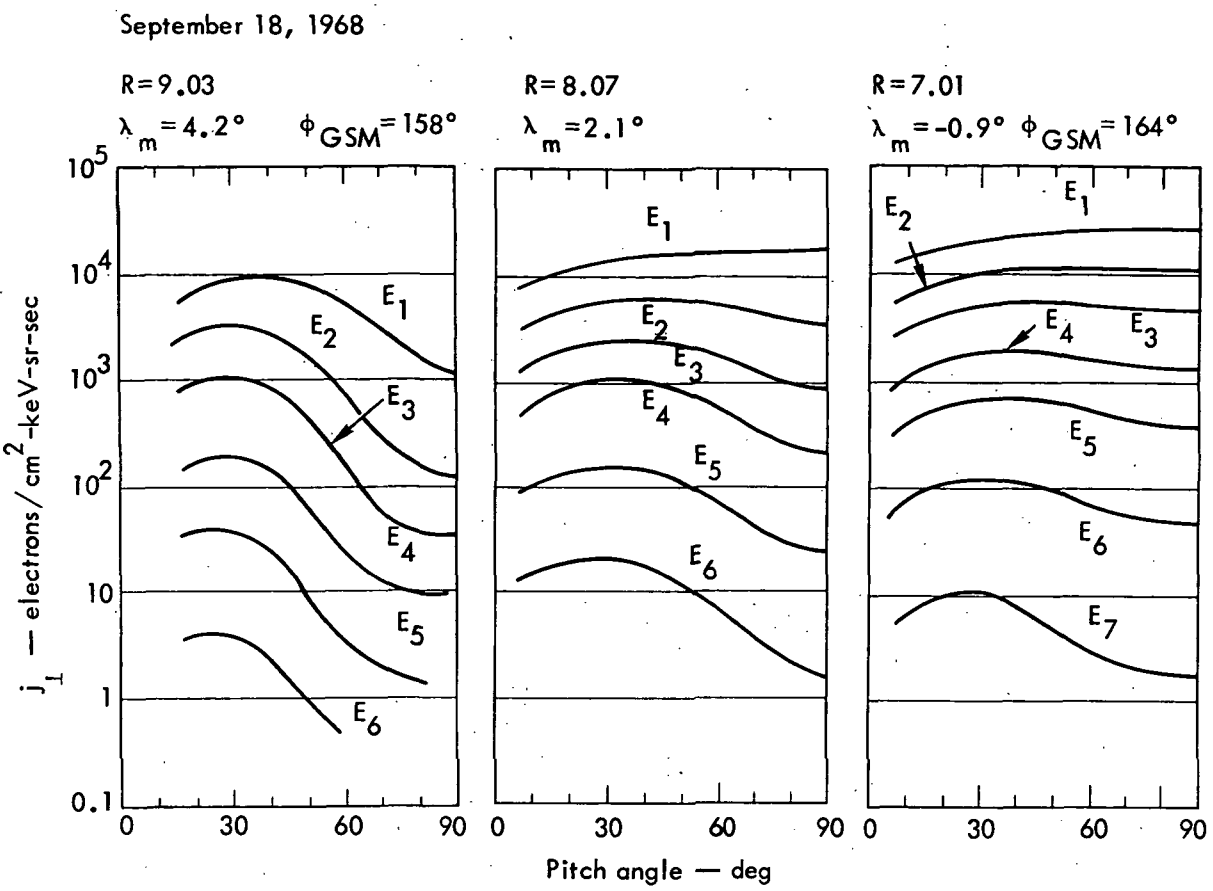

Fig. 34. Pitch-angle distributions obtained just before midnight September 18, 1968. These distributions inside roughly 9 R_E are typical of the entire nighttime sector.

electron pitch-angle effects are made evident by the degree of modulation. Isotropy shows as no modulation except for statistical scatter. When we observe modulation in this region of the magnetosphere, it is always due to the butterfly distribution. Following the 2012 UT substorm, we note the onset of enhanced modulation in E_2 at ~2100 UT and in E_1 at ~2110 UT. A new substorm growth period began as the field started to become more tail-like; at ~2210 UT, we note the abrupt transition from the butterfly distribution to isotropy. Following the onset of expansion of the 0108 UT substorm, we note the emergence of the butterfly distribution in E_2 at ~0124 UT and in E_1 at ~0200 UT. It will be noted that the proton fluxes P_1 also reflect substorm effects. The pitch-angle distributions of the protons are generally isotropic and do not show the reemergence of the butterfly during expansion. The butterfly distribution, however, is usually found in the nighttime magnetosphere at roughly 6 to 9 R_E. Modulation in the proton fluxes in Fig. 37 is to be noted, but, as discussed later, this is due to plasma sheet gradient effects.

Even during a quiet period, electrons cannot drift through the nighttime magnetosphere to dusk without a considerable modification occurring in the butterfly distributions. Figure 38 shows data

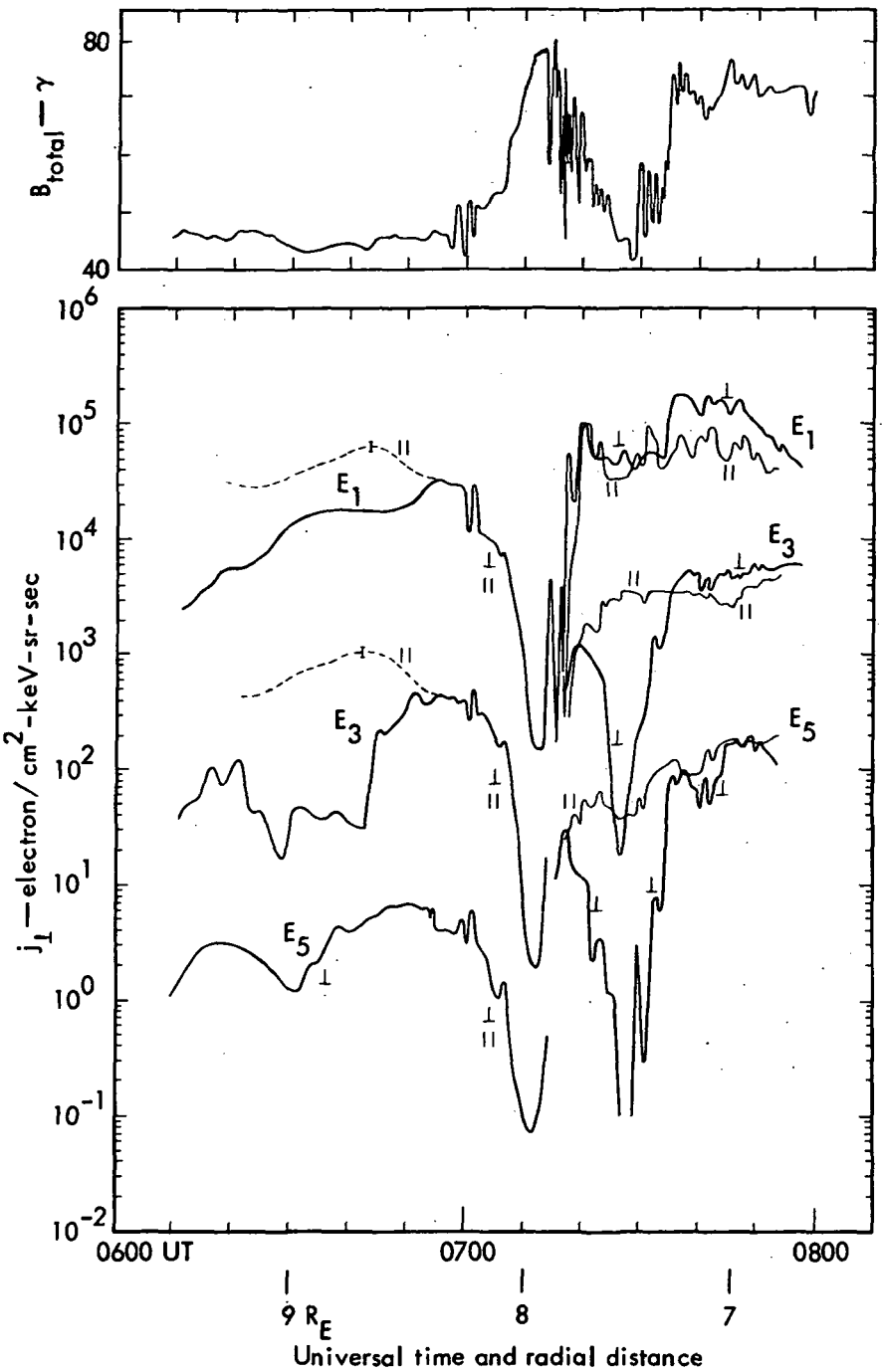

Fig. 35. Perpendicular and parallel electron flux during the 0714 UT substorm on August 15, 1968. The electron energy channels E_1, E_3, and E_5 are centered at 79, 266, and 822 keV, respectively. The $j_\parallel$ shown dotted prior to ~0655 UT was obtained from the UCLA experiment and tacked onto the LLL data. The error bars are an estimate of the uncertainty in this procedure. The flux, $j_\parallel$, is actually the peak flux in the angular range 135 to 150 deg with respect to $\vec{B}$. The total magnetic field in the top panel was obtained from the UCLA magnetometer experiment.

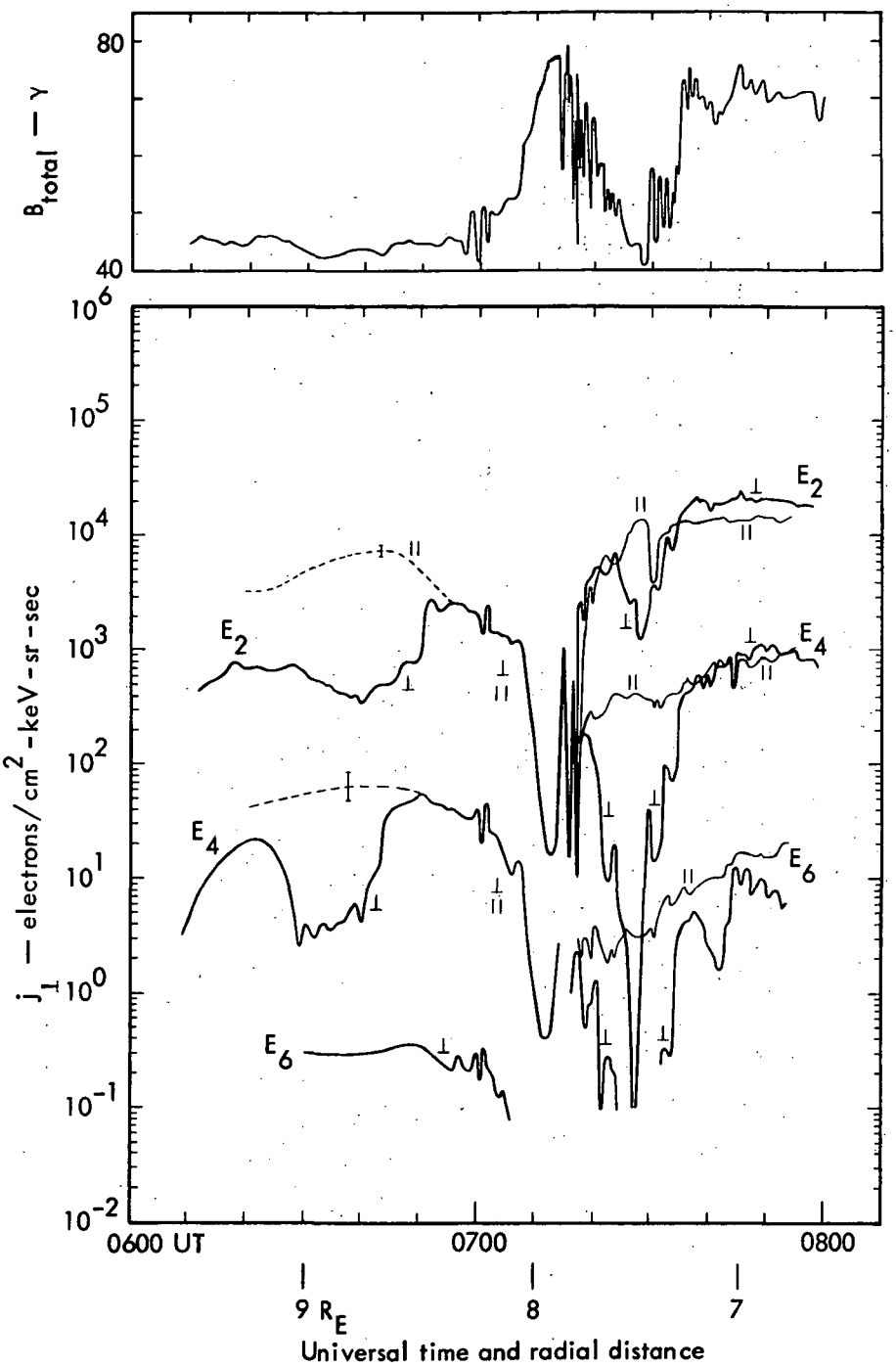

Fig. 36. Perpendicular and parallel electron flux during the 0714 UT substorm on August 15, 1968. This is the same as for Fig. 34 except the electron channels E_2, E_4, and E_6 are 158, 479, and 1530 keV, respectively.

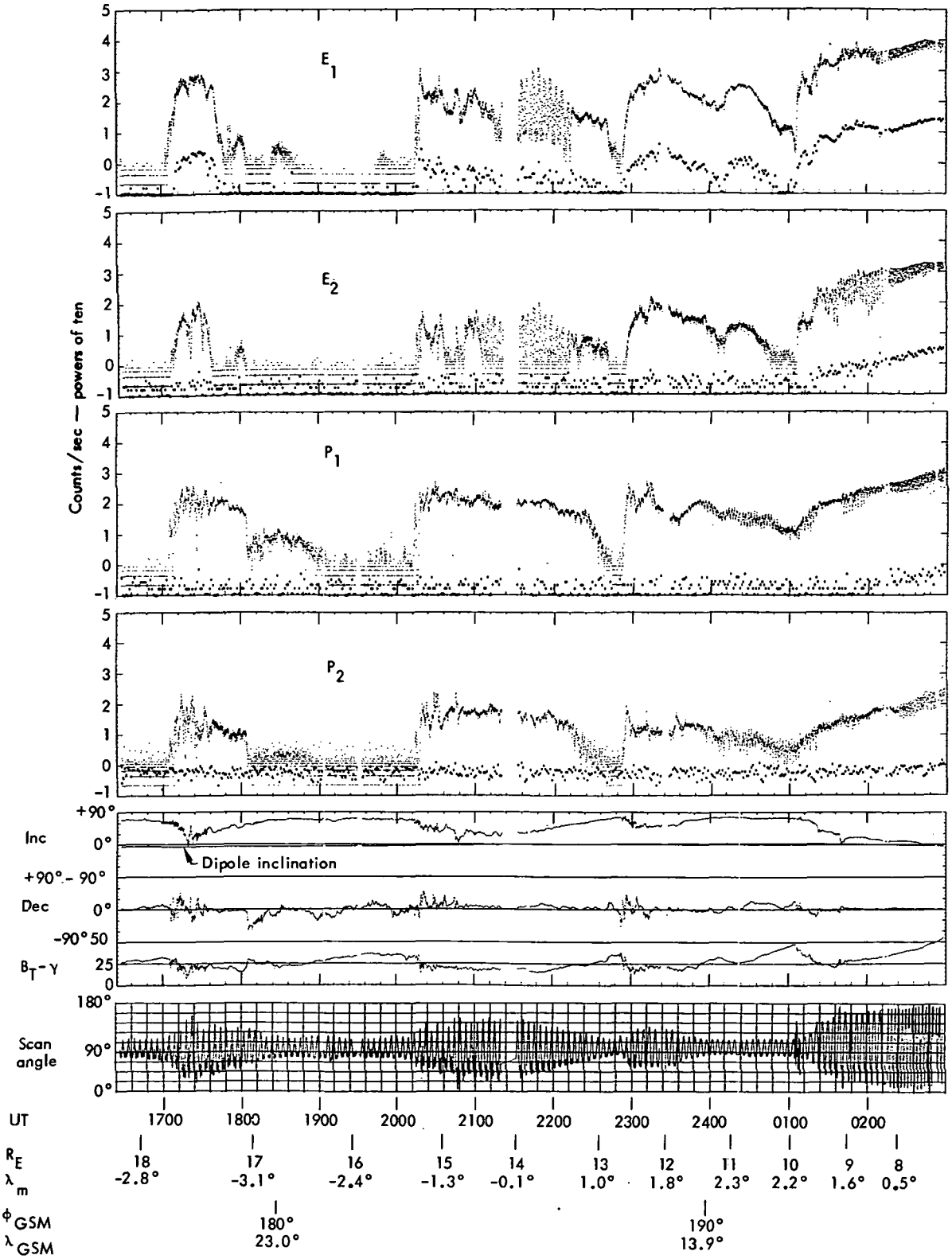

Fig. 37. Scatter plot of data acquired during an inbound pass near midnight August 9, 1968. The small dots show the data at 4.6-sec averages obtained at all pitch angles reached by the experiment scan, whereas the large dots indicate the backgrounds. The panel labeled "scan" shows the range of pitch angles observed by the experiment; the outer envelope is equivalent to the field inclination and its complement. The data show four well-defined substorms.

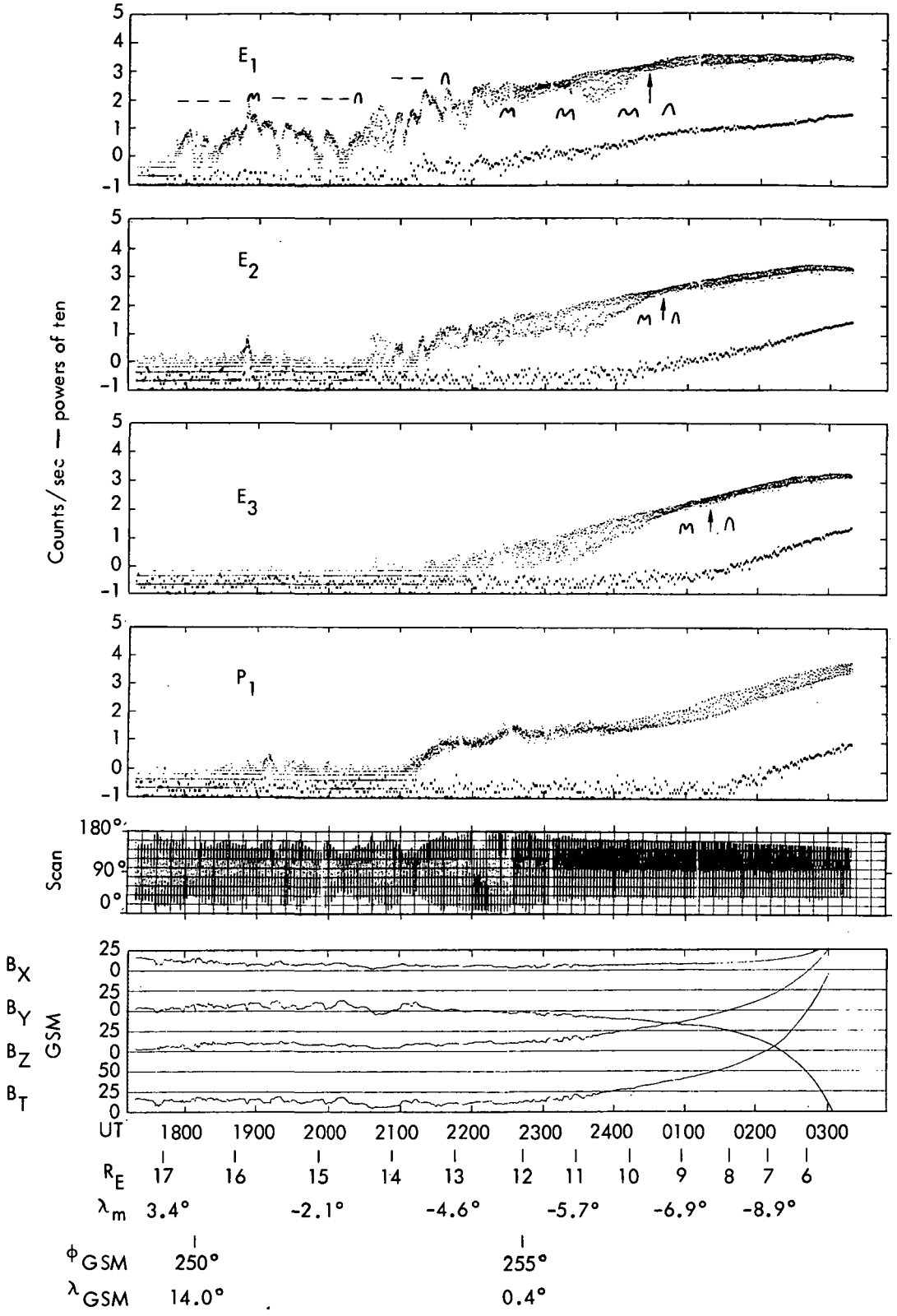

Fig. 38. Scatter plot of data during an early morning inbound pass while in the plasma sheet June 5, 1968. See Fig. 37 for an explanation of the plots. The electron data are annotated to show the character of the pitch-angle distributions evident in the various regions.

acquired in the plasma sheet on an inbound pass at ~0500 local time, during which K_p was 2^-. Figures 39 and 40 show the corresponding pitch-angle distributions. Note that as we approach dawn, the change in the field configuration leads to the demise of the butterfly distribution inside radial distances of about 9 R_E. Beyond this distance, the loss of the butterfly distribution is due to the disruptive influence of tail-like magnetic fields and plasma sheet noise. Figure 41 provides a resumé of the pitch-angle results.

We believe this resumé of our pitch-angle results provides the proper overall view of the effects occurring to the electrons as they drift eastward around the earth. The story is not complete, however. An area of major interest is the noontime magnetopause (noon plus or minus a few hours and plus or minus about 50 deg in magnetic latitude). Here there are questions about the mechanisms that produce the magnetopause shadowing effects we observe from a few hours past noon extending into the nighttime magnetosphere. It may be that the near equatorially-mirroring particles leave the magnetosphere directly at the magnetopause. Or it may be that they are scattered by wave activity near the magnetopause so as either to enhance the fluxes at small pitch angles or cause them to leave the trapping regions. There is the possibility also that the equatorial drift paths for electrons, rather than mapping to the magnetopause near noon, may split north and south through regions of minimum B (that is, through minima in B along the field line which are not at the equator) and then come back together an hour or two past noon. The possibility of this mechanism was suggested by Shabansky (1971) and discussed by Roederer (1969) in his presentation of field models. Roederer pointed out that these high-latitude regions have not been shown to connect topologically to the rest of the magnetosphere; however, we find copious quantities of electrons mirroring in what would appear to be high-latitude minimum-B regions, judging from the experimental results of Sugiura et al. (1971). The population of the regions is associated with a general high-latitude buildup of fluxes near the magnetopause for both electrons and protons. Our guess is that the action of the minimum-B paths

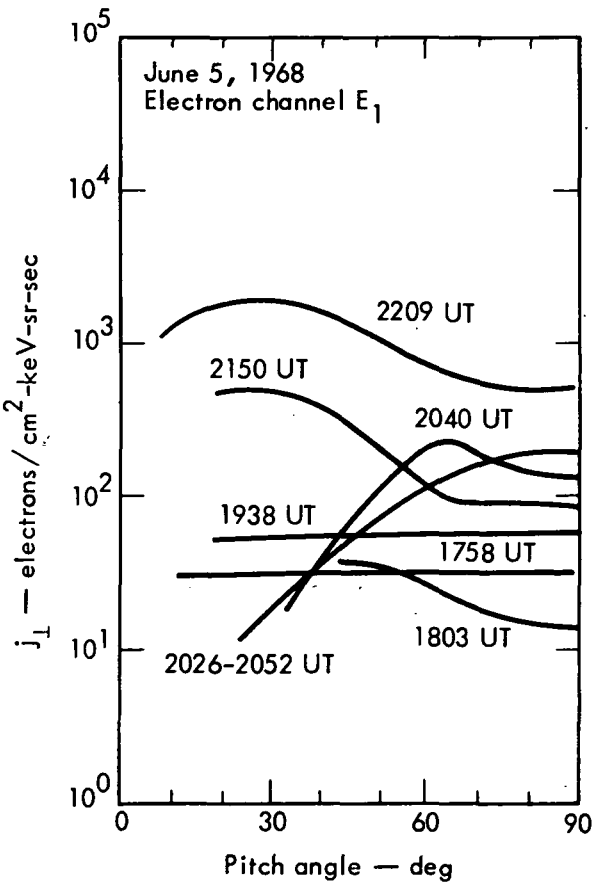

Fig. 39. Pitch-angle distributions for E_1 at various times during the inbound pass June 5, 1968.

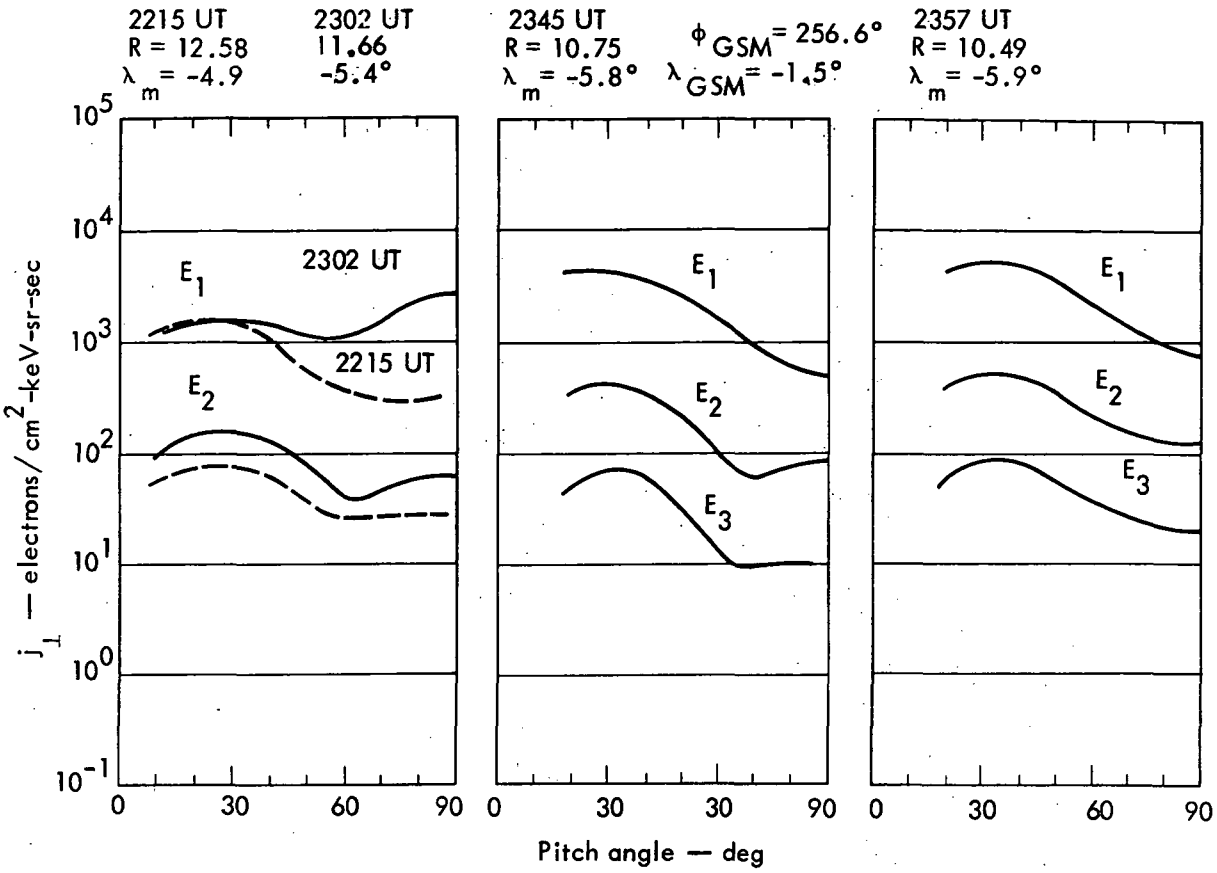

Fig. 40. Pitch-angle distributions for E_1, E_2, and E_3 at various times during the inbound pass June 5, 1968.

is important in determining the particle motions.

Proton data may provide some insight into the problem of azimuthal particle drift by the noon magnetopause. One would expect to find magnetopause shadowing effects in the prenoon magnetosphere. Although these effects are occasionally found and become pronounced at ~0600 LT and earlier (that is, in the nighttime magnetosphere), they do not show in the same convincing way as for electrons. For example, at 9 R_E at 0900 LT, the typical pitch-angle distribution is a narrow "normal" distribution sitting on an isotropic background. We have a very real problem in reconciling the proton data to the clear effects of magnetopause shadowing obtained for the electrons.

PLASMA SHEET BOUNDARY MOTION DURING A SUBSTORM

The plasma sheet boundary motion was was studied in detail during the 0714 UT, August 15, 1968, substorm (Buck et al., 1973). Figure 42 shows the geometry existing at the start of this substorm's growth phase. The experiment scanned looking out perpendicular to the earth's radius vector, looking alternately from west to east. It saw particles whose

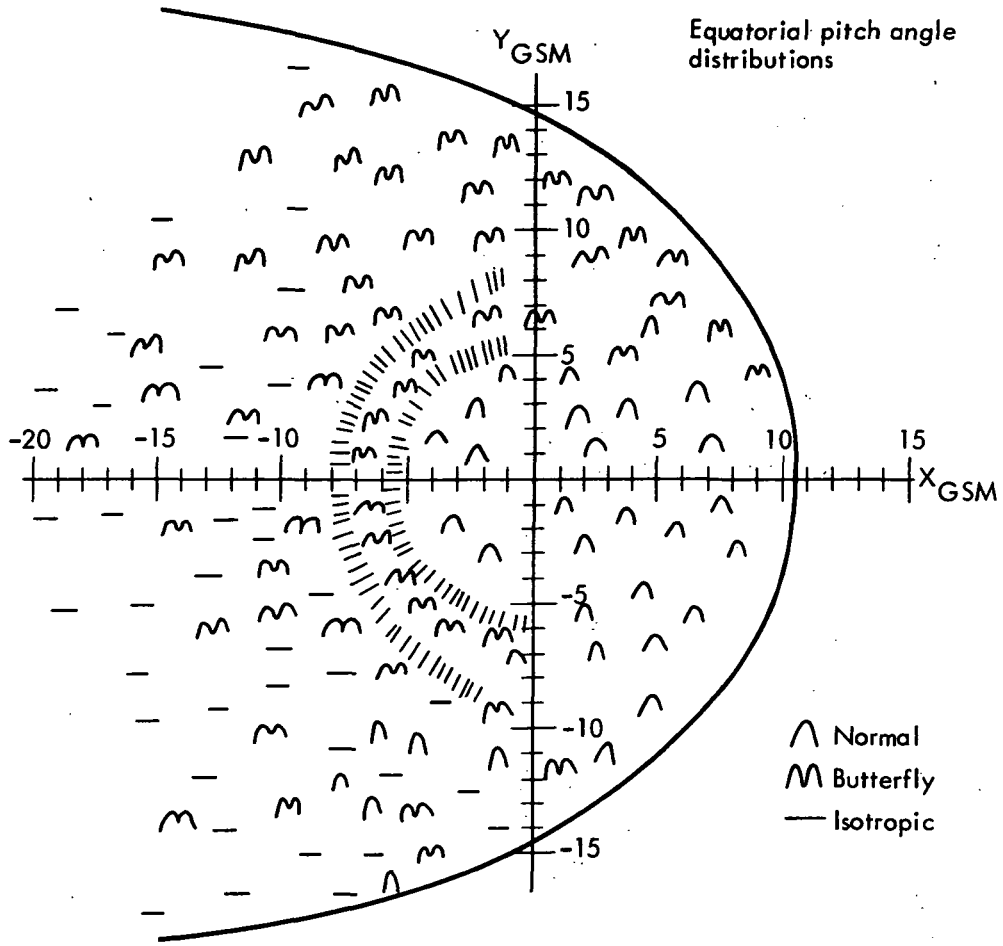

Fig. 41. Survey of equatorial pitch-angle distributions throughout the magnetosphere. In those nighttime regions beyond ~9 R_E where a mixture of distributions prevail, the results are statistical.

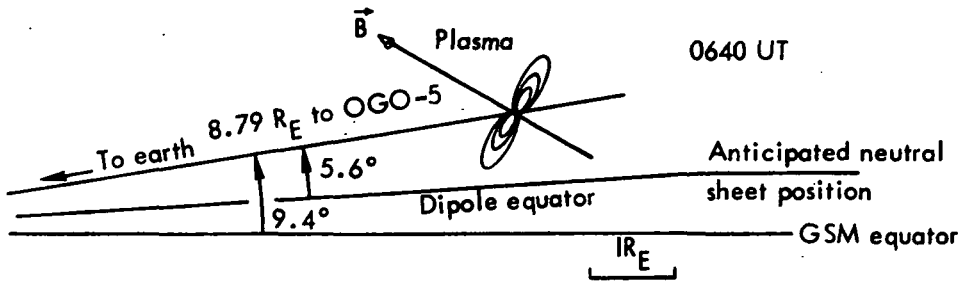

Fig. 42. Scale drawing in the X_{GSM} - Z_{GSM} plane showing the situation at the start of the growth phase of the August 15, 1968, substorm. The magnetic field had almost doubled by the end of the growth phase, so at that time the proton orbits were about half the size shown here.

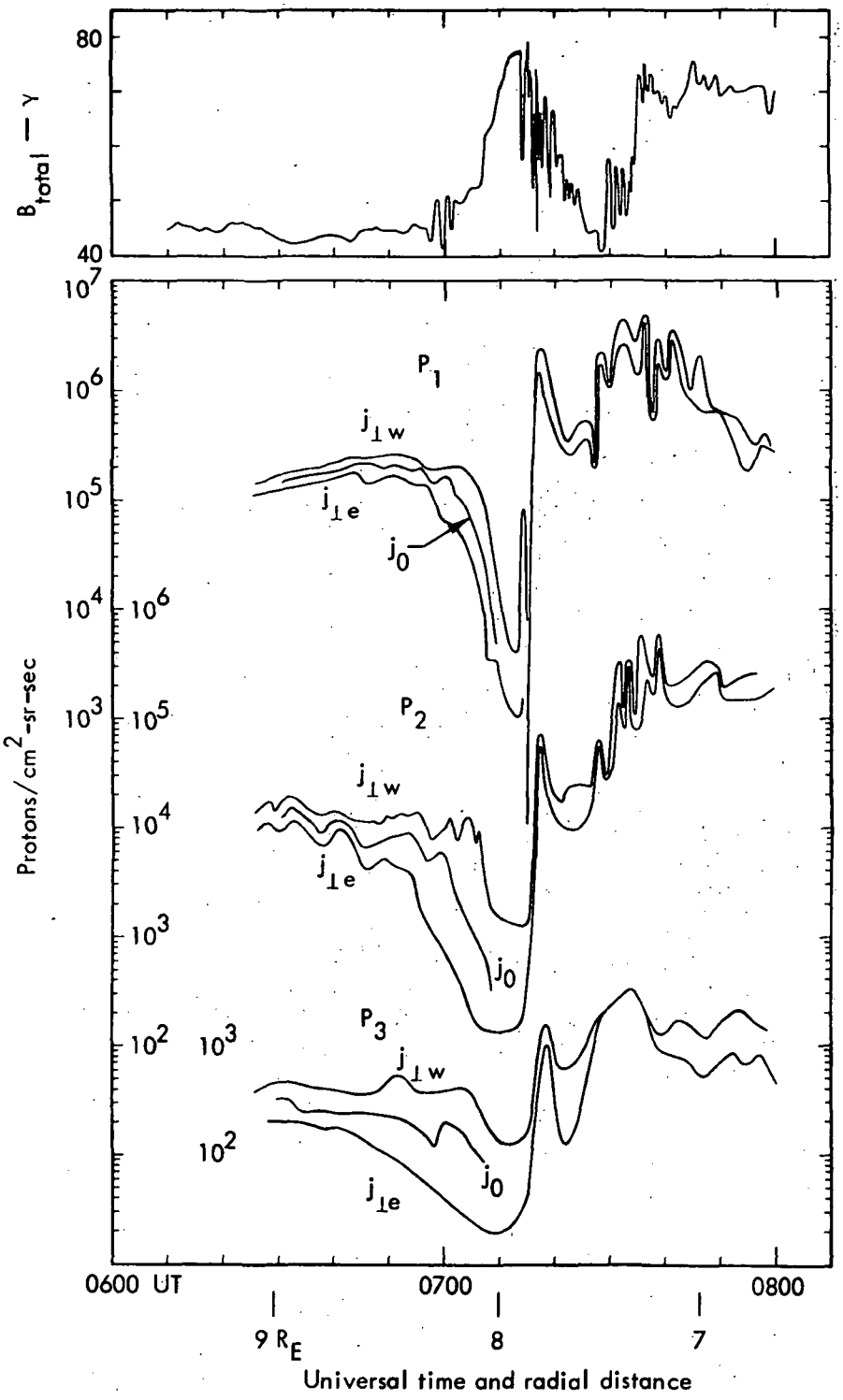

Fig. 43. East and west proton fluxes measured during the 0714 UT August 15, 1968, substorm. The top panel shows the scalar magnetic field variation during the substorm. $j_{\perp e}$ and $j_{\perp w}$ are the peak fluxes (average energies P_1 = 0.12 MeV, P_2 = 0.33 MeV, and P_3 = 0.81 MeV) measured perpendicular to $\vec{B}$ in the approximate east and west directions. j_0 is the value of the flux at the radial position of OGO-5 at pitch angles of about 110 deg.

gyro centers varied in position from above the spacecraft to below the spacecraft. The complete scan took about 1 min; hence, every minute or so we were able to generate a flux gradient by assigning the measured fluxes to their average position of motion. For perspective we show, in Fig. 43, a radial profile of fluxes measured below the spacecraft ($j_{\perp w}$), at the spacecraft (j_0), and above the spacecraft ($j_{\perp e}$). The flux gradient history is shown in Fig. 44. The e-fold boundary lengths and boundary velocities are given in Figs. 45 and 46, respectively. These data indicate that, in the region of the midnight cusp where these data were taken, the plasma sheet virtually collapsed just prior to substorm expansion. This observation has led to the suggestion by McPherron et al. (1973) that reconnection near the midnight cusp may be the causitive factor in the initiation of the substorm's expansive or explosive phase.

We studied boundary motions during several other substorms; a preliminary account was presented by Buck et al. (1972). In these studies, a steepening

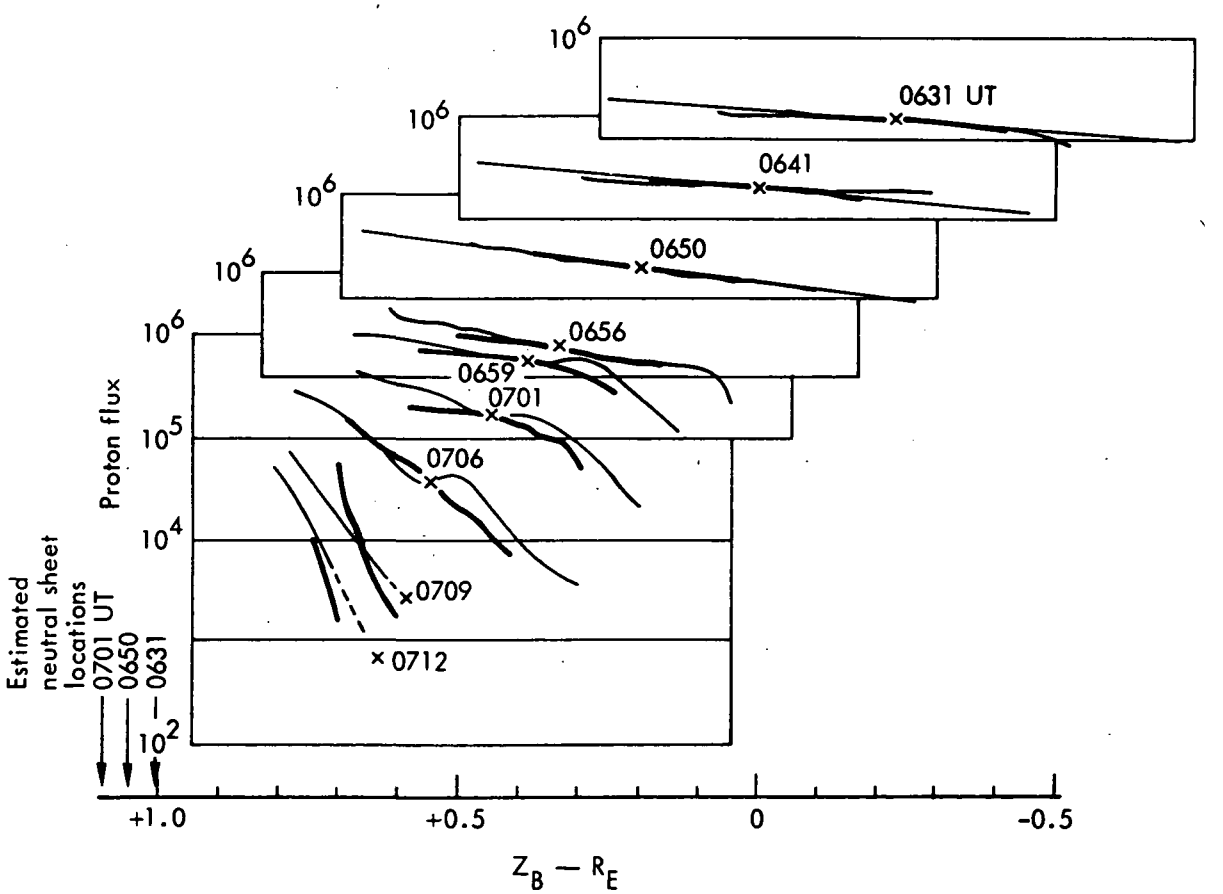

Fig. 44. Proton flux profile evolution during the substorm. Each set of curves is a profile obtained from one full scan of the experiment aperture at the indicated times. The thinning wave at the plasma sheet boundary became apparent about 0656 UT. The anticipated position of the neutral sheet (magnetic equator) is indicated at various times to the left. The data are representative of the flux in P_1 in units of protons/cm^2-sr-sec. The heavy line is P_1; the light lines are P_2 and P_3, the latter being longer. The P_3 data after 0650 UT are deleted from the plots.

and thinning of the boundary always occurred. However, in each case, OGO-5 was too high above the expected position of the neutral sheet to determine the extent of sheet collapse. Also, OGO-5 was deeper in the magnetotail than for the 0714 UT August 15 substorm. These data are not inconsistent, however, with the suggestion that reconnection near the midnight cusp may be the causitive factor in substorm expansion.

THE APRIL 1969 SOLAR PARTICLE EVENT

This interesting event (the largest electron event ever recorded) was due to a flare on April 10, 1969, behind the sun's east limb. Figure 47 shows the time history of the electrons as observed on

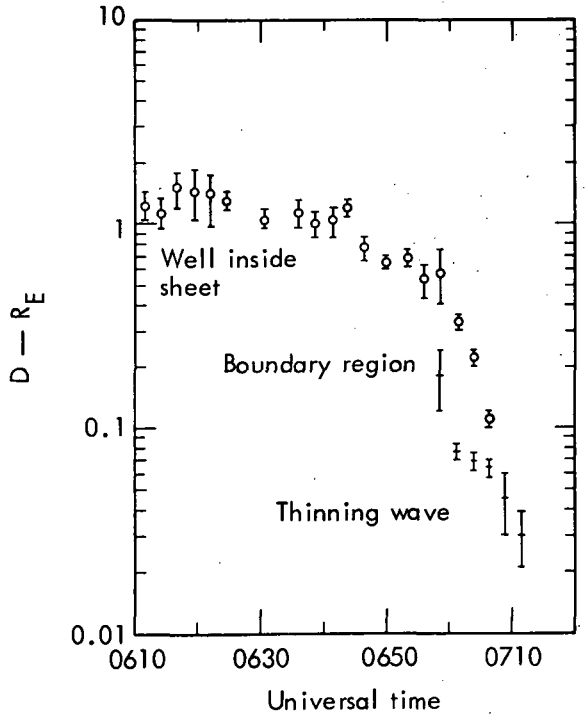

Fig. 45. The characteristic e-fold lengths of the boundary. The data show both the slowly varying region deep in the sheet and the boundary wave that became apparent at ~0656 UT.

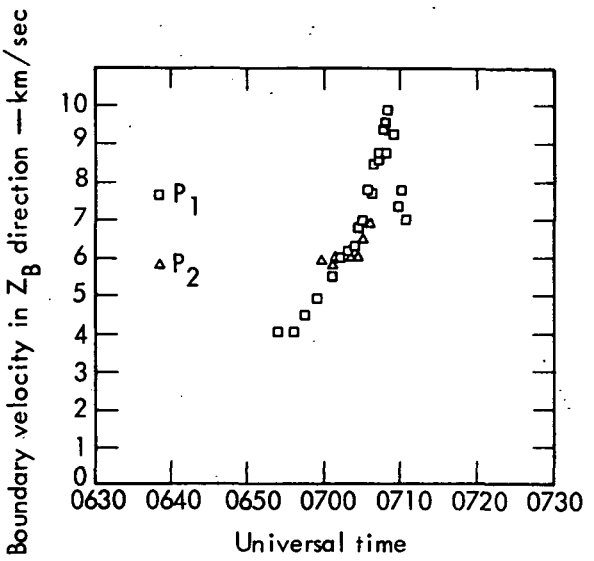

Fig. 46. Boundary velocity perpendicular to $\vec{B}$ (Z_B-direction). The slow variation is associated with the variations deep in the sheet during the early growth phase, whereas the rapid variation near the end is associated with the advance of the thinning wave. The velocity in the $-Z_{GSM}$ direction was ~0.9 of that shown in this figure.

OGO-5. Similar data have been obtained for protons, but as yet we have done nothing with these data. In contrast to west-limb events, where the particles can take advantage of the spiraling interplanetary magnetic field in their transport to Earth, the particles from this east-limb event had to arrive at Earth by indirect means (diffusion, convection, drift, etc.). It would appear that this event is perfect for the diffusive analysis of electron transport, but our early attempts to this end have not been successful. Possibly some of the more recent theoretical formulations will work.

By chance, during the course of the event, a similar magnetic spectrometer*

*A. L. Vampola, Space Physics Laboratory, The Aerospace Corporation, Los Angeles, California.

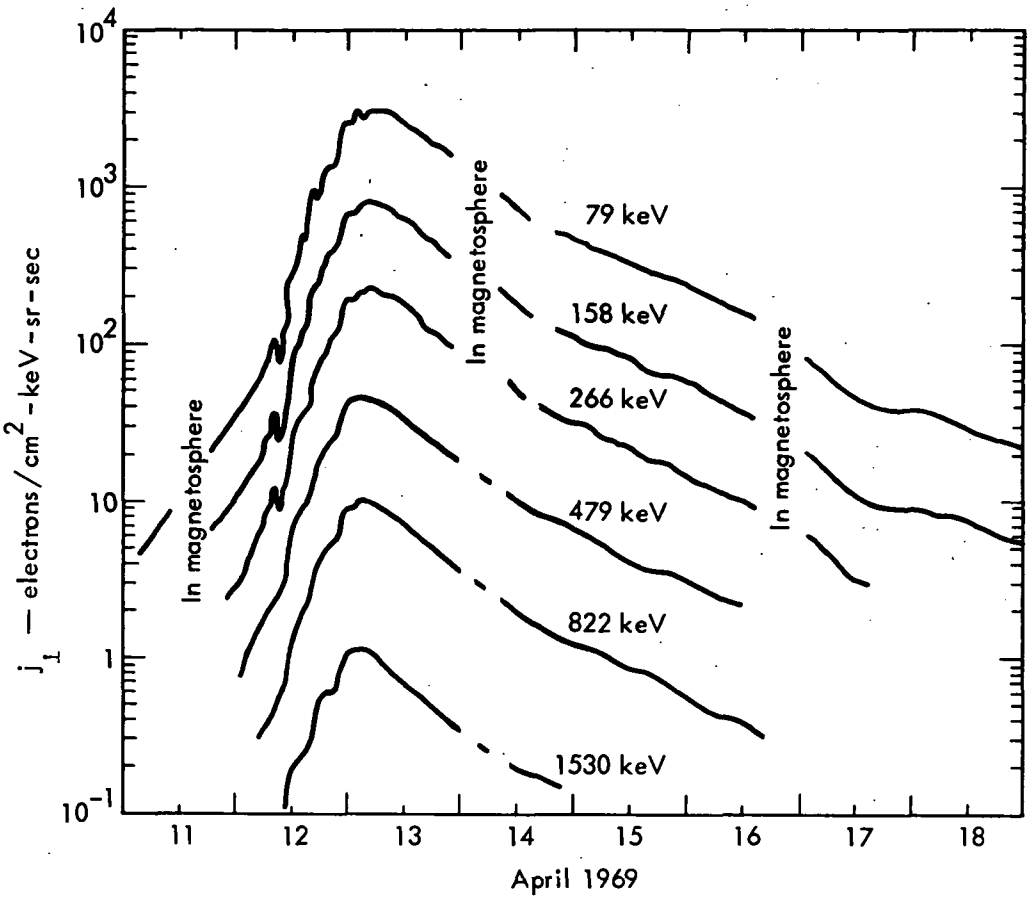

Fig. 47. The time history of the April 1969 solar-particle event as observed by the magnetic electron spectrometer on OGO-5. Data obtained in the magnetosphere that clearly represented trapped radiation are excluded from this plot. Normally, the solar fluxes could be identified well inside the magnetosphere, with no sign of discontinuity at the magnetospheric boundary except for the superposition of trapped radiation.

was collecting data on the polar orbiting Airforce Satellite OV1-19. This experiment provided for good data correlation (West and Vampola, 1971) between the polar caps and the interplanetary region. The two experiments tracked $j_\perp$ values during the event's history. A comparison at the peak of the event is shown in Fig. 48.

To summarize these observational data data, we have:

(1) Absolute flux intensities and energy spectra: There was tracking of fluxes and spectra between the interplanetary region and over the north and south polar caps during the entire history of the event.

(2) Pitch-angle distributions: (a) The interplanetary pitch-angle distributions were isotropic. (b) The pitch-angle distributions over the polar caps were isotropic except for the single loss cone when looking towards Earth. (c) Sharp discontinuities were observed in pitch-angle distribution (energy-independent) when transiting from the quasitrapping region (double loss cone) to the polar caps (single loss cone) on the sunward

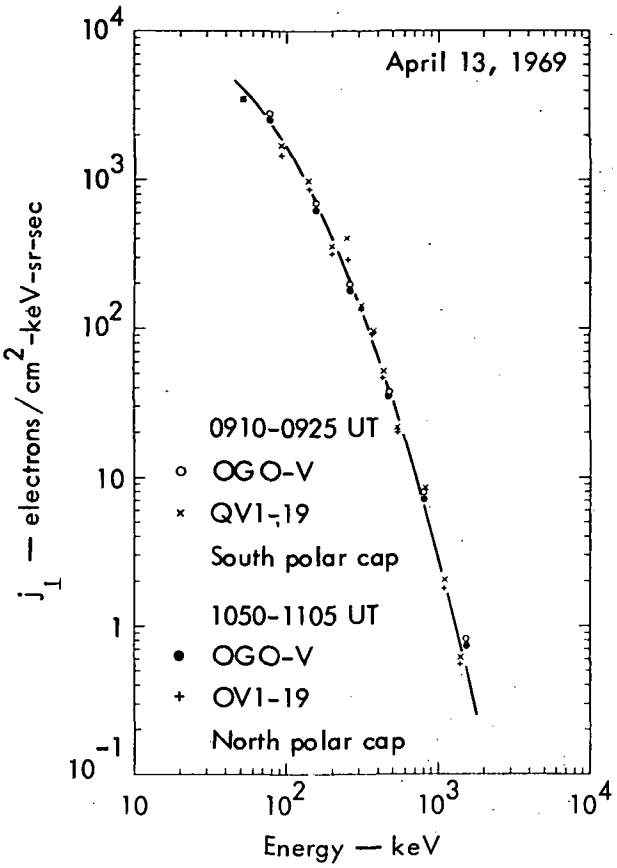

Fig. 48. Comparison of electron-spectrometer data obtained on OGO-5 and OV1-19 near the peak of the solar-particle event on April 13, 1969. For the 0910-0925 UT data, OV1-19 was over the south polar cap, altitude >4500 km; for the 1050-1105 UT data, it was over the north polar cap, altitude <2000 km.

side of Earth. (d) Sharp discontinuities were observed in pitch-angle distribution (energy-independent) when transiting from the outer zone to the polar cap at local midnight.

(3) Polar flux profiles: (a) Uniform particle distributions were observed over the polar caps. (b) There were sharp discontinuities of particle fluxes in transiting from quasitrapping region to polar caps.

(4) Solar magnetic-field sector boundary effects: No particle effects were obvious at OGO-5 or OV1-19 during the ~1140 UT, April 13 interplanetary solar magnetic sector crossing.

Observations 1, 2a, 2b, 2c, 3a, and 3b can be explained through a picture of adiabatic motion. We allow the polar field lines to connect to the solar field in the interplanetary medium. The electrons are expected to start off in the interplanetary region where they are in diffusive equilibrium, to spiral along the field lines to the region over the polar caps, then to mirror and return to the interplanetary region. This picture is in strong support of the model of the "open" magnetosphere.

The pitch-angle and flux discontinuity at the polar plateau (observations 2c and 3b) would at first glance appear to be a crowning achievement of the "open" magnetosphere model. However, one would anticipate no energy dependence in the latitude of the pitch-angle discontinuity (observation 2d), as is found to occur near local midnight. On April 13, near the peak of the event, the transition occurred at 64.89 ± 0.05 deg invariant latitude for 50-keV electrons and 64.43 ± 0.05 deg for 1.1-MeV electrons. Also, there was no obvious effect in the OV1-19 data during the April 13 interplanetary sector crossing, which occurred near the peak of the particle event. In the presence of appreciable direct connection, we would expect to find an effect due to rearrangement of the magnetic-field configuration. These two observations weaken the arguments for the "open" magnetosphere model.

THE NOVEMBER 18, 1968 SOLAR PARTICLE EVENT

A preliminary account of this work was presented by D'Arcy et al. (1970).

This solar particle event was the result of a west-limb flare. Relativistic protons were observed on Earth by neutron monitors. OGO-5 was on the dusk side of Earth, in position to observe the scatter-free propagation of electrons and protons along the spiraling interplanetary magnetic field leading from the sun to the vicinity of Earth. The early arrival is shown in Fig. 49 by the scatter plot of the E_1 electrons (79 keV). The data points are shown in time sequence as the experiment scanned about an axis (the earth's radius vector, inclined about 34 deg to the plane of the ecliptic), so that the experiments aperture viewed largely in the north-to-south direction. The experiment looked somewhat west of the sun when

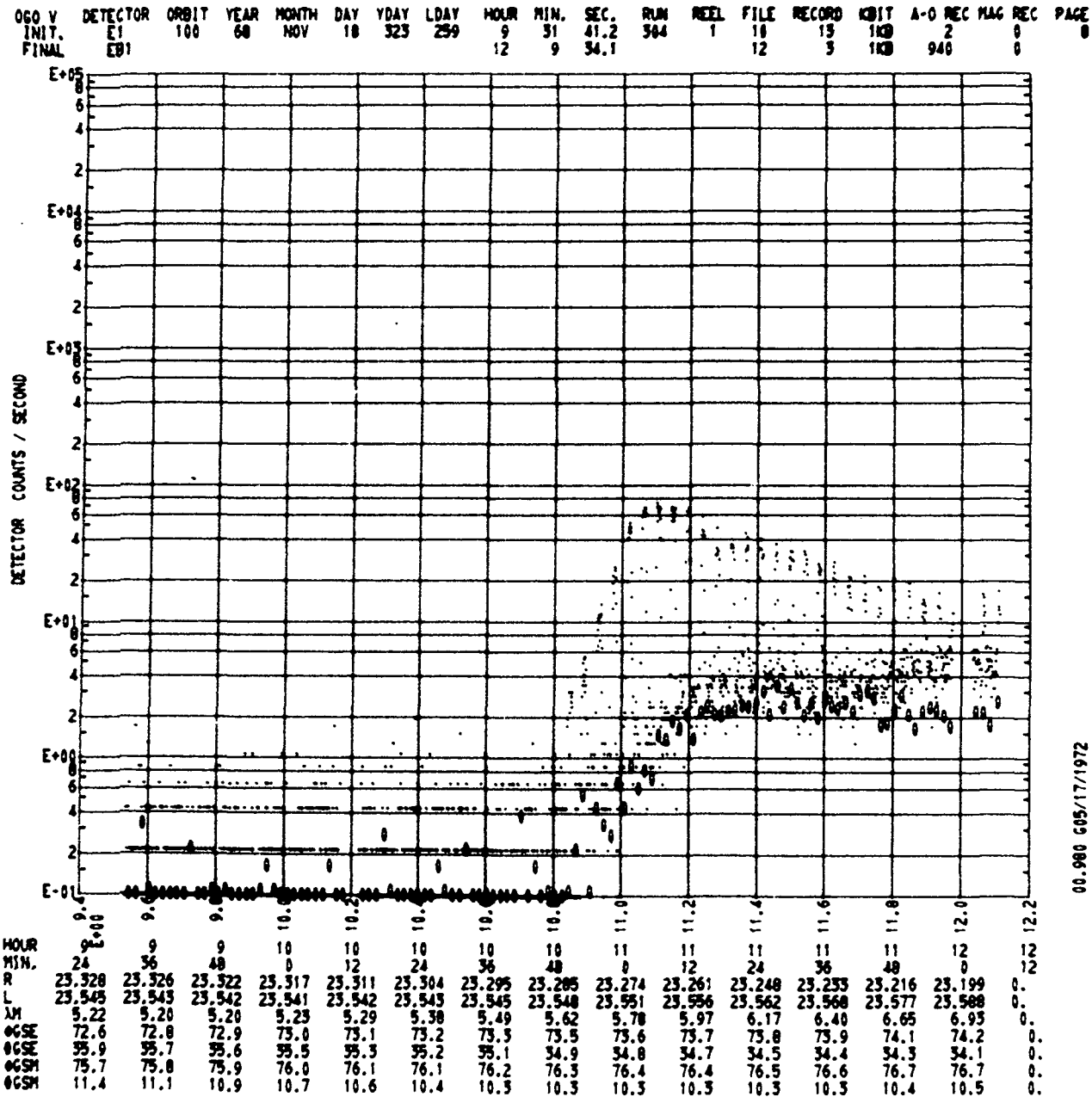

Fig. 49. E_1 fluxes obtained during the early time history of the November 18, 1968, solar particle event.

viewing in the ecliptic plane. The upper envelope of the data is due to electrons arriving from the direction of the sun; the lower envelope is the back-scattered component. These data, including proton data, are being analyzed by workers at the Bartol Research Foundation, Swarthmore, Pennsylvania.

HIGHLY-ANISOTROPIC PROTON DISTRIBUTIONS OBSERVED INTERPLANETARY

Our experiment made numerous measurements of highly-anisotropic proton distributions in the interplanetary medium. Some of these observations are associated with a well-defined solar particle event;

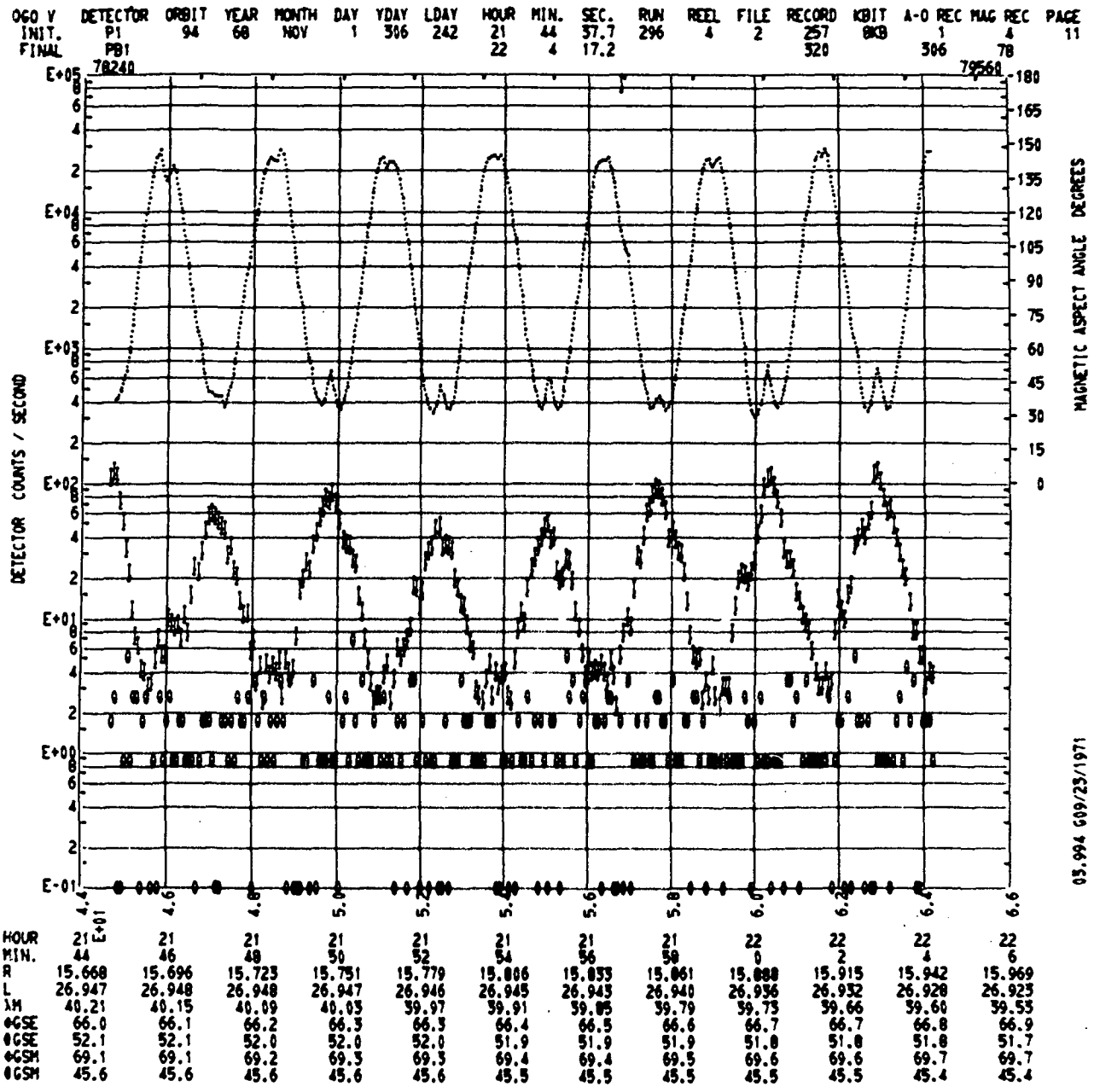

Fig. 50. Example of highly directed solar protons obtained on OGO-5. Note that these low energy protons (~100-150 keV) are directed along the field line.

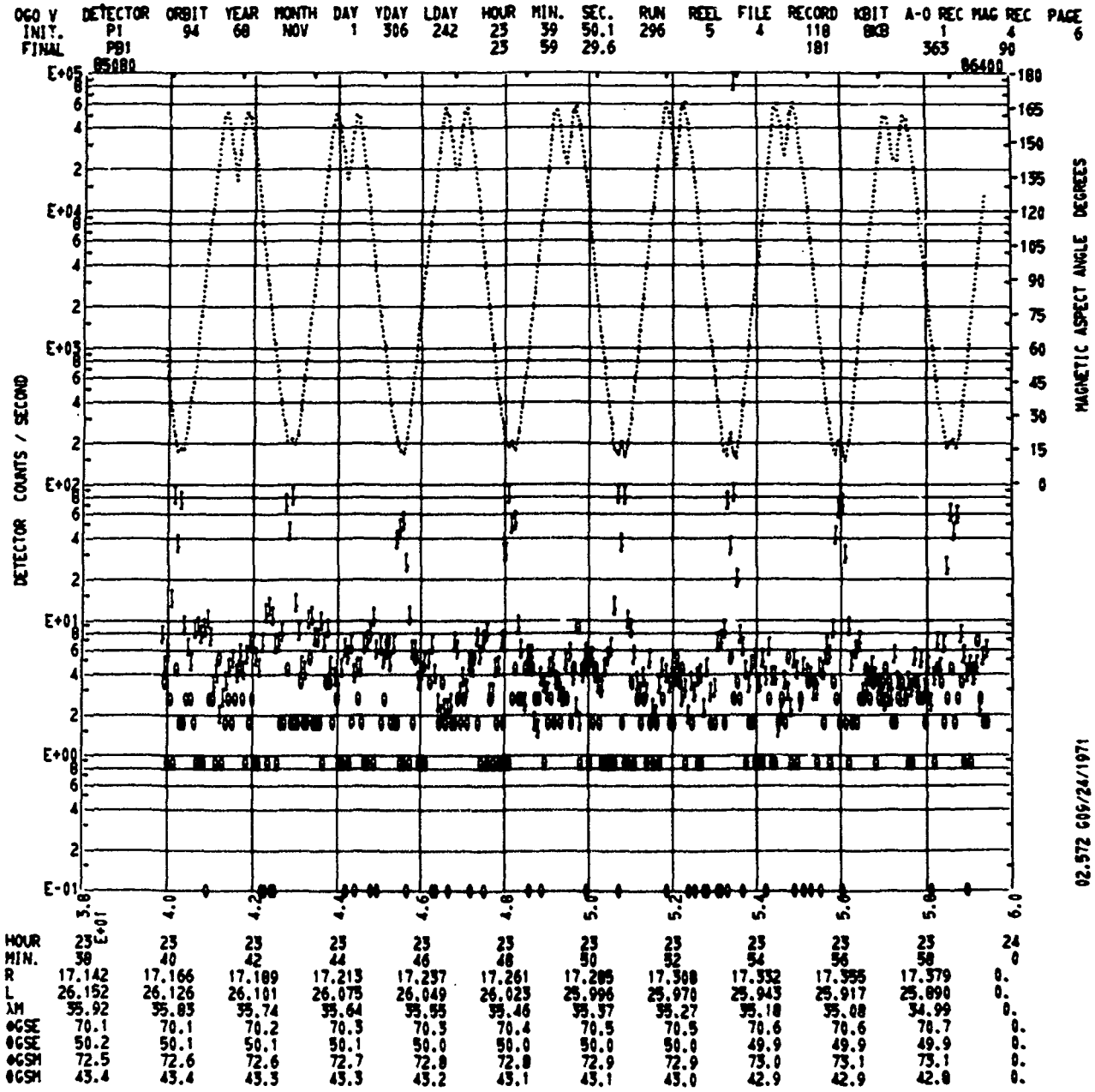

Fig. 51. Example of highly directed solar protons obtained on OGO-5. Note that these low energy protons (~100-150 keV) are directed along the field line.

others seem to be isolated bursts of protons lasting from minutes to tens of minutes. During a well-defined solar particle event, we find the usual increase in anisotropy as we go to lower energies. The lowest-energy channels, however, can show high degrees of anisotropy. In the cases we examined, the protons may be observed coming from roughly the solar direction. Other examples of large anisotropy are shown in Figs. 50 and 51. These data were acquired during the solar particle event accompanying the intense magnetic storms of October 31- November 1, 1968.

Concluding Remarks

This experiment made significant advances in several areas:

- The electron distributions and dynamics of the inner belt were provided for 1968 and 1969. These data will be useful in studying the diffusive transport of particles in the inner magnetosphere.
- A partial study was carried out covering the electron pitch-angle distributions and dynamics of the slot and outer belt regions.
- A rather complete survey was made of the electron pitch-angle distributions throughout the equatorial regions of the outer magnetosphere, with special insight into magnetopause-shadowing drift-shell effects, field-configuration-change drift-shell-splitting effects, and substorm effects. These data provide a good view of the azimuthal drift motions of electrons in the distorted-field regions of the outer magnetosphere.
- Detailed motions of the plasma sheet in the tail were observed during a substorm, using the proton east-west effect. These data show the almost complete collapse of the tail field prior to substorm expansion for the case studied.
- The transport of solar electrons to the polar caps was studied via correlative data from both the OGO-5 and OV1-19 satellites. These data provide insight into magnetospheric structure.

There is still considerable work to be done with our OGO-5 data that we believe to be significant:

- The detailed organization of the slot and the outer-belt data needs to be completed so that theoreticians can study the transport problem in the trapping regions following storm-time injection (our inner belt data already are organized adequately).
- Electron pitch-angle distributions need to be studied more thoroughly in light of the recent theoretical advances in our understanding of pitch-angle diffusion in the plasmasphere.
- Electron and proton distributions need to be studied near the noon magnetopause to assess their azimuthal drift motions through minimum-B regions in the earth's magnetic field.
- Electron pitch angles need to be studied more thoroughly in the pre-midnight magnetosphere to permit better understanding of the pitch-angle signature in the study of magnetic field topology, especially with regard to substorms.
- A complete survey of proton pitch-angle distributions needs to be conducted at all local times in the equatorial regions.
- The proton east-west effect needs to be exploited more fully in the study of plasma-sheet dynamics, especially during substorms. This seems to be the most effective way of studying boundary motions on a single satellite.
- The manner in which electrons drift azimuthally through the region

of the midnight cusp so as to maintain some semblance of the butterfly pitch-angle distribution needs to be understood. This will provide additional insight into field topology for dynamic and static periods.

- Well-defined plasma sheet oscillations, observed past midnight in terms of particles and B-fields, need to be understood. Are these effects associated with the solar wind?
- The appearance of energetic electrons and protons in the magnetosheath near the high latitude magnetopause needs to be understood. There may be a tie-in to reconnection.
- The highly directed solar protons observed interplanetary need to be investigated. Do these low energy particles follow the convective flow of the solar wind?
- The scatter-free propagation of solar electrons from the sun to the earth needs to be investigated further in order to enhance our understanding of particle transport.
- The April 1969 solar particle event needs to be understood more thoroughly in terms of particle transport. As a follow up on this work, there are several other events that should be studied.
- The manner in which solar protons gain access to the near-earth trapping regions (~3 R_E) needs to be understood.

The above list is by no means complete. This experiment has provided a veritable goldmine of information. It is hoped that a significant portion will reach the printed page.

Acknowledgments

Many people contributed to the success of this experiment. Those assisting in the construction phase are cited in the instrument report. In the data reduction and analysis phase, we acknowledge the continued support of E. Mercanti (Program Manager), K. Meese (Program Coordinator), J. Meenen (Operations), and H. Lindner (Data Processing) of GSFC. We thank P. J. Coleman and C. T. Russell of UCLA for the ready availability of their OGO-5 vector magnetometer data. In addition, we thank C. T. Russell, R. L. McPherron, Margaret G. Kivelson, and T. A. Farley, all of UCLA, for many stimulating discussions during the course of data analysis.

The people directly assisting the authors at Lawrence Livermore Laboratory were M. M. Zeligman and Bettie Myers. They were responsible for handling the large amounts of data produced by the experiment. R. G. D'Arcy, Jr., who was responsible for the proton spectrometer while at Livermore, has continued with the data reduction of these data at the Bartol Foundation.

The work covered in this report was performed under the auspices of the U. S. Atomic Energy Commission, funded in part by NASA under P. O. S-70014-G.

References

Buck, R. M., H. I. West, Jr., and R. G. D'Arcy, Jr., "Evidence for thinning of the plasma sheet during the August 15, 1968 substorm," EOS Trans. Amer. Geophys. Union 51, 810, 1970.

Buck, R. M., H. I. West, Jr., and R. G. D'Arcy, Jr., "Energetic protons as probes of magnetospheric particle gradients," EOS Trans. Amer. Geophys. Union 53, 486, 1972.

Buck, R. M., H. I. West, Jr., and R. G. D'Arcy, Jr., "Satellite studies of magnetospheric substorms on August 15, 1968: 7. OGO-5 energetic proton observations—Spatial boundaries," J. Geophys. Res. 78, 3103, 1973.

Fairfield, D. H., "Average magnetic field configuration of the outer magnetosphere," J. Geophys. Res. 73, 7329, 1968.

Haskell, G. P., "Anisotropic fluxes of energetic particles in the outer magnetosphere," J. Geophys. Res. 74, 1740, 1969.

Lyons, L. R., R. M. Thorne, and C. S. Kennel, "Pitch angle diffusion of radiation belt electrons within the plasmasphere," J. Geophys. Res. 77, 3455, 1972

McPherron, R. L., M. P. Aubry, C. T. Russell, and R. J. Coleman, "Satellite studies of magnetospheric substorms on August 15, 1968: 9. Phenomenological models for substorms," J. Geophys. Res. 78, 3131, 1973.

McQuaid, J. H., "An electron and proton spectrometer detector system for an OGO-E satellite experiment," IEEE Trans. Nucl. Sci. NS-13 No. 1, 515, 1966.

Pfitzer, K., "The spectra and intensity of electrons in the radiation belts," Space Res. 6, 702, 1966.

Pfitzer, K. A., and J. R. Winkler, "Experimental observation of a large addition to the electron inner radiation belt after a solar flare event," J. Geophys. Res. 5792, 1968.

Roederer, J. G., "On the adiabatic motion of energetic particles in a model magnetosphere," J. Geophys. Res. 72, 981, 1967.

Roederer, J. G., "Quantitative models of the magnetosphere," Rev. Geophys. 77, 77, 1969.

Serlimitsos, P., "Low energy electrons in the dark magnetosphere," J. Geophys. Res. 71, 61, 1966.

Shabansky, V. P., "Some processes in the magnetosphere," Space Sci. Rev. 12, 299, 1971.

Speiser, T. W., "Particle trajectories in model current sheets: (Part 1). Analytical solutions," J. Geophys. Res. 70, 4219, 1965.

Speiser, T. W., "Particle trajectories in model current sheets: (Part 2). Aplications to auroras using a geomagnetic tail model," J. Geophys. Res. 72, 3919, 1967.

Speiser, T. W., "The Dungey model of the magnetosphere, and astro-geophysical current sheets," Radio Sci. 6, 315, 1971.

Sugiura, M., B.G. Ledley, T.L. Skillman, and J.P. Heppner, "Magnetospheric-field distortions observed by OGO-3 and 5," J. Geophys. Res. 76, 7553, 1971.

West, H.I., Jr., L.G. Mann, and S.D. Bloom, "Some electron spectra in the radiation belts in the Fall of 1962," Space Res. 5, 423, 1965.

West, H.I., Jr., "Some observations of the trapped electrons produced by the Russian high altitude nuclear detonation of October 28, 1962," in Radiation Trapped in the Earth's Magnetic Field (B.M. McCormac, ed.), Dordrecht, Holland: D. Reidel Publishing Company, 634, 1965.

West, H.I., Jr., J.H. Wujeck, J.H. McQuaid, N.C. Jenson, R.G. D'Arcy, Jr., R.W. Hill, and R.M. Bogdanowicz, "The LRL electron and proton spectrometer on NASA's Orbiting Geophysical Observatory V(E) (instrumentation and calibration)," Lawrence Livermore Laboratory, Rept. UCRL-50572, June 1969.

West, H.I., Jr., R.W. Hill, J.R. Walton, R.M. Buck, and R.G. D'Arcy, Jr., "Electron and proton pitch-angle distributions in the outer magnetosphere," EOS Trans. Amer. Geophys. Union 50, 659, 1969.

West, H.I., Jr., R.M. Buck, and J.R. Walton, "Electron spectra in the slot and the outer radiation belt," EOS Trans. Amer. Geophys. Union 51, 806, 1970.

West, H.I., Jr., R.M. Buck, and J.R. Walton, "The butterfly pitch-angle distribution of electrons in the postnoon to midnight region of the outer magnetosphere as observed on OGO-5," EOS Trans. Amer. Geophys. Union 53, 486, 1972a.

West, H.I., Jr., R.M. Buck, and J.R. Walton, "Shadowing of electron azimuthal-drift motions near the noon magnetopause," Nature Phys. Sci. 240, 6, 1972b.

West, H.I., Jr., R.M. Buck, and J.R. Walton, "Electron pitch-angle distributions throughout the magnetosphere as observed on OGO-5," J. Geophys. Res. 78 1064, 1973a.

West, H.I., Jr., R.M. Buck, and J.R. Walton, "Satellite studies of magnetospheric substorms on August 15, 1968: 6. OGO-5 energetic electron observations — Pitch-angle distributions in the nighttime magnetosphere," J. Geophys. Res. 78, 3093, 1973b.

Distribution

DoNoT PRINT

LLL Internal Distribution

Roger E. Batzel
J. S. Kane
W. E. Nervik
H. L. Reynolds
J. E. Carothers
J. N. Shearer
R. D. Neifert
H. I. West, Jr. 100
R. M. Buck
J. R. Walton
LBL Library
TID File 30

External Distribution

K. Meese
E. Mercanti
Office of Director
Office of Assistant Director, Projects 3
Office of Assistant Director, T&DS 3
Office of Assistant Director, SS 3
Office of Technical Services 3
Library 2
Negotiator
Technical Information Division
National Space Science Data Center 5
Technical Director 7
Goddard Space Flight Center
Greenbelt, Maryland

M. Pomerantz
The Bartol Research Foundation
of the Franklin Institute
Swarthmore, Pennsylvania

R. G. D'Arcy, Jr.
Cambridge, Massachusetts

A. Schardt
E. Schmerling
L. Kavanaugh
Code SG
NASA Headquarters
Washington, D. C.

Technical Information Center 2
Oak Ridge, Tennessee

CSM/rt/edas